The Pennsylvania State University
The Graduate School

EXTRACELLULAR VESICLE -MEDIATED EPITHELIAL TO MESENCHYMAL TRANSITION AS A DISEASE MECHIANISM IN RETINAL PIGMENT EPITHELIA

A Dissertation in

Biomedical Sciences

by

Mi Zhou

Submitted in Partial Fulfillment

of the Requirements

for the Degree of

Doctor of Philosophy

August 2022

The dissertation of Mi Zhou was reviewed and approved by the following:

Jeffrey M. Sundstrom
Assistant Professor, Department of Ophthalmology
Dissertation Advisor
Chair of Committee

John Wills
Distinguished Professor, Department of Microbiology and Immunology

Xuemei Huang
Distinguished Professor, Department of Neurology

James Connor
Distinguished Professor, Department of Neuroscience and Anatomy and Department of Neurosurgery

Patricia Grigson-Kennedy
Professor, Department of Neural and Behavioral Sciences

Nicholas Buchkovich
Associate Professor, Department of Microbiology and Immunology

Ralph Keil
Associate Professor of Biochemistry and Molecular Biology
Chair of the Biomedical Sciences Graduate Program

ABSTRACT

Retinal pigment epithelial (RPE) cells play a central role in maintaining the health and functional integrity of both photoreceptors and the choroid. This functional unit is required for maintaining proper visual function. Numerous retinal degenerative diseases are initiated by RPE dysfunction, including several inherited retinal degenerations and age-related macular degeneration (AMD). However, the molecular mechanisms underlying RPE dysfunction in retinal degeneration remain largely unknown.

To investigate the role of protein misfolding in retinal pigment epithelial (RPE) cell dysfunction, the effects of R345W-Fibulin-3 expression on RPE cell phenotype were studied. Primary RPE cells were cultured to confluence on Transwells and infected with lentivirus constructs to express wild-type (WT)- or R345W-Fibulin-3. Barrier function was assessed by evaluating zonula occludens-1 (ZO-1) distribution and trans-epithelial electrical resistance (TER). Polarized secretion of vascular endothelial growth factor (VEGF), was measured by Enzyme-linked immunosorbent assay (ELISA). Differentiation status was assessed by qPCR of genes known to be preferentially expressed in terminally differentiated RPE cells, and conversion to an epithelial–mesenchymal transition (EMT) phenotype was assessed by a migration assay.

Compared to RPE cells expressing WT-Fibulin-3, ZO-1 distribution was disrupted and TER values were significantly lower in RPE cells expressing R345WFibulin-3. In cells expressing mutant Fibulin-3, VEGF secretion was attenuated basally but not in the apical direction, whereas Fibulin-3 secretion was reduced in both the apical and basal directions. Retinal pigment epithelial signature genes were downregulated and multiple genes associated with EMT were upregulated in the mutant group. Migration assays revealed a faster recovery rate in ARPE-19 cells overexpressing R345W-Fibulin-3 compared to WT. The results suggest that expression of R345W-Fibulin-3 promotes EMT in RPE cells.

Extracellular vesicles (EVs) play a critical role in cell-cell communication and modulate cellular differentiation. While RPE cells have been shown to secrete EV, the

potential role of EVs in regulating RPE differentiation has not been studied. We next investigate the size, cargo, and function of extracellular vesicles (EVs) derived from RPE cells expressing WT-Fibulin-3 compared to RPE cells expressing the R345W-Fibulin-3 mutation, and determine the role of these EVs in RPE cell dysfunction.

ARPE-19 cells were infected with luciferase-tagged wild-type (WT)- Fibulin-3 or luciferase-tagged R345W-Fibulin-3 (R345W) using lentiviruses. EVs were isolated from the media of ARPE-19 cells by conventional ultracentrifugation or density gradient ultracentrifugation. Transmission electron microscopy (TEM) and cryogenic electron microscopy (Cryo-EM) were performed to study the morphology of the EVs. The amount and size distribution of EVs were determined by Nanoparticle Tracking Analysis (NTA). EV protein concentrations were quantified using the DCTM Protein Assay (Bio-Rad). EV markers were validated by conducting Western blot analysis. EV cargo were analyzed by unbiased proteomics using LC-MS/MS with subsequent pathway analysis (Advaita). The EV-associated transforming growth factor beta 1 (TGF-β1) protein was measured by enzyme-linked immunosorbent assay (ELISA). EV incubated with trypsin were conducted to determine the orientation of WT-Fibulin-3 and R345W-Fibulin-3 in EV. EV uptake was investigated by using PKH67-labeled vesicles and was analyzed by confocal imaging. The EV transplant study was conducted, and migration ability was evaluated in ARPE-19 cells with or without exposure to EVs by conducting scratch assays. Pan-TGF-β-neutralizing antibody was used to determine whether EVs derived from RPE cells induce EMT via TGF-β signaling. mRNA expression levels of EMT markers were measured after EV treatment using RT-PCR.

TEM imaging revealed concave-appearing vesicles, and Cryo-EM imaging showed spherical vesicles with two subpopulations of EVs: a group with diameters around 30 nm and a group with diameters over 100 nm. Imaging also indicated a greater number of small EVs (~30 nm) in the R345W group compared to the WT group. This result was further confirmed by NTA showing that, in the R345W group, the particle size distributions were smaller than those of the WT-ARPE-EV. There were no significant differences in EV protein concentrations per EV between WT and R345W groups. Pathway analysis revealed

that primary cilia and sonic hedgehog (SHH) pathways were found to be 3- to 5-fold more abundant in EVs derived from WT ARPE-19 cells. In contrast, EMT drivers, lysosome components, and ribosome components were 3- to 7-fold more abundant in EVs secreted from R345W ARPE-19 cells. Subsequent studies revealed enhanced content of TGF-β1 associated with R345W-ARPE-EVs compared to WT-ARPE-EVs. Fibulin-3 can be digested with a low concentration of trypsin, but not EGFR, Flotillin-1, or ALIX, indicating that Fibulin-3 is outside of EV rather than within them. There were no significant differences in EV uptake between WT and mutant groups. Critically, EV transplant studies showed that treatment of recipient RPE cells with R345W-ARPE-EV was sufficient to induce an enhanced migration ability and elevated EMT marker expression in RPE cells. The effects were significantly inhibited after the addition of pan-TGF-β-neutralizing antibody.

In conclusion, the expression of R345W-Fibulin-3 alters the size, cargo, and function of EVs. Notably, EVs derived from RPE cells expressing R345W-Fibulin-3 are sufficient to enhance the rate of wound healing closure and elevate EMT marker expression in untransfected RPE cells.

TABLE OF CONTENTS

LIST OF FIGURES

LIST OF TABLES

LIST OF ABBREVIATIONS

Abbreviation	Term
ADVIRC	Autosomal dominant vitreoretinochoroidopathy
AF4	Asymmetric flow field-flow fractionation
AFM	Atomic Force Microscopy
AJs	Adherens junctions
AMD	Age-related macular degeneration
ANOVA	One-way analysis of variance
AREDS	Age-Related Eye Disease Study
BEST1	Bestrophin-1
BiP	Binding immunoglobulin protein
BMPs	Bone morphogenetic proteins
BSA	Bovine serum albumin
CDH2	Cadherin 2
CDK4	Cyclin-dependent kinase 4
CHOP	C/EBP homologous protein
CLIC4	Chloride intracellular channel 4
CNV	Choroidal neovascularization
CRALBP	Retinaldehyde-binding protein
Cryo-EM	Cryogenic Electron Microscopy
CSF	Cerebrospinal fluid
DHMD	Doyne honeycomb macular dystrophy
DME	Diabetic macular edema
DMEM	Dulbecco's Modified Eagle's Medium
Dox	Doxycycline
EGF	Epidermal growth factor
ELISA	Enzyme-linked immunosorbent assay
EMT	Epithelial-mesenchymal transition
ER	Endoplasmic reticulum
ERAD	ER-associated degradation
ESCRT	Endosomal sorting complex required for transport
EVs	Extracellular vesicles
FDR	False discovery rate
GFP	Green fluorescent protein
GLuc	*Gaussia* Luciferase
GLUT	Glucose transporter
GM130	Golgi matrix protein 130
GRP-78	Glucose regulated protein-78
GSK-3β	Glycogen synthase kinase-3 beta
HEPES	4-(2-hydroxyethyl)-1-piperazineethanesulfonic acid
hfRPE	Human fetal RPE

HRF	Hyperreflective foci
ICC	Immunocytochemistry
iPSC-RPE	Induced pluripotent stem cell-derived RPE
IRDs	Inherited retinal degenerations
JNK/p38-MAPK	c-Jun N-terminal kinase and p38 mitogen-activated protein kinase
Log_2DE	Log differential expression
MCT1	Proton-coupled monocarboxylate transporters 1
MET	Mesenchymal-epithelial transition
miRNAs	MicroRNAs
MVBs	Multivesicular bodies
MOPS	3-(N-morpholino) propanesulfonic acid
MS	Mass spectrometry
NAM	Nicotinamide
NTA	Nanoparticle tracking analysis
OCT	Optical coherence tomography
PBS	Phosphate-buffered saline
PBS-T	0.1% Triton-X-100 in PBS
PCR	Polymerase chain reaction
PED	Pigment epithelium detachment
PEDF	Pigment epithelium-derived factor
PEG	Polyethylene glycol
pH	Potential of hydrogen
PPAR	Peroxisome proliferator-activated receptor
PVR	Proliferative vitreoretinopathy
RAR	Retinoic acid receptor
RNAi	RNA interference
ROCK	Rho-associated protein kinase
RPE	Retinal pigment epithelial
RPE65	Retinal pigment epithelium-specific 65 kDa protein
RPS	Resistance pulse sensing
SDS-PAGE	Sodium dodecyl sulfate-polyacrylamide gel electrophoresis
SD-OCT	Spectral domain optical coherence tomography
SEM	Scanning Electron Microscopy
SHH	Sonic hedgehog
TBS	Tris-buffered saline
TBST	Tris-buffered saline and Polysorbate 20
TEM	Transmission electronic microscopy
TER	Trans-epithelial electrical resistance
TGF-β	Transforming growth factor-beta
TJs	Tight junctions
TIM23	Mitochondrial import inner membrane translocase subunit Tim23
TRPM	Transient receptor potential cation channel
UPR	Unfolded protein response
VEGF	Vascular endothelial growth factor

VIM	Vimentin
WB	Western Blots
WT	Wild-type
ZEB1	Zinc Finger E-Box Binding Homeobox 1
ZO-1	Zona-occludens-1
ZONAB	ZO-1–associated Y-box factor

ACKNOWLEDGMENTS

First and foremost, I would like to thank my mentor Dr. Jeffrey Sundstrom. The opportunities that you have provided have been invaluable. I am forever grateful for the time we have worked together. You are more than a great mentor to me. You are also a good friend. Thank you for guiding me through this journey. Thank you for your kindness and endless support.

I have been very fortunate in the support I have received at Penn State. No graduate career can flourish without the overall guidance of the faculty. I would like to thank the Biomedical Sciences Graduate Program, our outstanding program chair, Dr. Ralph Keil. Especially, I want to thank Dr. Xuemei Huang and Dr. Richard Mailman for their guidance and incredibly support on my career development. My committee members have been wonderful. Thank my dissertation committee: Dr. John Wills, Dr. Xuemei Huang, Dr. Sue Grigson, Dr. James Connor, and Dr. Nicholas Buchkovich. Thank you for your time, encouragement, and suggestions. Your constructive comments and advice made me who I am today.

It is also important that I express my appreciation to all my lab members. You made the lab environment welcoming and enjoyable. Special thanks to Dr. Alistair Barber for your continued support, help, and care throughout my training. I thank Dr. Yuanjun Zhao for teaching me how to do experiments and giving me plenty of help and advice every step of the way. Your patience and kindness are greatly appreciated. I thank Dr. Stephanie Grillo for discussing projects and interacting with me almost every day. I thank Sarah Weber and Jasmine Geathers for being wonderful friends and always being there for me.

Finally, I would like to express my sincere appreciation to my family. I thank my parents, Rui Yan and Qingxun Zhou for their unconditional and unlimited love, understanding, and support. Your love keeps me happy, content, and grateful. I thank my intelligent husband, Xinghai Xia, for accompanying me during this journey. You always inspire me and motivate me to be the best I can be. Your support enabled me to reach my full potential in my career development.

CHAPTER 1.

ROLE OF EPITHELIAL-MESENCHYMAL TRANSITION AND EXTRACELLULAR VESICLES IN RETINAL PIGMENT EPITHELIUM DYSFUNCTION.

Chapter 1 was previously published as a review paper and a book chapter written by Mi Zhou (Zhou et al., 2020, Frontiers in Cell and Developmental Biology and Zhou et al., 2020, Exosomes: A Clinical Compendium). The text has been reformatted for this dissertation**.**

Abstract

Retinal pigment epithelial (RPE) cells maintain the health and functional integrity of both photoreceptors and the choroidal vasculature. Loss of RPE differentiation has long been known to play a critical role in numerous retinal diseases, including inherited rod-cone degenerations, inherited macular degeneration, age-related macular degeneration, and proliferative vitreoretinopathy. Recent studies in post-mortem eyes have found upregulation of critical epithelial-mesenchymal transition (EMT) drivers such as TGF-β, Wnt, and Hippo. As RPE cells become less differentiated they begin to exhibit the defining characteristics of mesenchymal cells, namely, the capacity to migrate and proliferate. A number of preclinical studies, including animal and cell culture experiments, also have shown that RPE cells undergo EMT. Taken together, these data suggest that RPE cells retain the reprogramming capacity to move along a continuum between polarized epithelial cells and mesenchymal cells. We propose that movement along this continuum toward a mesenchymal phenotype be defined as RPE Dysfunction. Potential mechanisms include impaired tight junctions, accumulation of misfolded proteins and dysregulation of several key pathways and molecules, such as TGF-β pathway, Wnt pathway, nicotinamide, microRNA-204/211 and extracellular vesicles. We synthesize the evidence implicating

RPE undergoing EMT in post-mortem eyes, animal studies, primary RPE, iPSC-RPE and ARPE-19 cell lines.

Extracellular vesicles (EVs) are released from cells under both physiological and pathophysiological conditions. EVs are a class of extracellular vesicles that originate from intraluminal membranes, and their diameters vary from 30 to 150 nm. Like hormones and cytokines, EVs play a critical role in cell-cell communication. Proper methods for EV isolation and characterization facilitate accurate downstream analyses. Both conventional and novel techniques for EV isolation and characterization were summarized as well as their advantages and limitations. Novel methods for fractionating EV subsets, defining EV cargo, tracking EV *in vivo*, and determining whether a protein is associated with the inside or outside of EVs are also included in this chapter.

Introduction

The epithelium to mesenchyme continuum

Epithelial cells and mesenchymal cells exhibit different characteristics and functions in the human body. Major hallmarks of terminally differentiated epithelial cells are expression of junctional complexes and apical-basal polarization. Epithelial cells reside on a basal membrane that separates them from other tissue components. In contrast to epithelial cells, mesenchymal cells are non-polarized cells with invasive and migratory behavior. Throughout embryogenesis, the capacity of cells to alternate between epithelial and mesenchymal states is vital for the development of the human body (1, 2). These processes are known as epithelial to mesenchymal transition (EMT) and mesenchymal to epithelial transition (MET). In healthy tissues, fully differentiated epithelial cells typically exert specific functions after development and are thought not to oscillate between two states. However, EMT can be activated under pathological circumstances, such as inflammation, wound healing, and carcinogenesis, enabling epithelial cells to obtain an enhanced migration ability and increase their production of extracellular matrix components.

Historically, EMT is classified into three subtypes: type I EMT occurs in the early stages of embryogenesis; type II EMT is associated with tissue regeneration and organ fibrosis; type III occurs in cancer cells and enables invasion and metastasis (3). Loss of epithelial markers, including zona-occludens-1 (ZO-1), E-cadherin, and cytokeratin, and gain of expression of mesenchymal drivers, including vimentin, N-cadherin, and fibronectin, are encompassed in the classical definition of EMT. However, this definition remains heavily debated and is thought to be oversimplified. Indeed, gain of invasive and migratory abilities is not necessarily accompanied by the completely loss of epithelial traits. Ovarian cancer cells are heterogeneous, as some cells lose E-cadherin but do not gain N-cadherin (4, 5). As such, it has been proposed that EMT and MET exist on a continuum, and an intermediate phenotype exists (6). Across this continuum, factors that drive the transition from epithelial to mesenchymal remain to be determined. Herein, the transition from fully differentiated epithelial cells toward mesenchymal cells (including the intermediate states) is defined as RPE dysfunction. Potential mechanisms involved in RPE dysfunction may include aging, loss of tight junctions, accumulation of misfolded protein, and inflammation (**Figure 1-1**).

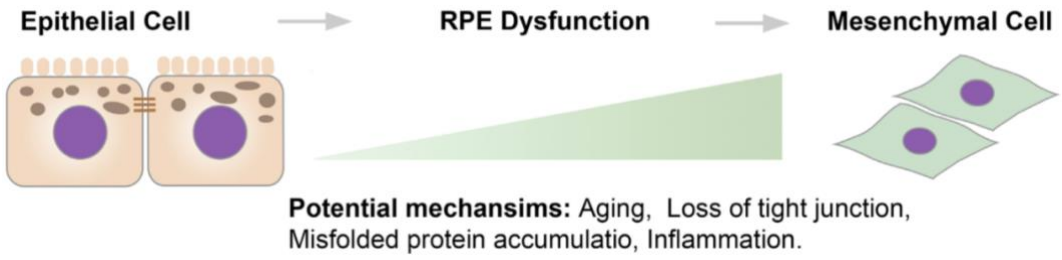

Figure 1-1. There is a continuum between epithelial cells and mesenchymal cells. Across the continuum, the transition starts from well-differentiated RPE cells that exhibit barrier integrity and cellular polarity to intermediate stages, where RPE cells become dedifferentiated and lose functions, to mesenchymal-like cells that exhibit an increased proliferative rate and migrate into the neuroretina.

Retinal Pigment Epithelial (RPE) cells

The RPE form a single layer of highly polarized cells juxtaposed between the photoreceptors and choroid. There are approximately 3.5 x 10^6 RPE cells in each adult human eye. Classically, RPE cells are thought to be terminally differentiated throughout

life (7). Several signaling pathways have been reported to be involved in RPE differentiation, including Sonic hedgehog (SHH), Wnt/β-catenin, and Notch (8-11). MicroRNAs (miRNAs) also play a role; previous studies have shown that miRNA-204/211 are critical for maintaining RPE differentiation (12, 13). RPE cells display morphological polarity, with apically located microvilli, tight junctions, and melanosomes, and basally located nuclei and basal infoldings. Melanin pigment granules in RPE cells absorb light, contributing to visual function and protecting against photo-oxidative stress (14). Basally, RPE cells attach to Bruch's membrane, which consists of a mixture of collagen type IV, laminin, and fibronectin that is similar to other basement membranes and functions to separate the RPE from the choriocapillaris (15).

The structure of RPE cells is optimized for their many functions. Proper RPE function requires specific polarized distribution of transmembrane proteins. For example, Na^+/K^+-ATPases (16), chloride intracellular channel 4 (CLIC4) (16), mannose receptors (17), proton-coupled monocarboxylate transporters 1 (MCT1) (18) are restricted to the apical aspect of RPE cells. CD36 that functions in phagocytosis is also apically located (19). In contrast, integrins, MCT3 (20), and Bestrophin-1(21), a chloride anion channel, are located basally. In addition to the polarized distribution of membrane proteins, RPE cells secrete proteins in a polarized manner. Vascular endothelial growth factor (VEGF) is primarily secreted in the basal direction to promote the growth of the choroidal vasculature, whereas pigment epithelium-derived factor (PEDF), an angiogenic inhibitor, is apically secreted (22). Some proteins lack a polarized distribution, including ezrin (23) and Glucose transporter (GLUT) 1 (24), which exist on both apical and basal aspects of the cell (**Figure 1-2**).

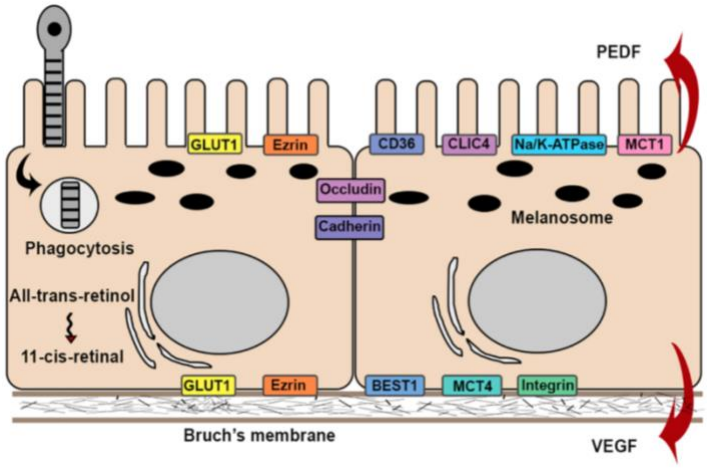

Figure 1-2. Schematic illustration of the structures and functions in RPE cell. RPE cells attach to Bruch's membrane in a single monolayer with apical microvilli and melanosomes, and basal nuclei. Barrier function is maintained by expression of occludin and cadherins. RPE cells exhibit physiological functions, such as phagocytosis and visual cycles. RPE cells exhibit functional polarity by polarized secretion of proteins and apical-basal distribution of membrane proteins.

Clinical and preclinical evidence of EMT in RPE cells

Overview

Together, photoreceptors, RPE, and the choroid form a functional unit that is required for proper visual function. RPE cells are the central component of this unit, as they maintain the health and functional integrity of both photoreceptors and the choroid. RPE dysfunction is often an initiating or early factor in retinal disease, manifesting as a loss of RPE barrier function, disrupted RPE polarization, and downregulated microRNA-204/211 expression. Emerging evidence shows that RPE cells become less differentiated and subsequently undergo EMT with upregulated mesenchymal cell markers and enhanced migration ability in several degenerative retinal diseases (25-27) (**Figure 1-3**). Clinical evidence suggesting that RPE cells undergo EMT in macular degenerations and proliferative vitreoretinopathy (PVR), as well as potential underlying mechanisms, are discussed in the following sections.

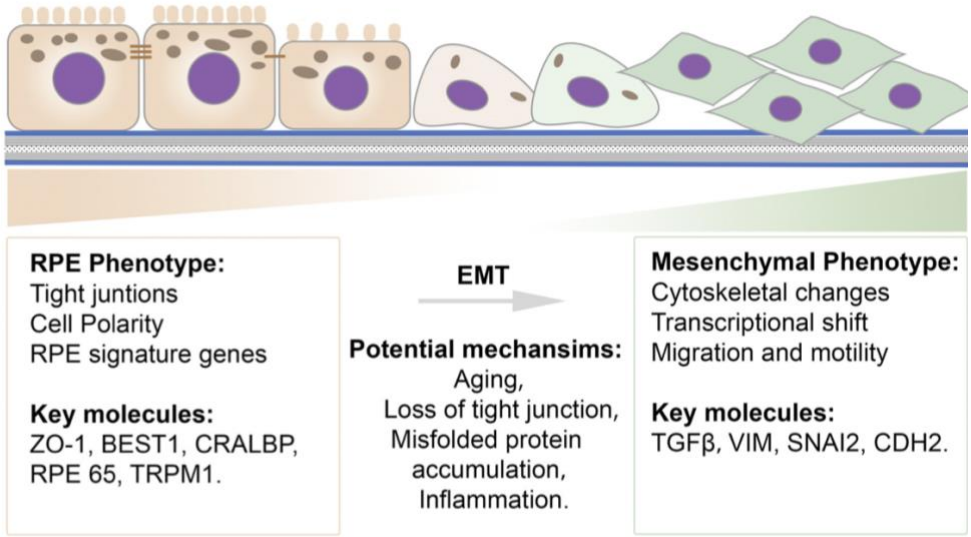

Figure 1-3. Schematic illustration of the transition spectrum in RPE cells. Common epithelial and mesenchymal cell features and key molecules are listed. RPE cells exhibit a well-differentiated epithelial phenotype that is characterized by integrated tight junctions, high polarization, and proper RPE signature gene expression. A mesenchymal-like phenotype exhibits cytoskeletal changes, a transcriptional shift, and an increased ability for migration. Potential mechanisms contributing to EMT in RPE cells include aging, loss of tight junctions, misfolded protein accumulation and inflammation.

Hyperreflective Foci

Hyperreflective foci (HRF) are well-circumscribed lesions with equal or greater reflectivity than the RPE band that spread over various retinal and choroidal layers in spectral domain optical coherence tomography (SD-OCT) images (28, 29). Numerous clinical studies have shown that retinal HRF appear in optical coherence tomography OCT images in retinal diseases, including age-related macular degeneration (AMD), inherited rod-cone degenerations, and inherited macular degenerations (30-32). HRF in choroid have been reported in Stargardt disease (32) and diabetic macular edema (DME) (28). The cellular origins of HRF were initially hypothesized to be migrated RPE cells, macrophages, or hard exudates. Emerging evidence confirms that a portion of HRF are RPE cells (30, 33). A previous study investigated the origin of HRF by combining polarimetry with auto-fluorescence imaging, enabling differentiation between RPE cells, inflammatory cells, and hard exudates. The Results revealed that, in early stages of AMD, a portion of HRF are

likely secondary to RPE migration (30). Moreover, histopathological studies confirmed that HRF represent cells of RPE origin, substantiating the idea that RPE cells have the capacity to migrate into neuroretina (33) **(Figure 1-4)**.

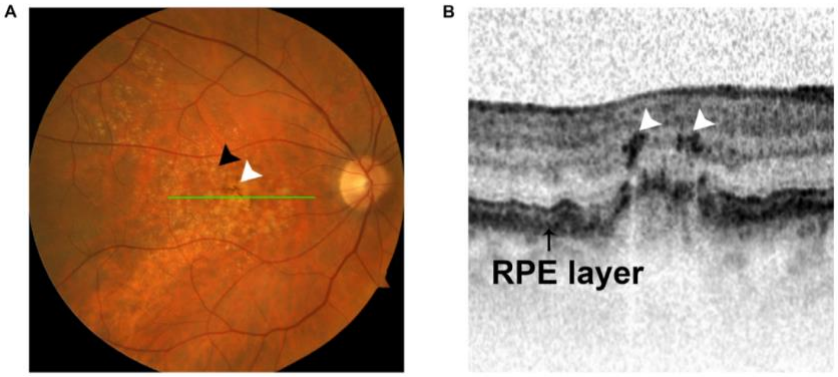

Figure 1-4. Intraretinal hyperreflective foci (HRF) appear in OCT images in intermediate AMD. (A) Fundus photograph showing two hallmarks of intermediate AMD: sub-RPE deposits (black arrow) and pigment changes (white arrow). (B) OCT image demonstrating the presence of intraretinal HRF (white arrows) in intermediate AMD. The HRF correlate with pigment on funduscopic imaging (green line).

In numerous retinal degenerative diseases, HRF were found to correlate with disease stage. In AMD, HRF were found to correlate with pigmentary changes on fundus imaging and were seen with increased frequency in advanced forms of AMD, including geographic atrophy and choroidal neovascularization (CNV) (34). In the latter case, anti-VEGF treatment has been shown to significantly decrease the amount of HRF (35). In addition to AMD, HRF appear to hold clinical significance in inherited retinal degenerations. For example, in Stargardt disease, an inherited macular degeneration caused by a single mutation in the *ABCA4* gene, the appearance of HRF was found to correlate strongly with poor visual acuity, decreased central macular thickness, and increased disease duration (32). In retinitis pigmentosa, HRF were observed more often in the inner nuclear layer in early stages, whereas they were more frequently observed in the outer nuclear layer in later stages, indicating that HRF location correlates with disease stage (31). Thus, HRF may be viewed as a predictive marker for disease progression, and migratory RPE cells can be seen as a sign of poor prognosis.

Evidence of EMT in age-related macular degeneration (AMD)

Clinical evidence

AMD is a leading cause of irreversible vision loss, accounting for 13.4 million cases worldwide (36). The primary pathology of AMD occurs at the level of the RPE cells. As RPE cells become atrophic, the hallmark clinical lesions of AMD ensue; sub-RPE lipoprotein deposits, known as drusen and drusenoid deposits and RPE pigment disruption become visible within the macula. Most AMD begins after the age of 55 as the 'dry' form of macular degeneration. In 10-15% of AMD cases, it progresses to the 'wet' form of the disease, which is defined by CNV. Drusen deposits typically form between the RPE and Bruch's membrane, which can create a mechanical tension that negatively impacts cell-cell contacts. A prior study showed that the volume of drusenoid pigment epithelium detachment (PED) was inversely correlated with visual acuity (37). An increase in drusenoid PED size promotes the disintegration of RPE layer and facilitates RPE migration (37). Likewise, in wet AMD patients, increased area of serous PEDs is strongly associated with RPE layer disruption (38). In CNV, abnormal vessel growth and retinal hole formation directly disrupt cell-cell contact between RPE cells.

The Age-Related Eye Disease Study (AREDS) identified two clinical risk factors for disease progression, namely, drusen burden and the presence of pigment abnormalities (39). Patients with either large drusen or macular pigment are at a 13% and 12.5% risk of developing advanced AMD, respectively. Interestingly, when the drusen burden is large and pigment is present, the risk of progression increases synergistically to 47.3%. However, the molecular mechanisms that drive RPE dysfunction and lead to pigment accumulation in macular degeneration remain to be determined.

As mentioned in the previous section, HRF are observed on OCT in AMD patients and correlate with abnormal pigment on fundus imaging, suggesting that HRF and pigmentary changes represent RPE cells that have migrated into the neuroretina (34, 40). This concept is substantiated by studies demonstrating EMT of RPE cells in AMD. Upregulated expression of the EMT transcriptional markers vimentin and Snail1 and

downregulated expression of E-cadherin in RPE cells were found in post-mortem human dry AMD eyes relative to age-matched controls, suggesting that RPE cells in dry AMD patients had undergone EMT (26). Snail is co-localized with RPE65-positive cells in 11 human CNV eyes (41). Additionally, Snail- and α-SMA-double-positive RPE cells were strongly associated with RPE fibrotic changes, indicating that RPE cells undergo epithelial-myofibroblast transition and that this transition leads to retinal fibrosis, an end-stage manifestation of wet AMD (42, 43) (**Figure 1-5A**).

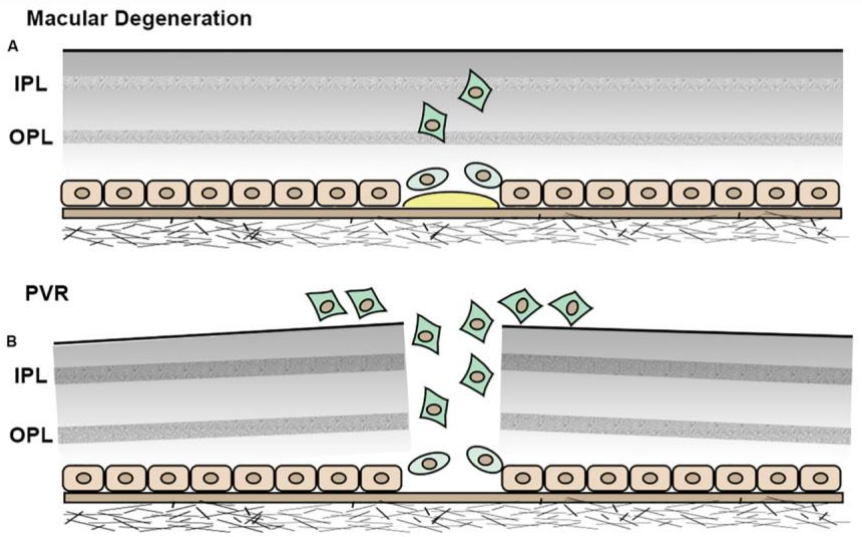

Figure 1-5. Schematic illustration of EMT in RPE cells. (A) In macular degeneration, RPE cells become less differentiated, undergo EMT and migrate into neuroretina. (B) In PVR, RPE cells undergo EMT and migrate into the epiretinal area.

Here, we hypothesize that pigment abnormalities represent RPE cells that have undergone EMT and migrated into the neuroretina. A contradiction to this hypothesis is that RPE cells should, in theory, become less pigmented with EMT; therefore, would not result in a pigmented macula. However, it is possible that migrating RPE cells become less differentiated, but remain pigmented to, perhaps, a lesser degree. It is also possible that macular hyperpigmentation results from a cluster of RPE cells that have migrated to this area in order to make up for the reduction in pigmentation. Another possibility is that migrating RPE cells undergo MET in the neuroretina and become more pigmented. Further

studies should focus on the molecular mechanisms that drive RPE dysfunction and lead to pigment accumulation in macular degeneration.

Preclinical evidence

Published studies using animal models of AMD have shown that proteins, such as PCG-1-alpha, MRTF-A and PTEN, are involved in the EMT of RPE cells, as inhibiting their activity attenuated the severity of disease progression (44-46). Interestingly alpha-beta-crystallin, a protein linked to AMD pathophysiology, was found to modulate EMT through SNAIL and SLUG. They showed that suppressing alpha-beta-crystallin Results in the inhibition of EMT development in RPE cells (47).

Evidence of EMT in proliferative vitreoretinopathy (PVR)

Clinical evidence

PVR is a scarring process that occurs following the treatment of rhegmatogenous retinal detachment. The incidence of post-operative PVR is estimated to be 5%-10% (48, 49). PVR is initiated by a retinal break, which is followed by persistent inflammation and wound healing. RPE cells are believed to contribute to the healing process by undergoing EMT and migrating to the epiretinal area (50-52). The resultant formation and contraction of PVR membranes ultimately lead to retinal folds and loss of vision (**Figure 1-5B**).

Several studies have shown that cytokeratin, an RPE cell marker, co-localized with vimentin in PVR membranes (50-52). Additionally, in human PVR membranes, cells positive for cytokeratin were co-expressed with α-SMA (53). By counting the cells positive for both cytokeratin and α-SMA, the study showed that the majority of myofibroblasts in human PVR membranes originated from RPE cells, suggesting that RPE cells are capable of undergoing EMT and migrating into neuroretina, and that this process plays a major role in the pathogenesis of PVR.

Preclinical evidence

A number of PVR animal studies have shown that RPE cells undergo EMT when PVR is induced (54-57). Following retinal detachment, one study found that RPE cells would stain positive for alpha-SMA in wild-type mice, but RPE cells in Smad3-null mice would be negative, indicating that EMT is attenuated when Smad3 is absent (54). The same investigation also found that Smad3-null mice had decreased residual subretinal fibrosis. Additionally, PVR in mice induced by dispase injection, has been shown to increase retinal alpha-SMA-positive cells (55). Together, these *in vivo* studies suggest that RPE cells undergo EMT following PVR, whereby suppressing the EMT process can greatly reduce the severity of PVR.

Evidence of EMT in inherited retinal degenerations (IRDs)

Clinical evidence

A subtype of Best disease, autosomal dominant vitreoretinochoroidopathy (ADVIRC) is a chorioretinal degeneration caused by a mutation in the Bestrophin-1 (*BEST1*) gene, and evidence suggests that EMT of RPE cells plays a role in its pathogenesis. In a study of ADVIRC post-mortem human eyes, Morton et al. demonstrated minimal expression of TGF-β within the RPE cell monolayer. In contrast, RPE cells that had migrated into the neuroretina have been characterized as having downregulated RPE-65 and upregulated expression of TGF-β, suggesting that RPE cells become dedifferentiated once they start to migrate (58). In inherited retinitis pigmentosa, proliferative and displaced RPE cells have been observed in regions up to the internal limiting membrane in several patient samples (59-62). One study showed that RPE cells in a spared region of retina had apically displaced nuclei (loss of polarization) and abundant melanolysosomes, whereas RPE cells in areas of more severe disease were flattened and depigmented (60). In photic maculopathy, transmission electronic microscopy (TEM) indicated that RPE cells were displaced and proliferative with depigmentation, loss of infoldings, and irregular shape (63). Another study demonstrated RPE cell proliferation in retinal detachment and found that new cells did not display typical RPE cell polarity (64).

In choroideremia and chorioretinal atrophies, regions of proliferating and attenuated RPE cells were observed, with abrupt transitions in between them (65-67).

Mechanisms of EMT in RPE cells

Overview

The molecular mechanisms that drive RPE dysfunction and lead to retinal degeneration remain to be determined. Emerging evidence suggests that the impairment of tight junctions and accumulation of misfolded proteins drive EMT in RPE cells. Moreover, upregulations of TGF-β and Wnt pathway have been implicated to play a critical role in RPE de-differentiation and promoting EMT. In contrast, Nicotinamide and microRNA 204/211 have been shown to enhance RPE phenotype and prevent EMT in multiple RPE cell model systems. Extracellular vesicles that have been shown to regulate EMT in numerous other tissues are also discussed in the following sections.

Roles of junctional proteins in EMT

Cell-cell contact is critical for maintaining epithelial phenotype. The RPE acts as part of the outer blood-retina barrier by way of tight junctions (TJs) and adherens junctions (AJs) between neighboring RPE cells (68). At a molecular level, the major proteins that constitute TJs in RPE cells are occludin and claudins, while cadherins serve as the major AJ proteins (69, 70). The extracellular domains of these molecules form an intact blood-retinal barrier that results in a high transepithelial resistance.

A prior study showed that RPE cells in the center of cultured sheets maintained a well-differentiated phenotype with proper expression of RPE signature genes and pigment, whereas RPE cells at the edges of the sheet lost epithelial morphology and were less pigmented (71). Moreover, this study showed upregulated expression of vimentin and N-cadherin in RPE cells at the edges, suggesting that loss of cell-cell contact leads to RPE cell de-differentiation and facilitates EMT of RPE cells. In C57/Bl6 mice, utilizing shRNA to target and disrupt junctional proteins, like ZO-1 induce RPE cell proliferation and hyperpigmentation of the retina (72). The RPE cells were found to be undergoing EMT,

whereby the absence of ZO-1 induced the expression of key EMT markers and reduced the expression of epithelial markers in the affected RPE cells (72). This data shows that the loss of the tight junction protein causes RPE cell dedifferentiation and induces EMT.

The mechanism by which TJs and AJs maintain an epithelial phenotype involves sequestration of EMT signals within their complexes. The junctional protein ZO-1 binds to ZO-1–associated Y-box factor (ZONAB), a transcription factor that is able to upregulate cell proliferation rate by regulating nuclear expression of cyclin-dependent kinase 4 (CDK4) (73, 74). Loss of ZO-1 Results in a release of ZONAB into the cytoplasm, enabling a subsequent translocation of ZONAB (70). ZONAB then binds to the transcriptional factor for CDK4, increasing expression of CDK4 and promoting cell proliferation. Similarly, E-cadherin sequesters β-catenin on the cell membrane, and downregulation of E-cadherin leads to a release of β-catenin into the cytoplasm. β-catenin subsequently translocate into the nucleus and activates promoters of EMT and proliferation, including Snail and Cyclin D1 (75) (**Figure 1-6A**). The Hippo-YAP pathway, an important regulator of RPE cell differentiation, depends strongly on cell junction complexes. TJ and AJ complexes inhibit YAP/TAZ translocation (two effectors of the Hippo pathway) into the nucleus. Loss of TJs or AJs enables activation of YAP/TAZ. Activated YAP/TAZ bind to TEAD and upregulate ZEB1, promoting EMT (76). A previous study showed that knockdown of YAP in primary mouse RPE cells downregulated MITF expression and upregulated ZEB1 expression, indicating that loss of YAP attenuates RPE differentiation and induces RPE cells to undergo EMT (77). Thus, RPE cell-cell junctions are critical regulators of EMT.

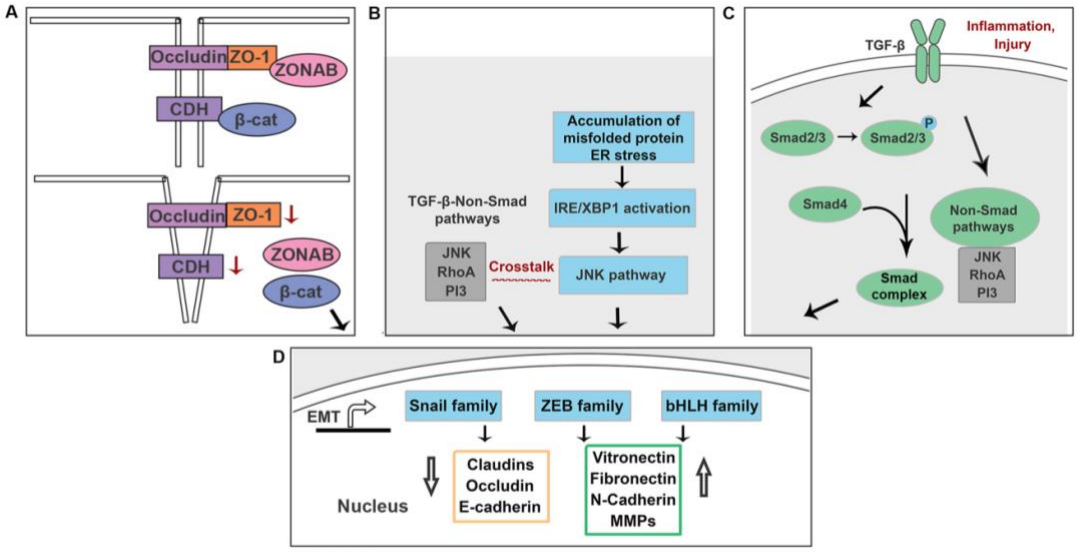

Figure 1-6. Schematic illustration of the potential mechanisms underlying EMT in RPE cells. (A) Loss of ZO-1 and E-cadherin lead to a release of ZONAB and β-catenin. (B) Accumulation of misfolded proteins activate NK/p38-MAPK pathway that crosstalks with TGF-β-induced non-Smad pathways in an IRE-dependent manner. (C) Increased production of TGF-β is associated with inflammation and injury in RPE cells. (D) Above signals promote EMT by upregulating EMT drivers including Snail, Zeb and bHLH family.

Roles of misfolded proteins in EMT

Emerging evidence suggests that the unfolded protein response (UPR) and EMT signaling interact in several different organs (78-81) (**Figure 1-6B**). Mutations in *BEST1* cause its mislocation and results in retinitis pigmentosa and other retinal dystrophies (82, 83). Recessive mutations in *BEST1* activate the UPR with upregulated expression of XBP1. In ADVIRC patient, a chorioretinal degeneration caused by a mutation in the *BEST1* gene, RPE cells that had migrated into the neuroretina have been characterized as having downregulated RPE-65 and upregulated expression of TGF-β (58). A previous study showed that accumulation of intracellular amyloid-β attenuates TJs of RPE cells by down-regulating occludin and claudin-1 proteins, supporting the idea that accumulation of abnormal proteins in RPE cells attenuates RPE differentiation (84). Crystallin is a protein expressed in the eye and is classified into three types: α, β, and γ-crystallins. βA3/A1-crystallin localizes to the lysosome and plays a critical role in the clearance functions of lysosomes, including phagocytosis and autophagy (85). A prior study demonstrated that the expression level of βA3/A1-Crystallin in polarized primary human RPE cells is 23.75-

fold higher than that of non-polarized primary human RPE cells (26). Moreover, knockdown of βA3/A1-Crystallin in human and murine RPE cells results in upregulated expression of Snail and vimentin and an enhanced migration ability (26). This evidence suggests a connection between the protein misfolding and EMT in RPE cells. Doyne honeycomb macular dystrophy (DHC) results from an R345W mutation in Fibulin-3 (86, 87), an extracellular matrix protein and downstream target of HTRA1 (88). The R345W mutation causes Fibulin-3 misfolding, poor Fibulin-3 secretion, and activation of the UPR (89, 90). In our lab, we found that overexpression of R345W-Fibulin-3 in primary human RPE cells activates the UPR via the IRE1α/XBP1 pathway, attenuates RPE differentiation and facilitates EMT in RPE cells (91). Taken together, these data suggest that the accumulation of misfolded proteins in RPE cells contributes significantly to EMT and likely accelerates the disease process in patients who have inherited macular degenerations.

UPR activation involves several mechanisms aimed at reducing the load of aberrant protein accumulation, including attenuated protein translation to avoid worsening the accumulation, increased transcription of endoplasmic reticulum (ER) chaperones to aid in the folding process, and an increase in ER-associated degradation (ERAD). Three ER transmembrane sensors, IRE1α/XBP1, PERK, and ATF6, regulate the UPR and determine the appropriate adaptive response, directing the cell to proliferate, change shape, or undergo apoptosis (92, 93). Several studies have shown that the UPR and TGF-β-induced EMT signaling pathways interact at the level of c-Jun N-terminal kinase and p38 mitogen-activated protein kinase (JNK/p38-MAPK) in an IRE1-dependent manner (94-96). The activation of IRE1α/XBP1 signaling promotes EMT by upregulating JNK and EMT drivers, including Snail and Zeb family members, in different organs and tissues, including the breast, lung, and liver (96-99).

Key pathways and molecules

TGF-β pathway

TGF-β acts as an anti-inflammatory cytokine; increased production of TGF-β is associated with injury and inflammation. TGF-β signaling induces EMT by activating

either Smad or non-Smad pathways (100). In the Smad-dependent pathway, phosphorylation of TGF-β receptor (Type I and Type II) recruits Smad2 and Smad3 (101). The phosphorylation of Smad2 and Smad3, then recruits Smad4 and facilitates the formation of the Smad-complex. The Smad-complex translocates into the nucleus and binds regulatory elements that in turn induce the transcription of several key genes associated with EMT (75). In the Smad-independent pathway, TGF-β cross-talks with the JNK/p38-MAPK pathway to regulate EMT in an IRE1α-dependent manner (102, 103) (**Figure 1-6C**).

Previous studies have shown that the amount of TGF-β in the vitreous from eyes with PVR is three times higher than that of eyes without intraocular fibrosis (104, 105). Subconfluent culturing of primary human RPE cells, which mimics a wound stimulus, has been shown to result in acquisition of a mesenchymal phenotype by activating the TGF-β pathway (106). Treatment with TGF-β and TNF-α has been found to accelerate EMT in adult human RPE stem cell –derived RPE cell cultures (107). Blockage of TGF-β and FGF/MAPK pathways has been shown to markedly promote RPE differentiation efficiency during the induced pluripotent stem cell (hiPSC)-derived RPE cell culture (108).

Most of the *in vivo* investigations of EMT mechanisms in RPE cells involve genetic (54, 109) or pharmacological (55, 56, 110) manipulation of the TGF-β pathway. Ishikawa et al. (2015) used a PVR rabbit model to pharmacologically inhibit transforming growth factor-β2(TGF-β2)-induced EMT of RPE cells using Resveratrol, a compound that deacetylates SMAD4 (110). To determine the effect of notch inhibition on TGF-β1-induced EMT, Zhang and colleagues (2017) injected ARPE-19 cells that had been pre-incubated with a γ-secretase Notch inhibitor (LY411575) in a PVR mouse model, and found EMT was attenuated when Notch signaling was inhibited (56). In a PVR *in vivo* rat model, miR-194 decreased the ZEB1 protein. ZEB1 can synergize with SMAD and lead to TGF-β-dependent gene transcription, therefore suppression of this process repressed EMT in RPE cells (111). The absence of Galactin-1, a galactoside-binding lectin family protein which modifies the TGF-β pathway as well as others, in a knockout mouse following CNV resulted in reduced CNV severity, level of subretinal fibrosis and expression of EMT-

related markers in RPE cells (109). Taken together, these results show the importance of the different components of the TGF-β pathway in the RPE-EMT process.

Wnt pathway

Wnt-β-catenin is another well-characterized pathway that mediates EMT in the eye. A previous study showed that, in mouse eyes, laser photocoagulation activated the Wnt/β-catenin pathway and facilitated RPE proliferation and EMT (112). In ARPE-19 cells, EMT was promoted by the overexpression of β-Catenin and was blocked by a Wnt Inhibitor (XAV939) (113). Light exposure has also been shown to induce EMT in RPE cells by activating the Wnt/β-catenin pathway (114).

β-catenin is a key element in the Wnt signaling pathway. Without the activation of Wnt signaling, β-catenin is sequestered by a complex of glycogen synthase kinase-3 beta (GSK-3β) and axin. Activation of Wnt signaling leads to a release of β-catenin from the complex, enabling the subsequent translocation of β-catenin. Nuclear β-catenin then binds to the transcriptional factors for Snails, leading to increased expression levels of Snail and promotion of EMT.

Extracellular vesicles and EMT

Extracellular vesicles (EVs) play a critical role in cell-cell communication, modulate cellular differentiation, and promote aggregate formation (115, 116). EVs can originate from either multivesicular bodies (MVBs) or from the plasma membrane. Prior studies have shown that alterations in EV cargo are representative of the phenotypic status of their parental cells (117, 118). EVs contribute to the regulation of EMT and promote cancer metastasis in numerous tissues, including the lungs, breasts, liver and brain (117-120). EVs derived from $p85\alpha^{-/-}$ fibroblasts that possess greater mesenchymal features promoted breast cancer cells migration and invasion compared with EVs from WT fibroblasts (119). Myofibroblast-derived EVs are sufficient to induce normal fibroblasts to become myofibroblasts that possess greater mesenchymal features, by upregulating TGF-β pathways and EMT drivers (120). Although the specific role of EVs in mediating RPE

cell EMT remains to be determined, they appear to be involved in numerous mechanisms relating to EMT in RPE cells. In the following section, EV secretion mechanisms, EV as biomarkers, and methods for EV isolation and characterization were summarized.

EV secretion

Extracellular vesicles are released from nearly all cell types under both physiological and pathological conditions (121). EVs are found in numerous types of body fluid, including blood, urine, cerebrospinal fluid (CSF), vitreous, ascites, and breast milk (122-127). The mechanisms of EV formation are debated. A common theory is that EVs form through an endosomal sorting complex required for transport (ESCRT)-dependent pathway (128). Another theory of MVB formation and EV biogenesis is the ceramide-dependent pathway (129). Ceramide, a lipid, is thought to facilitate invagination of the MVB membrane. Rab27, a member of the Rab family of small GTPases, has also been shown to control the EV secretion pathway, specifically functioning in MVB docking at the plasma membrane (130, 131) (**Fig. 1-7**). Due to their heterogeneity, it is critical to select an appropriate method for isolation and detection of these small vesicles.

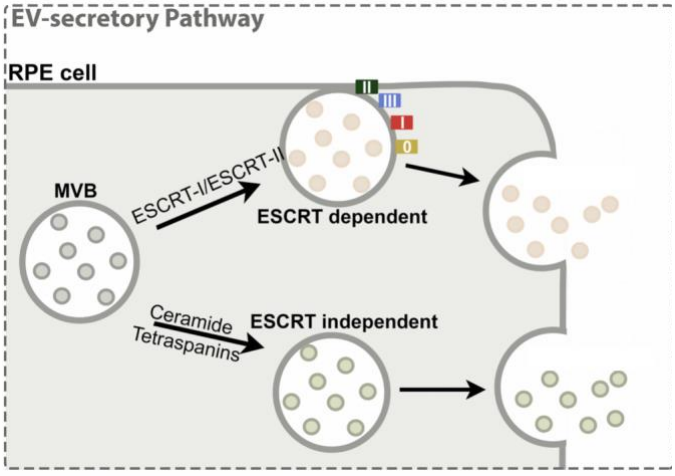

Figure 1-7. EV secretion pathways. EVs are secreted via the ESCRT-dependent pathway or the ESCRT-independent pathway.

Methods for Extracellular Vesicle Isolation

To advance EV research in both basic science and clinical contexts, proper preparation and characterization techniques are critical. Current techniques for EV isolation and characterization and address their experimental limitations were reivewed. The discussion of isolation techniques includes differential centrifugation, ultrafiltration, density gradient centrifugation, precipitation, and immunoaffinity capture-based isolation. For EV characterization, we discuss common methods for EV visualization with a focus on transmission electron microscopy techniques (TEM). The discussion also includes several techniques for EV quantification, including nanoparticle tracking analysis (NTA), asymmetric flow field-flow fractionation (AF4), and resistance pulse sensing (RPS). We address flow cytometry and the ExoView^{TM} (NanoView Biosciences, Boston, MA) platform as tools for EV surface marker detection and subset characterization. Lastly, we discuss methods for tracking EVs and defining EV cargo, including proteomic and microRNA sequencing techniques.

Differential Centrifugation

Differential centrifugation was initially developed to isolate EVs from reticulocytes and is currently the most commonly used method for EV isolation (132). The basis of this method is the removal of cells, cell debris, and large vesicles by successive centrifugation steps. Briefly, experimental samples are centrifuged at 300, 2,000, and 10,000 x g to remove cells, dead cells, and cell debris, respectively. EVs are obtained by centrifugation at 100,000 x g. This method is suitable for experiments involving a large volume of the initial sample, as quite a substantial number of vesicles are lost during the process. According to a study from Kowal et al., 70% of the EV fraction obtained by this method consists of vesicles 50-150 nm in diameter, with the remaining vesicles having diameters of > 150 nm (20%) or < 50 nm (10%) (133).

Filtration and Ultracentrifugation

Filtration is another common method for EV isolation. The principle behind this method is that the use of membranous filters enables separation of EVs from other sample components based on their molecular weights and sizes. This method has two main steps: 1) separation of EVs from larger particles, such as cells, cell debris, and microparticles, using membrane filters with pore diameters of 0.1-0.22 µm and 2) separation of EVs from smaller particles, such as soluble proteins and protein aggregates, using filters with a molecular weight cut-off of 3-100 kDa. Several commercial membranous filters have been developed, such as the Corning Disposable Bottle-Top Filter with a 500 mL volume and a pore size of 0.22 µm and the Amicon Centrifugal Filter Ultra for proteins ranging from 3-100 kDa. If additional volume reduction is needed, samples containing EVs can be centrifuged at 100,000-200,000 x g to pellet EVs (**Figure 1-8A**).

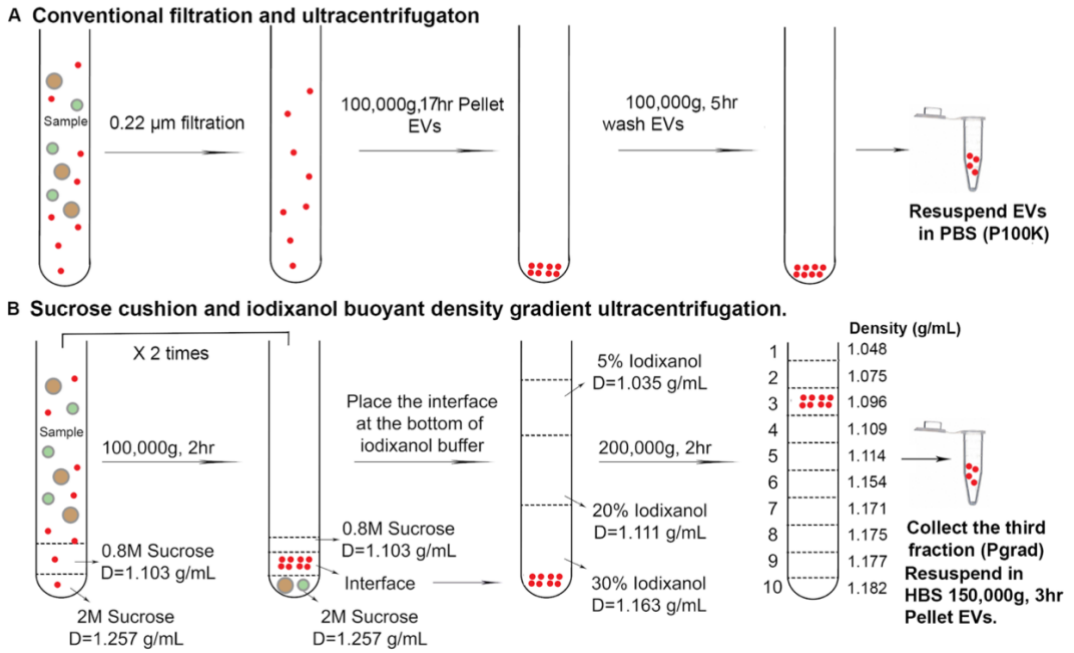

Figure 1-8. Methods for EV Purification. (A) Conventional filtration and ultracentrifugation were used to isolate EVs for Western blot and other studies. (B) Sucrose cushion and iodixanol buoyant gradient ultracentrifugation was used to isolate EVs for proteomics studies.

Density Gradient Centrifugation

Density gradient centrifugation takes advantage of differences in vesicle sizes and mass densities to isolate EVs via creation of a discontinuous density gradient. During the centrifugation step, the particles travel through the gradient until they reach the point at which their density matches that of the surrounding solution. Sucrose and iodixanol are two common media used to create the gradient. Iodixanol is more stable and less viscous relative to sucrose (134). There are two ways to load the samples: top-loading and bottom-loading. Bottom-loading has an advantage over top loading as soluble proteins will remain at the bottom during ultracentrifugation, whereas soluble proteins will sediment through the gradient if the sample is top-loaded.

Greening et al. reported a density-based separation method using iodixanol from OptiPrep (MilliporeSigma, US) that uses sample top-loading (135). In this method, the experimental sample is first ultracentrifuged at 100,000 x g for 2 hours. Crude EV pellets are then resuspended in phosphate-buffered saline (PBS) and top-loaded into an iodixanol gradient buffer. After ultracentrifugation at 100,000 x g for 18 hours, 12 fractions remain in the tube, with EVs in the seventh fraction from the top. The 12 fractions are then collected and subjected to downstream analyses.

In contrast, Choi et al. reported a method for EV isolation and downstream proteomic profiling using sample bottom-loading instead (136). In this method, experimental samples are added to the 0.8 M and 2 M sucrose cushions, and ultracentrifugation is conducted. After repeating this process twice, EVs can be found at the interface between two sucrose cushion buffer layers. The interface solution is collected and placed at the bottom of an iodixanol gradient buffer. An additional ultracentrifugation yields 10 remaining fractions, with EVs in the third fraction from the top. The 10 fractions are then collected and can be subjected to downstream analyses (**Figure 1-8B**).

Precipitation

EV precipitation is a faster and more efficient method for EV isolation relative to the those described above. The objective of this method is to capture EVs by incubating

them with polymers, which allows EVs to be obtained at low speeds of centrifugation in combination with polymers. The most commonly used polymer for this purpose is polyethylene glycol (PEG). ExoQuick™ EV Precipitation Solution (System Biosciences, Palo Alto, CA) and Invitrogen™ Total EV Isolation Reagent (Thermo Fisher Scientific, Waltham, MA) are two popular commercial products for EV precipitation. According to the ExoQuick user manual, experimental samples are pre-cleared to remove cells and cellular debris. The cleared solution is then incubated with an appropriate volume of ExoQuick for 0.5-12 hours, depending on sample type. Lastly, EVs are collected by centrifugation at 1,500 × g for 30 minutes.

Immunoaffinity Capture-Based Isolation

Neither ultracentrifugation nor precipitation allows enrichment for EV subtypes. To date, immunoaffinity capture remains the only method for isolation of EV subgroups. By coating magnetic beads with specific antibodies, EVs with those surface antigens are able to be captured. CD9, CD63, and CD81 are the most common markers and are expressed on nearly all EVs (137). Additional markers may be used to isolate EVs derived from a specific cell type. For example, chondroitin sulfate peptidoglycan 4 antibody-coated beads have been used to capture melanoma cell-derived EVs (138). while magnetic beads coated with CD56 or CD171 antibodies have been used to capture neuronal cell-derived EVs (139, 140).

Summary of Methods for Extracellular vesicles Isolation

Selection of the proper EV isolation method is usually dependent on the volume and origin of samples, as well as the goals of downstream analyses. The most relevant characteristics to consider in selecting the best EV isolation method for a particular study are: 1) the EV recovery rate or yield of the method, 2) the purity of the obtained EV sample, and 3) the efficiency of the method in terms of time and labor. In the following section, we focus on these characteristics in the context of the methods described above.

Recovery Rate

Several studies have shown that PEG-based precipitation has the highest recovery rate compared to other methods, at around 80-90% (141-143). Differential centrifugation and ultrafiltration have a relatively low-to-medium yield. Multiple studies have shown that differential centrifugation has a recovery rate of only 20-40% due to loss of a large fraction of EVs during the process (142, 144, 145). Ultrafiltration has a higher recovery rate relative to differential centrifugation, at around 60% (144). Both differential centrifugation and ultrafiltration are commonly used in experiments, and selection of these two methods tends to be based on individual laboratory habits. Density gradient ultracentrifugation has the lowest EV recovery rate at around only 10% (141). As PEG-based precipitation has the highest EV recovery rate, this method is commonly used in experiments with a small starting sample volume, such as those involving clinical biofluid samples (e.g. plasma, urine, amniotic fluid, vitreous, and CSF). Differential centrifugation and ultrafiltration are usually used for isolation of EVs from cell culture media, as these studies tend to involve a large starting sample volume.

Purity

Density gradient ultracentrifugation is currently considered the gold-standard method for achieving the highest-purity EV samples, as they remove non-specifically bound proteins from vesicles (**Figure 1-9**) (141). As such, density gradient ultracentrifugation is commonly used to isolate EVs for EV proteomics and RNA sequencing studies (136). Although differential centrifugation and ultrafiltration can obtain relatively high sample purities, EV aggregates are a major artifact in these methods. As such, vigorous re-suspending of EV pellets is recommended. PEG-based precipitation tends to yield the lowest-purity EV samples. **Figure 1-10** shows EVs isolated from human vitreous using ExoQuick under TEM. It is difficult to separate EVs from associated polymers. As protein contaminants may skew experimental results, data interpretation in downstream studies should be performed with caution.

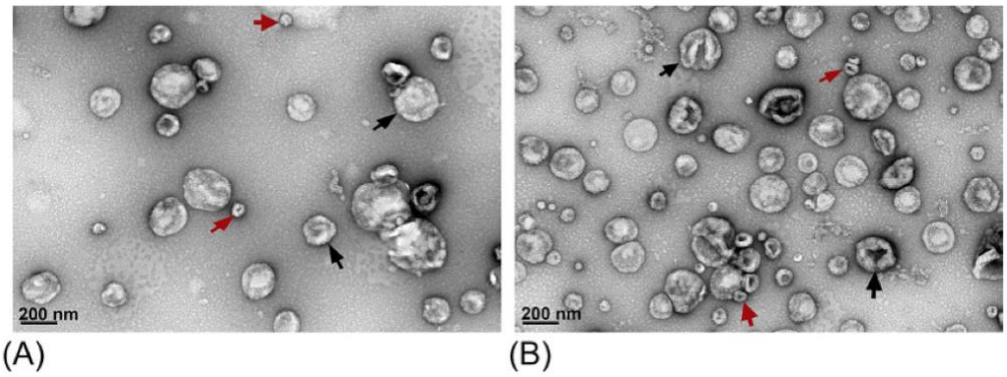

Figure 1-9. TEM showed two subpopulations of EVs, small vesicles (red arrows) and large vesicles (black arrows), isolated from (A) retinal pigment epithelial cells expressing wild-type fibulin-3 and (B) retinal pigment epithelial cells expressing R345W-fibulin-3, using sucrose cushion and iodixanol buoyant density gradient ultracentrifugation.

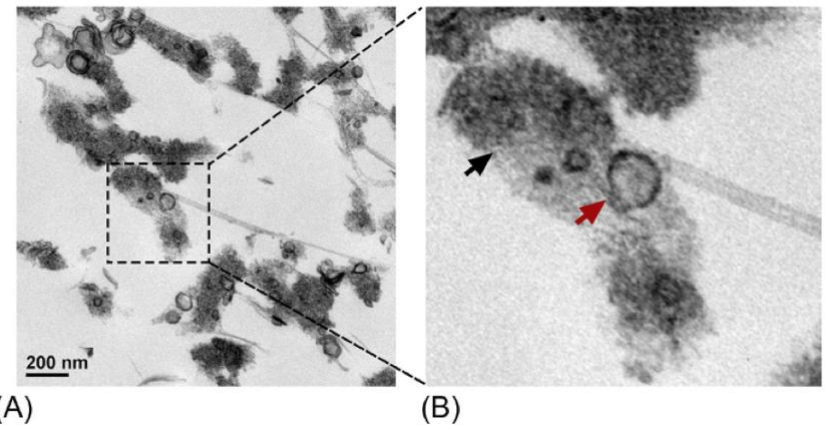

Figure 1-10. TEM of EVs isolated from human vitreous using ExoQuick. (A) TEM image of EVs isolated from human vitreous using ExoQuick. (B) Magnification of the indicated area shows that vesicles (red arrow) attach to the polymer (black arrow).

Time and Labor Cost

Of these methods, density gradient centrifugation requires the most time and labor, involving 2-3 days for completion of the process in its entirety. Although differential centrifugation requires more time than ultrafiltration, membrane filters and other ultrafiltration equipment cost more than the supplies required for differential

centrifugation, provided basic laboratory equipment has already been obtained. PEG-based precipitation is the least costly of these methods in terms of both labor and time.

Methods for Extracellular Vesicle Characterization

Ultrastructural Analysis

TEM

Due to the small sizes of EVs and the ease of sample preparation, TEM is the gold-standard method to study EV morphology. The resolution for TEM is about 1 nm, and the procedure of negative staining is simple and rapid, lasting only 2-3 hours. Briefly, EVs are fixed in 2% paraformaldehyde, deposited on Formvar carbon-coated TEM grids, and incubated for 20 minutes. The grids are then washed with PBS, incubated with glutaraldehyde, and washed with water. The vesicles are then stained with uranyl acetate solution and air dried (146). Regular TEM can be used to: 1) validate the existence of EVs in the solution, 2) assess the quality of EVs, and 3) study the morphology of EVs. TEM is rarely used for EV quantification due to limited reproducibility and inefficiency. Immuno-EM has been used to investigate EV surface markers and involves incubating EVs with primary antibodies and secondary antibodies attached to 5-40 nm gold particles.

Scanning Electron Microscopy (SEM)

Rather than using a broad beam as in TEM, SEM uses a fine point beam that scans samples line by line. As such, rather than the two-dimensional image generated by TEM, SEM focuses on the surface of samples to provide a three-dimensional image of EVs. Briefly, EVs are fixed with glutaraldehyde and dehydrated with an ascending sequence of ethanol. After samples are air dried at room temperature, EVs are ready for SEM analysis (147). Unlike the cup-shaped morphology observed under TEM, SEM showed round, bulging EVs without a central depression (148).

Cryogenic Electron Microscopy (Cryo-EM)

Cryo-EM is a type of TEM. In contrast to air drying samples as is done for TEM and SEM, cryo-EM allows samples to remain in their native aqueous environments. For cryo-EM analysis, suspended EVs are placed on a grid, which is then rapidly immersed in liquid ethane to allow vitrification of the sample. After samples are vitrified, they can then be analyzed under cryo-EM or transferred in liquid nitrogen for storage (149). Under cryo-EM, EVs have a clear bilayer structure and are sometimes surrounded by smaller vesicles (150).

Atomic Force Microscopy (AFM)

AFM has a high resolution of approximately 1 nm and is suitable for EV topography studies. multiple CD63 receptor sites on EVs were identified using AFM immunogold imaging (151). Briefly, the EV suspension is placed on a mica substrate and allowed to air dry at room temperature. Samples are then washed with ultrapure water and dried with nitrogen gas. Samples are viewed using AFM with silicon probes and analyzed with AFM software (**Figure 1-11**) (125).

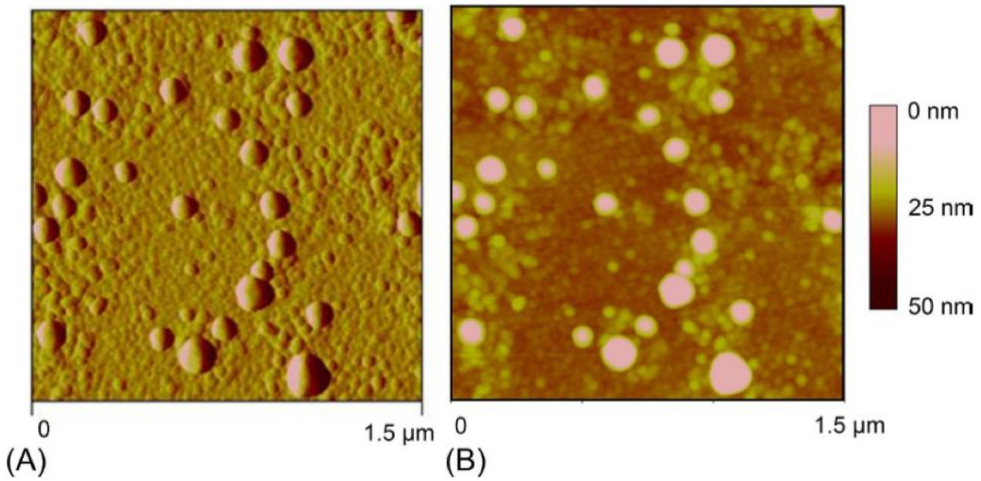

Figure 1-11. AFM of EVs. (A) AFM image and (B) AFM height image of EVs in human vitreous.

EV quantification

Nanopartical Tracking Analysis (NTA)

NTA is a sophisticated method for the measurement of EV concentration and size distribution. Compared to flow cytometry and TEM, NTA has better reproducibility. NTA has high resolution and is able to detect vesicles with diameters of 30-1000 nm. This technique takes advantage of dynamic light scattering and the Stokes-Einstein equation to quantify particle size and concentration. According to the NanoSight NS300 (Malvern Panalytical, Malvern, UK) user manual, under the scattered setting, each sample is loaded by syringe pump into the machine and five 60-second videos are generated. The entire process of sample measurement takes about 15 minutes. **Figure 1-12** shows NTA readouts of EVs derived from ARPE-19 cells, a human retinal pigment epithelial cell line, isolated using filtration and ultracentrifugation.

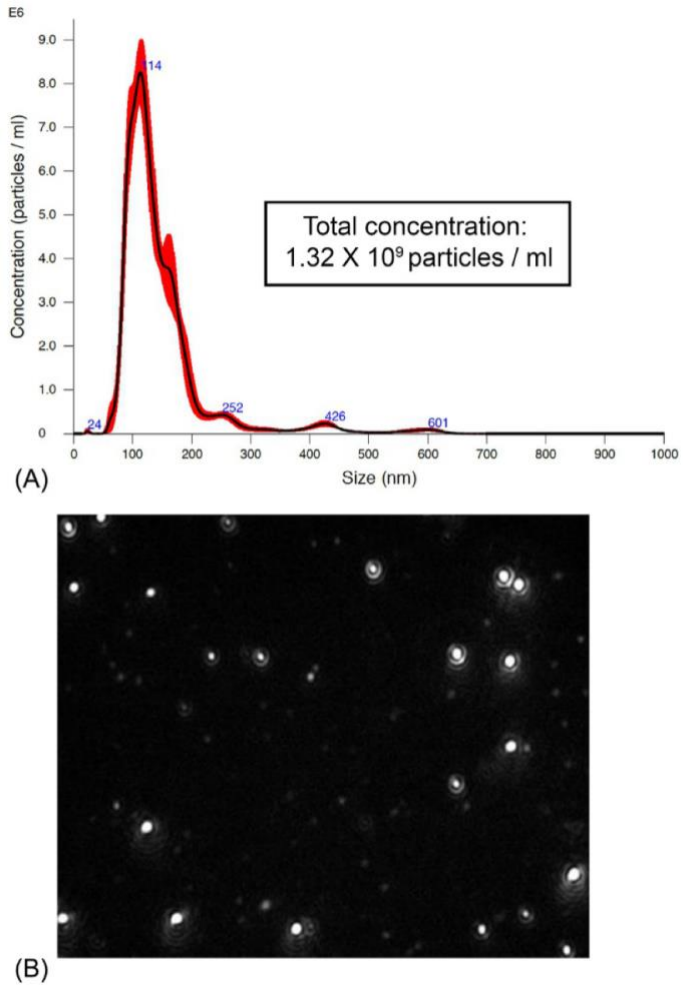

Figure 1-12. Representative NTA distribution profiles of EVs derived from ARPE-19 cells, including (A) a size distribution plot and (B) a screen shot of the corresponding video.

Asymmetric-flow field-flow fractionation (AF4)

AF4 is one of the few methods that is able to separate distinct subsets of extracellular vesicles. In this technique, EVs are separated based on their density and hydrodynamic properties. EVs flow through a forward laminar channel and, based on their Brownian motion, are sorted into different populations. Smaller particles have higher diffusion rates and tend to move faster; in contrast, larger particles have lower diffusion

rates and tend to move more slowly. Currently, there are two major companies that produce AF4 systems: Wyatt Technology and Postnova. Several studies have compared AF4 and NTA for EV quantification. In contrast to NTA, which in prior studies resolved only a single, broad peak from 50 to 150 nm, AF4 was able to distinguish two separate EV subpopulations, large EVs with sizes between 90-150 nm and small EVs with sizes around 30 nm (152-154). Therefore, AF4 is better able to address the size heterogeneity of EV samples and can be considered an advanced analytical technique for EV subset characterization.

Resistive Pulse Sensing (RPS)

RPS measures the size of vesicles based on their electrical resistance when they pass through a small orifice. RPS is able to detect vesicles with diameters of 50-1000 nm. Spectradyne, LLC is a leading company in the microfluidic measurement of nanoparticles. Compared to dynamic light scattering and NTA, RPS has both higher size resolution and better accuracy in measuring particle size distribution. Relative to NTA, EV concentrations obtained by RPS are closer to the count obtained from TEM. Grabarek et al. reported that EVs measured by NTA showed 5- to 10-fold higher concentration than RPS, as it failed to distinguish EVs from protein aggregates, liposomes, and bacteria (155).

Flow Cytometry

As EVs fall below the resolution limit of standard flow cytometers, which is between 300 and 500 nm, EVs cannot be detected directly by this method. Several studies have reported methods to semi-quantitatively measure EV subgroups by detecting specific membrane markers on their surface (156, 157). Briefly, EVs are attached to aldehyde/sulfate-latex beads via a 15-minute incubation with continuous rotation. The reaction is stopped by adding glycine and bovine serum albumin (BSA) solution. EV-bound beads are washed with PBS and blocked with BSA. Primary antibodies and fluorescence-labeled secondary antibodies are added in sequence for specific membrane marker detection. A negative control is obtained by incubating the EV-bound beads with

an isotype control followed by a secondary antibody, or in the absence of primary antibody. Using this method, Melo et al. found that EVs derived from pancreatic cancer cells carry more glypican-1 compared to EVs derived from non-tumorigenic cells (157).

ExoView^{TM} Characterization Platform

Recently, antibody-based EV arrays have been developed by NanoView Biosciences. This method enables fractionation of EV subpopulations with a very small sample volume. Briefly, antibodies against EV surface markers are arrayed on silicon chips. EV suspensions or biofluids containing EVs are incubated with the chips overnight. After incubation, chips are washed with PBS on a shaker and air dried. Captured EVs are detected using Single Particle Interferometric Reflectance Imaging Sensor technology. This technique allows enhanced contrast in the signal from particles. Daaboul et al. has used this method to successfully detect CD63-, CD8-, and CD9-positive EVs derived from a human embryonic kidney cell line, and CD171-positive EVs from human cerebrospinal fluid (158). Compared to flow cytometry, this method requires a smaller sample volume and is less time-consuming.

In vivo Extracellular vesicles Tracking

It is believed that EVs mediate intercellular communication in part by transporting their microRNA cargo from cell to cell. However, the details of how EVs carry out this function remain largely unknown. Two methods currently exist for analyzing the fate of Evs after leaving their parental cells. These EV labeling and tracking methods include: 1) staining EVs with lipophilic carbocyanine dyes, including PKH67 (green) and PKH26 (red) (Millipore Sigma, US); and 2) expressing EV markers, for example CD63, with green fluorescent protein (GFP) or mCherry in cells (159). To study the mechanisms by which EVs are endocytosed, confocal microscopy allows observation of the interaction between fluorescence-labeled EVs and the plasma membrane, as well as the co-localization of Evs and the recipient cell's organelles. To track the fate of circulating EVs *in vivo*, fluorescence-labeled EVs have been injected into mice via the tail vein and detected using the IVIS Spectrum system (160). GFP-CD63 genetic rats have been generated by

transfecting GFP-CD63 fusion protein into rat embryonic stem cells (161). In these transgenic rats, GFP-CD63-labeled EVs have been found in blood serum, breast milk, and amniotic fluid.

Extracellular vesicle cargo

Extracellular vesicles Proteins

Proteomics

Due to the heterogeneity of EVs, EV proteins have been analyzed by mass spectrometry (MS) in several types of cells and biofluids in an effort to gain a better understanding of EVs and to investigate whether they can be used as potential biomarkers for diagnosis (122, 123, 162). According to ExoCarta, a platform that provides information about EV proteins, 9,769 proteins have been identified in association with EVs. Advanced gene ontology analysis has shown that EV proteins are involved in several biological functions, including subcellular localization, protein binding, molecular transport, and others.

There are two common methods that are been employed for sample preparation in MS analysis: in-gel digestion and in-solution digestion. Compared to in-solution digestion, in-gel digestion has the advantage that contaminants can be removed from samples during electrophoresis. For the in-gel digestion method, EV proteins can be separated by sodium dodecyl sulfate-polyacrylamide gel electrophoresis. Following electrophoresis, the gel lanes are excised into multiple, equal-sized segments and processed by in-gel digestion with trypsin. The digested peptides can then be analyzed by MS coupled to a high-performance liquid chromatography system. Bioinformatic approaches such as pathway analysis and gene ontology can then be applied for further analysis of the EV protein profile (163).

Extracellular vesicles Proteins: Apical vs. Basolateral

Proper function of epithelial cells is highly contingent upon their polarity. Multiple studies have compared the cargo of apically vs. basolaterally secreted epithelial cell-derived EVs. Klingeborn et al. (164) found 299 unique proteins in EVs released apically from retinal epithelial cells, and 94 unique proteins in basolaterally secreted EVs. In intestinal epithelial cells, apical EVs were found to carry proteins involved in endosomal trafficking, whereas basolateral EVs contained proteins that function in adhesion and stimulation (165). These studies suggest that epithelial polarity impacts EV cargo and that EVs secreted from different directions conduct polarity-specific functions. Additional studies will be needed to investigate the underlying mechanisms and clarify the functional roles of these directionally secreted EV subpopulations.

Extracellular vesicles as Biomarkers

EVs encapsulate ‘messages’ from their parental cells in the form of biomolecules, including proteins, lipids, and nucleic acids. These messages manifest in diverse physiological and pathological contexts. For example, EVs derived from dendritic cells and T cells have been shown to carry cytokines to their recipient cells (166). EVs derived from cancer cells are involved in multiple steps in tumorigenesis and tumor metastasis, including tumor cell proliferation, tumor cell migration, immune escape, and angiogenesis (167). In addition, several studies have demonstrated that EVs are involved in the development of neurodegenerative diseases, such as Parkinson’s disease and Alzheimer’s disease, by spreading neural toxicity (116, 168).

In addition to their role in cell-cell communication, EVs may have useful clinical applications as well; they are increasingly being investigated as biomarkers sources for diagnosis and as drug-delivery vectors for therapeutic applications (169, 170). EV Diagnostics, a biotechnology company, has developed several breakthroughs EV-based diagnostic tools for lung and prostate cancer. EVs have been found to facilitate therapeutic targeting of oncogenic KRAS in pancreatic cancer (171). EV epidermal growth factor receptor VIII was shown to be expressed a higher level in patients with glioblastoma (172).

EV glypican-1 was shown to be elevated in pancreatic cancer patients (157), and EV CD26 and CD10 were suggested to be potential markers of liver injury (173). Proteomic analysis combined with validation via western blot or enzyme-linked immunosorbent assay is a widely used method for the discovery of EV biomarkers. Compared to liposomes, engineered EVs demonstrated enhanced efficacy of cancer suppression via delivery of RNA interference (RNAi) to specific targets.

Extracellular vesicles Proteins: Surface-Bound vs. Encapsulated

As with transmembrane and cytosolic proteins, surface-bound and encapsulated EV proteins should have distinct biogenesis mechanisms and carry out different functions. Fitzgerald et al. developed a method to systematically analyze the positions of cytokines in EVs (174). Triton X-100 and sonication are able to lyse the EV membrane. By comparing the protein concentration before and after Triton X-100 or sonication treatment, Fitzgerald et al. revealed the exact association between 33 cytokines and EVs. Additionally, EV sizes become smaller after treatment with proteinase K or trypsin due to digestion of surface proteins (175). In our lab, we found that low-concentration trypsin (0.1 g trypsin/1 g EV protein) only digests proteins located on the external surface of EVs without perturbing membrane-spanning or encapsulated proteins. In contrast, high-concentration trypsin (0.3-1 g trypsin/1 g EV protein) can destabilize the EV membrane, enabling access to the vesicle interior and digestion of proteins associated with both its external and internal aspects. This method provides an alternative approach for determination of the manner in which a given protein is associated with EVs.

Extracellular vesicles microRNA (miRNA; miR)

Like EV proteins, EV miRNAs have been investigated in several pathological contexts, including cancer, inflammation, and age-related degenerations. ExRNA is an open access platform that provides novel information, protocols, recent publications in the field of EV RNAs. miR-21 has been found to be increased in tumor-derived EVs in several cancers, including ovarian, lung, breast, and esophageal squamous cell cancers (176). EV miR-155 was shown to coordinate inflammatory responses (177). EV miR-9, miR-107,

and miR-124 have been shown to play a role in neuronal differentiation, and their downregulation is associated with Alzheimer's disease pathogenesis (178).

Tang et al. (142) compared different isolation methods for EV RNA and found that the Invitrogen™ Total EV RNA and Protein Isolation kit (Thermo Fisher Scientific) results in high extraction efficiency and purity compared to the SeraMir Exosome RNA Column Purification Kit (System Biosciences) and the Invitrogen™ TRIzol™ LS Reagent (Thermo Fisher Scientific). Next-generation sequencing techniques can generate global sequencing data that map all EV microRNA positions. miRNA arrays use hybridization to detect hundreds to thousands of miRNAs simultaneously. Real-time polymerase chain reaction and commercial miRNA and anti-miRNA antibody products are commonly used to validate results and mechanistic studies.

Concluding Remarks

In summary, emerging evidence suggests that RPE cells undergo EMT and migrate into the neuroretina in certain pathological conditions, manifesting clinically as HRF in OCT that correlate with pigmentary changes on fundoscopy. The data summarized here indicate that EMT of RPE cells is a significant predictor for disease prognosis. We summarized recent advances and potential mechanisms underlying this process. These advances may help clarify the role of EMT in retinal disease states and point to avenues that can be exploited for the development of new therapeutic targets.

The principles, procedures, advantages, and disadvantages of commonly used methods for EV isolation and characterization were summarized next. EV research is a new and rapidly progressing field. New methodologies are continuously being developed and will facilitate the translation of EV research to clinical applications.

CHAPTER 2.

EXPRESSION OF R345W-FIBULIN-3 INDUCES EPITHELIAL-MESENCHYMAL TRANSITION IN RETINAL PIGMENT EPITHELIAL CELLS

Chapter 2 was previously published as a research paper written by Mi Zhou (Zhou et al., 2020, Frontiers in Cell and Developmental Biology). The text has been reformatted for this dissertation.

Abstract

Purpose: To investigate the role of protein misfolding in retinal pigment epithelial (RPE) cell dysfunction, the effects of R345W-Fibulin-3 expression on RPE cell phenotype were studied.

Methods: Primary RPE cells were cultured to confluence on Transwells and infected with lentivirus constructs to express wild-type (WT)- or R345W-Fibulin-3. Barrier function was assessed by evaluating zonula occludens-1 (ZO-1) distribution and trans-epithelial electrical resistance (TER). Polarized secretion of vascular endothelial growth factor (VEGF), was measured by Enzyme-linked immunosorbent assay (ELISA). Differentiation status was assessed by qPCR of genes known to be preferentially expressed in terminally differentiated RPE cells, and conversion to an epithelial–mesenchymal transition (EMT) phenotype was assessed by a migration assay.

Results: Compared to RPE cells expressing WT-Fibulin-3, ZO-1 distribution was disrupted and TER values were significantly lower in RPE cells expressing R345W-Fibulin-3. In cells expressing mutant Fibulin-3, VEGF secretion was attenuated basally but not in the apical direction, whereas Fibulin-3 secretion was reduced in both the apical and basal directions. Retinal pigment epithelial signature genes were downregulated and multiple genes associated with EMT were upregulated in the mutant group. Migration

assays revealed a faster recovery rate in ARPE-19 cells overexpressing R345W-Fibulin-3 compared to WT.

Conclusions: The results suggest that expression of R345W-Fibulin-3 promotes EMT in RPE cells.

Introduction

Retinal pigment epithelial (RPE) cells, photoreceptors, and the choroid form a functional unit required for healthy vision. The unique structure and polarity of the RPE layer is critical to the ongoing maintenance of photoreceptors. Atrophy and dysfunction of the RPE with subsequent loss of photoreceptors plays a fundamental role in numerous retinal degenerations. RPE dysfunction manifests as a loss of barrier function, disrupted polarization, and downregulated expression of RPE signature genes and microRNA-204/211 (12, 13). Recent evidence suggests that RPE cells lose terminal differentiation and acquire a mesenchymal cell phenotype in occur in several retinal degenerations (26, 58, 109); misfolded proteins accumulate in RPE cells with age, however, the underlying mechanisms by which misfolded protein accumulation leads to RPE cell dysfunction remain unclear.

Epithelial–mesenchymal transition (EMT) is a process by which epithelial cells loss of epithelial markers, including zona-occludens-1 (ZO-1), E-cadherin, and cytokeratin, and gain of expression of mesenchymal drivers, including vimentin, N-cadherin, and fibronectin. Historically, it is thought that in healthy tissues, fully differentiated epithelial cells exert specific functions and maintain its phenotype after development. However, EMT can be activated under pathological circumstances, facilitating epithelial cells to obtain an enhanced migration ability and increase their production of extracellular matrix components. Clinical evidence has suggested that RPE cells undergo EMT with upregulated mesenchymal cell markers and enhanced migration ability in several degenerative retinal diseases, including inherited rod-cone degenerations, inherited macular degeneration, age-related macular degeneration, and proliferative

vitreoretinopathy. (25-27, 41, 58). However, the underlying mechanisms by which RPE cells undergo EMT are to be determined.

Emerging clinical evidence suggests that RPE dysfunction is a predictor for disease progression. Intraretinal hyperreflective foci (HRF) in optical coherence tomography (OCT) images have been observed in various retinal diseases, including age-related macular degeneration (AMD), inherited rod-cone degenerations, and inherited macular degenerations (30-32). In numerous retinal degeneration diseases, these foci were found to correlate with disease severity (31, 32, 34, 35). The postulated cellular origins of HRF include migratory RPE cells, macrophages, or hard exudates. Recently, a study used to combine polarimetry with auto-fluorescence imaging to discriminate between RPE cells, inflammatory cells, and hard exudates, to investigate the origin of HRF (30). The results revealed that, in early stages of AMD, a portion of HRF showed signs of RPE migration, substantiating the possibility that RPE cells have the capacity to migrate into the neuroretina (30). Moreover, histopathological studies have confirmed that HRF represent cells of RPE origin and correspond spatially to pigmentary abnormalities observed by fundoscopy (33). Notably, these pigmentary changes, along with sub-retinal deposit formation, represent the hallmark lesions of macular degeneration in its intermediate stage (179). Several studies have shown that pigmentary changes are important indicators of AMD prognosis (39, 180, 181). The mechanisms by which RPE cells migrate and whether their migration results in pigmentary changes still remain to be fully explored.

In other systems, it is well established that cellular stress frequently results in dedifferentiation via intracellular misfolded protein accumulation and activation of the unfolded protein response (UPR) (182, 183). Previously, a study showed that accumulation of intracellular amyloid-β leads to a loss of tight junctions in RPE cells, substantiating the idea that accumulation of abnormal proteins in RPE cells attenuates RPE differentiation (84). This evidence suggests an interaction of cellular signaling between the UPR and EMT in RPE cells, which also has been demonstrated in several different organs (78-81). Increased transcription of endoplasmic reticulum (ER) chaperones, binding immunoglobulin protein (BiP) also known as glucose regulated protein-78 (GRP-78) and

GRP-94 aimed at reducing the load of aberrant protein accumulation. Three ER transmembrane sensors, IRE1α, PERK, and ATF6, regulate the UPR and determine the appropriate adaptive response (92, 93). The activation of IRE1α-XBP1 signaling promotes EMT has been found in different organs and tissues, including the breast, lung, and liver (96-99). Several studies have shown that the UPR and TGF-β-induced EMT signaling pathways interact at the level of c-Jun N-terminal kinase and p38 mitogen-activated protein kinase (JNK/p38-MAPK) in an IRE1-dependent manner (94-96). Whether IRE1α-XBP1plays a role in RPE cell dysfunction is to be explored.

Fibulin-3 is a secretory protein and contains six epidermal growth factor (EGF)-like domains and a fibulin domain (184). Fibulin-3 is expressed throughout the body including the eyes. Several studies have shown that the single arginine-to-tryptophan point mutation, R345W, impairs the secretion rate of Fibulin-3 (89, 90, 185). Prior studies have also shown that mutant Fibulin-3 is misfolded and migrates faster than the wild-type form under non-reducing conditions (89). R345W-Fibulin-3 protein is responsible for the inherited macular degeneration, Doyne honeycomb retinal dystrophy (DHRD) (186, 187). Thus, overexpression of R345W-Fibulin-3 provides a useful model to study the impact of protein misfolding on RPE phenotype and dysfunction.

In this study, we investigated the role of fibulin-3 protein misfolding on RPE cell dedifferentiation and dysfunction. We infected primary RPE cells with lentivirus carrying luciferase-tagged R345W-Fibulin-3 to model an early-onset macular degeneration. Our results show that expression of R345W-Fibulin-3 activates ER stress via IRE1α/XBP1 pathway, which in turn attenuates differentiation in RPE cells, indicated by disrupted tight junctions, impairment of polarized proteins, and downregulated RPE signature gene expression. Moreover, we report that the expression of R345W-Fibulin-3 upregulates EMT markers and enhances the migration ability of RPE cells.

Results

Primary RPE cells exhibit terminal differentiation on Transwell filters.

Primary RPE cells were placed on Transwell filters, and several endpoints were used to test the differentiation status at four weeks. TEM imaging showed that primary RPE cells displayed appropriate structural polarity with apically located microvilli, tight junctions, and melanosomes, and basally located nuclei and basal infoldings (**Fig. 2-1 A-B**). Barrier function was assessed by quantifying TER over time. After four weeks, the TER plateaued at ~1,400 **Ω•**cm^2 (**Fig. 2-1 C**). Tight junction expression and distribution was confirmed by confocal imaging. ZO-1 immunoreactivity was abundant and continuous along the cell borders (**Fig. 2-1 D**). These data confirm that primary RPE cells grown on Transwells are polarized and differentiated.

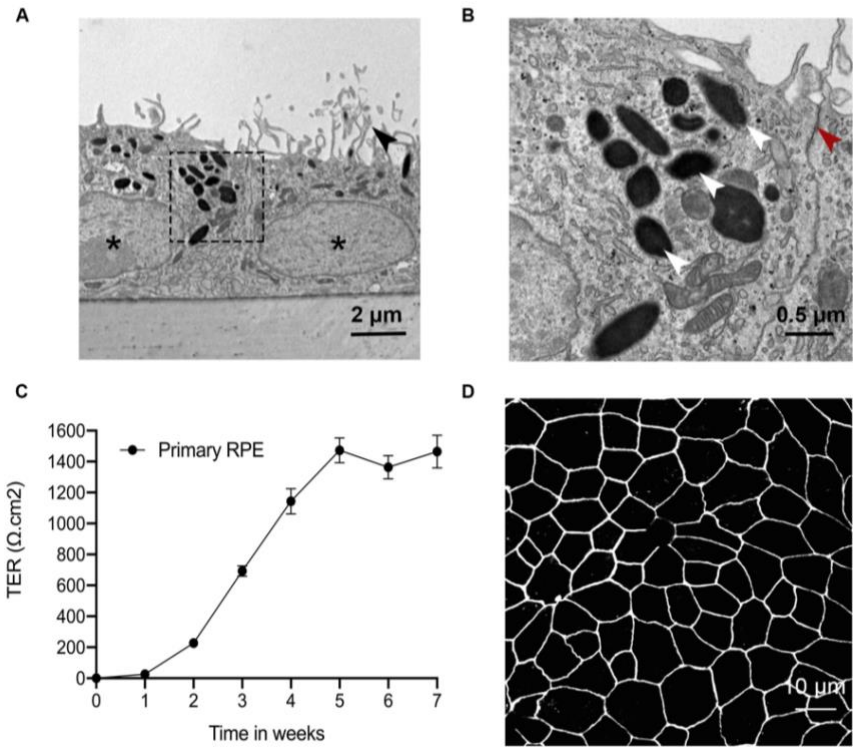

Figure 2-1 Primary RPE cells have a terminal differentiation phenotype on Transwell filters. Primary RPE cells were cultured on Transwell filters, and their phenotype was evaluated by TEM, TER and tight junction protein ICC. (A) RPE cells grew in a single monolayer with apical microvilli (black arrowhead), melanosomes, basal nuclei (asterisks), and membrane infoldings. (B) Magnification of the indicated area in A shows RPE cells with clearly visible tight junctions (red arrowhead) and melanosomes (white arrowhead). (C) Barrier function was assessed by quantifying TER over time. After four weeks, the TER plateaued at ~1,400 Ω cm 2. (D) ZO-1 immunoreactivity was continuous along the cell borders.

Expression of R345W-Fibulin-3 activates the IRE1α/XBP1 pathway in RPE cells.

Prior study has revealed that in ARPE-19 cells, expression of R345W-Fibulin-3 activates ER stress via the IRE1α/XBP1 pathway (185). This study showed that overexpression of R345W-Fibulin-3 induces the elevated expression of Binding immunoglobulin protein (BiP) also known as glucose regulated protein-78 (GRP-78) at both mRNA and protein levels and induces increased expression of XBP1 at mRNA level (185). To investigate the specific ER stress pathway(s) induced by mutant Fibulin-3 in primary RPE cells, total RNA was isolated at 14 weeks post-infection (n=3), and quantified by rtPCR. Consistent with the previous study, IRE1α/XBP1 pathway and transcription

factor C/EBP homologous protein (CHOP) were elevated in primary RPE cells expressing mutant Fibulin-3 compared to controls (**Fig. 2-2 A**). mRNA levels of ER chaperone, BiP/GRP-78 and GRP-94 were also elevated compared to cells expressing WT-Fibulin-3 (**Fig. 2-2 B**). These results suggest that expression of mutant Fibulin-3 activates ER stress in RPE cells primarily through the IRE1α/XBP1 pathway.

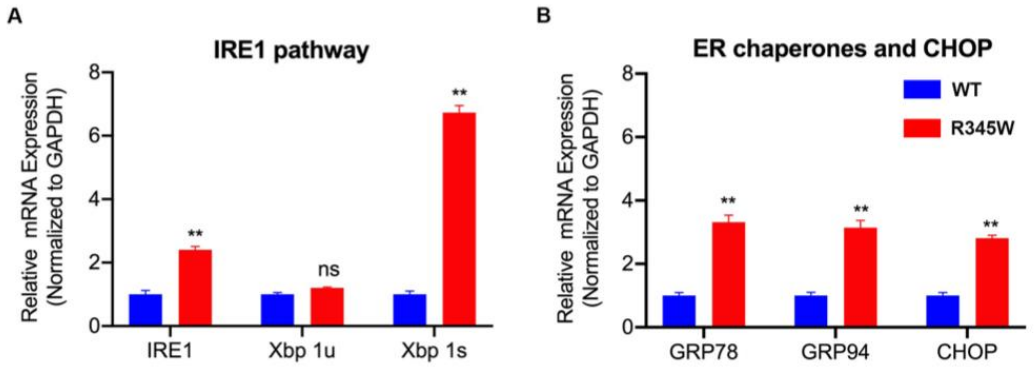

*Figure 2-2. Expression of R345W-Fibulin-3 elevates markers of ER stress in primary RPE cells. mRNA isolated from primary RPE transfected with WT or R345W-Fibulin-3 was quantified by rtPCR. (A) IRE1α/XBP1 mRNA were elevated in primary RPE cells expressing mutant Fibulin-3 compared to controls, while Xbp 1u was unaltered. (B) mRNA levels of ER chaperone, GRP-78 and GRP-94, and transcription factor CHOP were also elevated compared to cells expressing WT-Fibulin-3. (n = 3, values are mean ± SEM, **p < 0.01).*

Expression of R345W-Fibulin-3 in RPE cells disrupts tight junction protein distribution and impairs barrier function.

To investigate the effects of R345W-Fibulin-3 expression on RPE permeability barrier function, we first examined ZO-1 distribution using the primary RPE cell culture system described above. ICC was conducted at 9- or 12-weeks post-infection. Confocal imaging revealed that ZO-1 distribution was dramatically disrupted and disorganized in the mutant group relative to the WT group (**Fig. 2-3 A**). To quantify these changes, the number of RPE nuclei associated with continuous ZO-1 was counted in 9 regions of the 625 μm^2 confocal image. Relative to controls, continuous ZO-1 distribution in the mutant group was reduced by 38% ($p<0.01$) after 9 weeks of infection and by 90% after 12 weeks ($p<0.01$) (**Fig. 2-3 B**). These data indicate that the expression of mutant Fibulin-3 in RPE cells disrupts tight junction protein distribution.

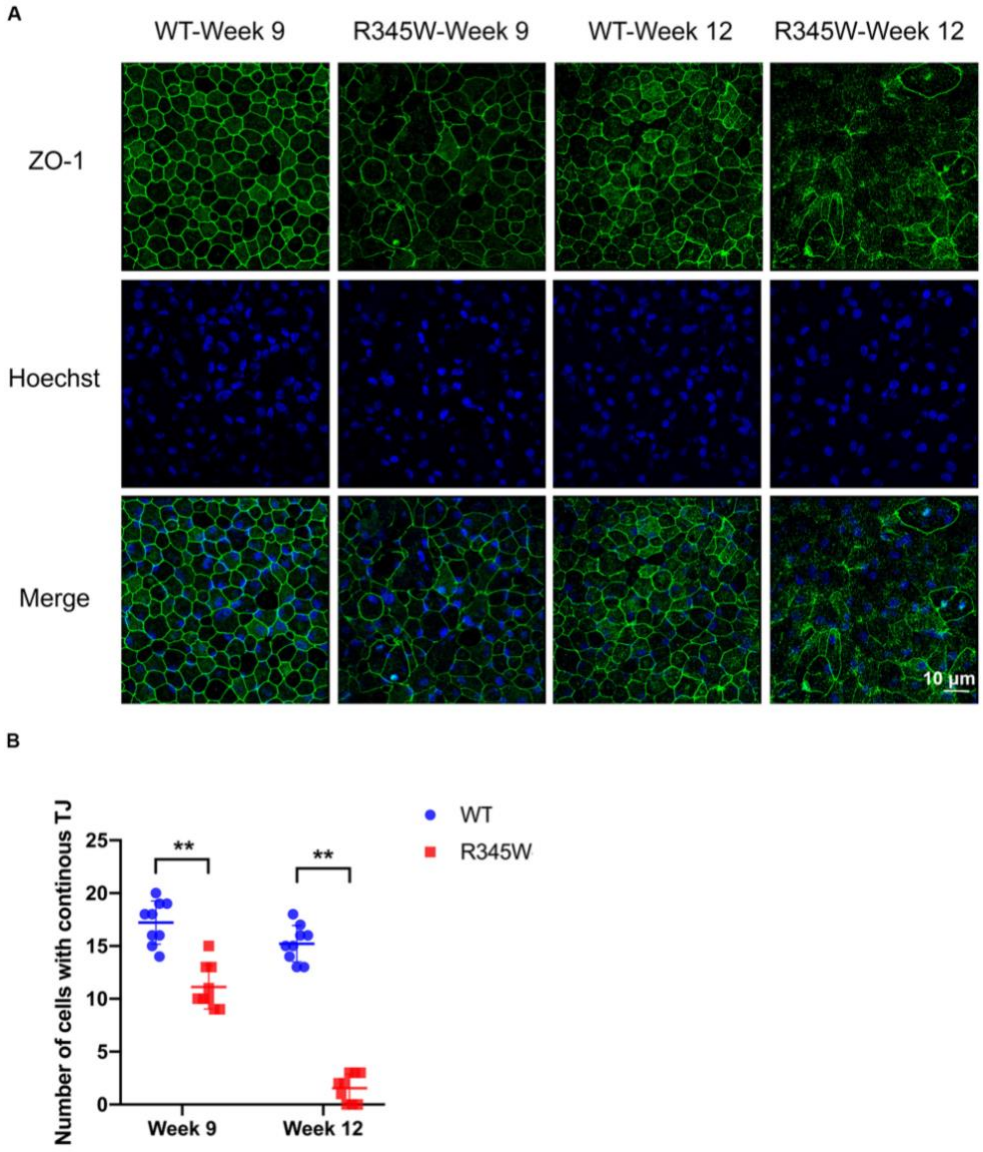

Figure 2-3. ZO-1 distribution is disrupted in primary RPE cells expressing R345W-Fibulin-3. The expression and distribution of ZO-1 tight junction protein was assessed in primary RPE cells 9 and 12 weeks after infection with WT- or R345W-Fibulin-3 ***(A)*** *Maximum projection confocal images of ZO-1 ICC. Green: ZO-1; Blue: Hoechst-stained nuclei. Confocal imaging reveals that ZO-1 distribution was dramatically disrupted in RPE cells expressing R345W-Fibulin-3 at 9- and 12-weeks post-infection.* ***(B)*** *Cells with continuous ZO-1 distribution were counted in nine different areas of 625 µm 2. The number of cells with continuous tight junctions was significantly lower in RPE cells expressing R345W-Fibulin-3 at 9- and 12-weeks post-infection compared to WT infected controls (n = 9, values are mean ± SEM, **p < 0.01).*

To assess the impact of disrupted tight junction protein distribution on a critical aspect of RPE cell function, trans-epithelial electrical resistance (TER) was monitored over

time. Four weeks after being seeded, the TER of all cells reached a plateau of approximately 1,400 Ω•cm^2. Seven weeks after seeding, cells were infected with GLuc-tagged WT-Fibulin-3, GLuc-tagged R345W-Fibulin-3, or GLuc tag only. At 3 weeks post-infection, the TER was reduced to 800-1,000 Ω•cm^2 in all three groups, but no significant differences were observed between groups. Starting at 4 weeks post-infection, the TER of cells expressing R345W-Fibulin-3 was significantly reduced relative to the GLuc-tagged WT-Fibulin-3 and GLuc tag only groups. TER in the GLuc-tagged R345W-Fib3 group was 70.7% lower at 9 weeks post-infection (n=8, p<0.01) and 78.4% lower at 12 weeks post-infection (n=8, p<0.01) (**Fig. 2-4**). These data are consistent with the altered ZO-1 distribution described above and further indicate that expression of mutant Fibulin-3 induces loss of RPE barrier function.

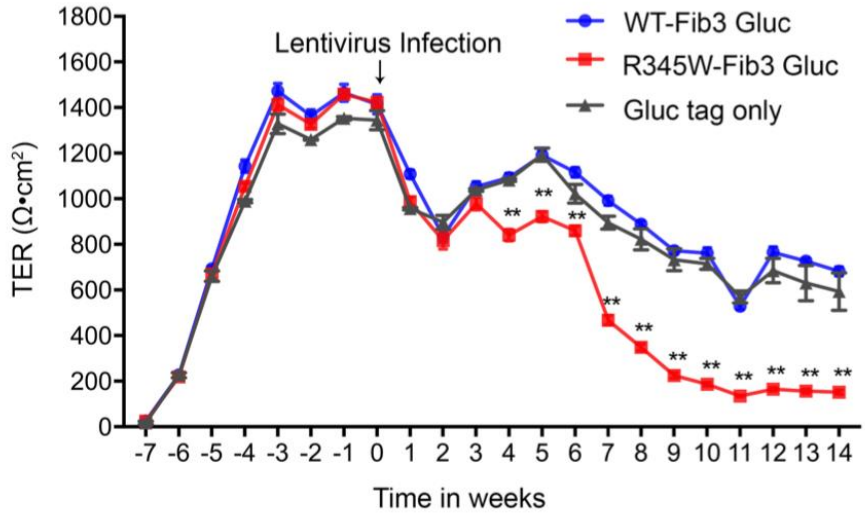

*Figure 2-4. Expression of R345W-Fibulin-3 decreases TER in primary RPE cells. Cell permeability was assessed by monitoring TER in RPE cells once a week for 21 weeks. At the beginning of the 4th week (week-3 on x-axis), RPE cells reached maturity with TER values maximizing between 1,300 and 1,500 Ω cm 2. In the beginning of the 7th week (week 0 on x-axis), RPE cells were infected with lentivirus with either luciferase-tagged WT-Fibulin-3 (blue), luciferase-tagged R345W-Fibulin-3 (red), or luciferase-tag only (gray) for five consecutive days. At 3 weeks post-infection, TER decreased to approximately 800 Ω cm 2 in all groups. At 4 weeks post-infection, TER continuously dropped in the mutant group (n = 8) and reached values significantly lower than the WT (n = 8) and tag-only groups (n = 2). (Values are mean ± SEM of individual wells, **p < 0.01).*

Expression of R345W-Fibulin-3 in primary RPE cells reduces the basal secretion of VEGF.

It is well established that polarized secretion of proteins by RPE cells is critical for RPE, photoreceptor, and choroidal homeostasis, and that the polarized secretion of VEGF is of particular significance (22, 188). In terminally differentiated RPE cells, VEGF is primarily secreted in the basal direction to promote the growth of the choroidal vasculature (189). To test whether mutant Fibulin-3 induction alters the polar secretion of growth factors, we quantified apical and basal VEGF secretion using the primary RPE cell culture system described above. Cell culture medium was collected from the apical and basal compartments of each well. VEGF165 was quantified using a validated ELISA. The apical VEGF concentration did not differ between groups (**Fig. 2-5A**). Compared to WT-Fibulin-3, basal VEGF secretion was significantly lower in the R345W-Fibulin-3 group at both 9- and 12-weeks post-infection (n=8, $p<0.01$) (**Fig. 2-5B**). These results suggest that expression of mutant Fibulin-3 alters the polarized secretion of VEGF.

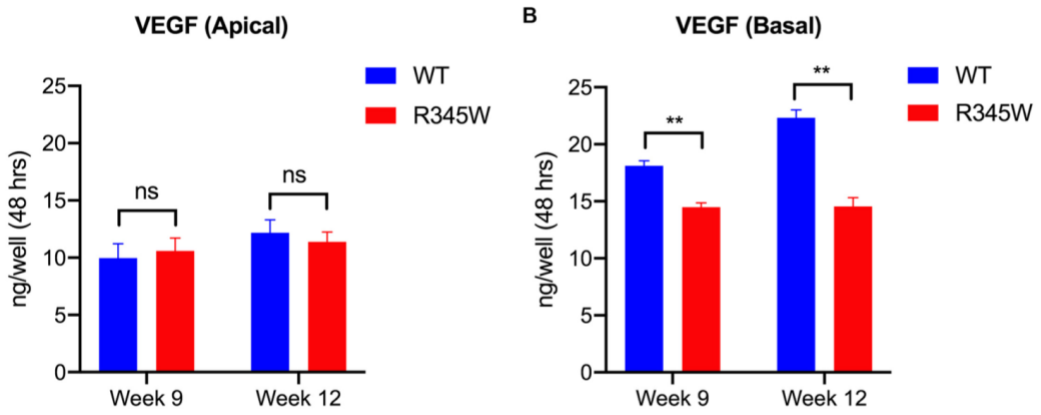

*Figure 2-5. VEGF secretion is impaired in primary RPE cells expressing R345W-Fibulin-3. VEGF secretion levels were quantified by ELISA. Cell culture media were collected from the apical and basolateral sides of primary RPE cells on Transwell filters at 9- and 12-weeks post-infection. (A) Apical VEGF secretion was not significantly different in the R345W-Fibulin-3 cells compared to WT, (B) Basal VEGF secretion was significantly lower in the mutant group compared to the WT group at 9- and 12-weeks post-infection. Values are the mean ± SEM of individual wells (n = 8, **p < 0.01).*

Expression of R345W-Fibulin-3 alters its polarized secretion in primary RPE cells.

To monitor the secretion of WT-Fibulin-3 and R345W-Fibulin-3, cell culture media were collected once a week for 12 weeks following infection. The results revealed that luciferase activity in basal cell culture media was significantly higher than that of apical cell culture media from RPE cells expressing both WT and mutant forms of Fibulin-3 ($n=8$, $p<0.01$) (**Fig 2-6A**). Luciferase activity in the cell culture media of primary RPE cells expressing mutant Fibulin-3 was significantly lower than that of cells expressing the WT form on both apical and basal sides. Moreover, we found that R345W-Fibulin-3 secretion was severely impaired in the basal direction and moderately impaired apically. The decreased basal:apical secretion ratio of R345W-Fibulin-3 suggests that R345W-Fibulin-3 expression impairs polarized Fibulin-3 secretion in RPE cells ($n=8$, $p<0.01$; **Fig. 2-6 A-B**).

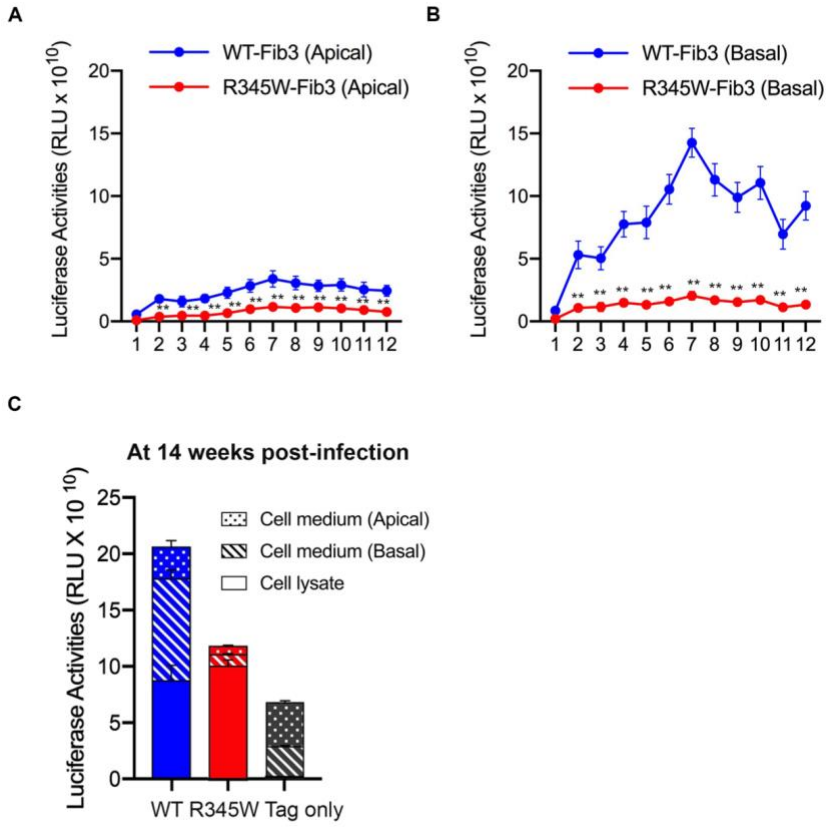

*Figure 2-6. Secretion of R345W-Fibulin-3 is impaired in both apical and basolateral directions. Fibulin-3 secretion levels were monitored by luciferase assay from media collected from the apical and basolateral sides of primary RPE cells. (A,B) Fibulin-3 was preferentially secreted to the basal side in both WT and mutant cells. R345W-Fibulin-3 secretion levels in mutant cells were significantly lower than those of WT cells over time (n = 8, **p < 0.01). (C) After 14 weeks of infection, primary RPE cells were harvested and cell media were collected. No significant differences in luciferase activities between the WT and mutant groups were observed. Luciferase activities were decreased in RPE cells expressing R345W-Fibulin-3 in both the apical and basolateral directions.*

At 14 weeks post-infection, cell lysates and cell culture media were harvested, and luciferase activity was quantified via a luciferase assay. Our results showed no significant differences in primary RPE cell lysate luciferase activities between WT and mutant groups, which is not consistent with previous studies in RPE-J cells or ARPE-19 cells that reported greater amounts of mutant Fibulin-3 within cells relative to the WT protein (89, 185). One possible explanation for the differing results is the differences between these cell culture systems. Consistent with previous studies (190), luciferase activity in the cell culture media of RPE cells expressing mutant Fibulin-3 was 73.6% and 88.8% lower on the apical and

basal sides, respectively, than that of cells expressing the WT form after 14 weeks of infection (n=8, $p<0.01$; **Fig. 2-6 C**). The reduction in total luciferase activity including both cell lysates and cell culture media in the mutant group may due to the increased degradation of mutant Fibulin-3.

Expression of R345W-Fibulin-3 leads to downregulated expression of RPE signature genes and upregulated expression of EMT markers.

To determine the differentiation state of the RPE cells in culture, we evaluated the expression levels of validated RPE cell signature genes. These genes were defined as mean expression values upregulated 10-fold or greater in native adult RPE cells relative to other cell types (191, 192). BEST1 (bestrophin-1), CRALBP (retinaldehyde-binding protein), RPE65 (retinal pigment epithelium-specific 65 kDa protein), and TRPM1 (transient receptor potential cation channel) are four RPE cell signature genes with functions in membrane transport, the visual cycle, and pigmentation pathways. We investigated whether R345W-Fibulin-3 expression influences RPE signature gene expression using the same cell culture system as above. After 14 weeks of infection, primary RPE cells were harvested for total RNA isolation. RT-PCR was conducted to examine signature gene expression in each group. BEST1, CRALBP, RPE65, and TRPM1 expression levels were normalized to GAPDH expression. RT-PCR results showed that BEST1, CRALBP, RPE65, and TRPM1 expression levels were significantly lower in the GLuc-tagged R345W-Fibulin3 group than in the GLuc-tagged WT-Fibulin-3 group (n=3, $p<0.01$), indicating that the expression of R345W-Fibulin-3 attenuates RPE cell differentiation (**Fig. 2-7A**).

It is thought that cell dedifferentiation is usually followed by trans-differentiation, namely, EMT, due to stress-induced cellular reprogramming which includes increased cell migration (182, 183, 193). Using RT-PCR, we compared the expression levels of TGFB2 (transforming growth factor beta-2), ZEB1 (Zinc Finger E-Box Binding Homeobox 1), VIM (Vimentin), and CDH2 (Cadherin 2) across groups using the primary RPE cell culture system described above. Compared to the WT group, the expression levels of all four EMT markers were significantly higher in the mutant group (n=3, $p<0.01$). Notably, the

magnitude of EMT induction was similar to prior work (12, 13), suggesting that expression of R345W-Fibulin-3 facilitates EMT in RPE cells (**Fig. 2-7B**).

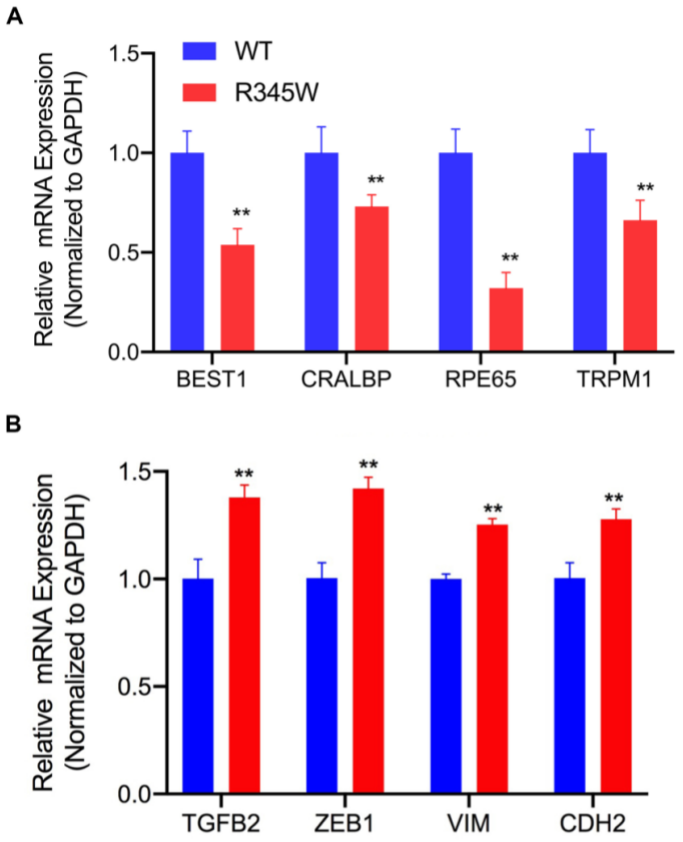

*Figure 2-7. RPE signature genes are downregulated and EMT markers are upregulated in primary RPE cells expressing R345W-Fibulin-3. (A) At 14 weeks post-infection, primary RPE cells were harvested and total RNA was isolated. RT-PCR was performed to quantify four RPE signature genes (BEST1, CRALBP, RPE65, and TRPM1). All expression levels are normalized to GAPDH expression. Relative to the WT group, mRNA for BEST1, CRALBP, RPE65, and TRPM1 were significantly reduced in RPE cells expressing R345W-Fibulin-3 (n = 3, **p < 0.01). (B) At 14 weeks post-infection, primary RPE cells were harvested, and total RNA was isolated. RT-PCR was performed to quantify four EMT markers, (TGFB2, ZEB1, VIM, and CDH2). All expression levels were normalized to GAPDH expression. The experimental results showed that, relative to the WT group, TGFB2, ZEB1, VIM, and CDH2 were significantly upregulated in RPE cells expressing R345W-Fibulin-3 (n = 3, **p < 0.01).*

Expression of R345W-Fibulin-3 leads to enhanced migration ability in RPE cells.

To evaluate whether the expression of R345W-Fibulin-3 leads to migratory changes in RPE cells, scratch assays were conducted in ARPE-19 cells overexpressing

either a dox-inducible GLuc-tagged WT-Fibulin-3 or R345W-Fibulin-3. We examined WT-Fibulin-3 and R345W-Fibulin-3 expression in this Tet-On ARPE-19 cell system by western blot. We found that the non-induced mutant group displayed a small but detectable amount of leaky expression of R345W-Fibulin-3 (**Fig 2-8 A-B**). In the cell culture media, the amount of "leaky" expression in the absence of dox is 7% (GLuc-tagged WT) and 34% (GLuc-tagged R345W) of the respective western blot signal with dox treatment for 48 hours. In the cell lysate, the amount of "leaky" expression in the absence of dox is 3% (GLuc-tagged WT) and 3% (GLuc-tagged R345W) of the respective western blot signal with dox treatment for 48 hours, consistent with previous study (194) (**Fig 2-8 A-B**).

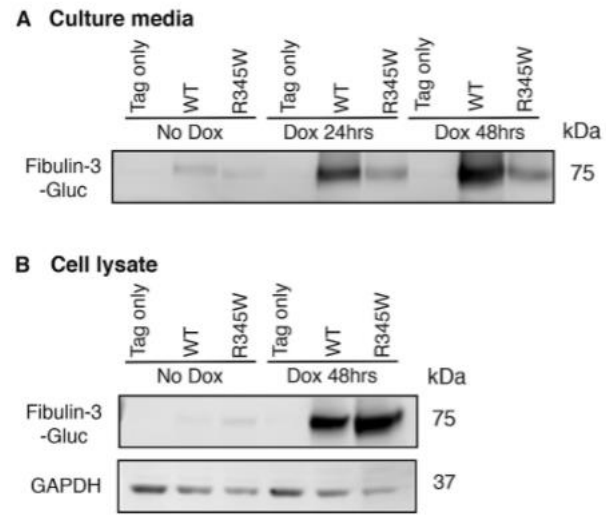

Figure 2-8. Western blot analysis of Fibulin-3 secretion and expression levels in ARPE-19 cells. Secretion and expression levels of WT-Fibulin-3 and R345W-Fibulin-3 were quantified in the cell culture media and cell lysate, respectively, from the Tet-On ARPE-19 cells by western blot. The results showed that, relative to R345W-Fibulin-3, more WT-Fibulin-3 was secreted into the cell culture media. Relative to WT-Fibulin-3, more R345W-Fibulin-3 was retained within the cells. Without dox induction, GLuc-tagged WT-Fibulin-3 and R345W-Fibulin-3 were still weakly detected in both cell culture media and cell lysates, suggesting slightly leaky Fibulin-3 expression in this Tet-On ARPE-19 cell system.

Expression of R345W-Fibulin-3 enhanced migration ability in a dose-dependent manner. Scratches were made after 48 hours of dox-induced expression of either WT-Fibulin-3 or R345W-Fibulin-3 in ARPE-19 cells. Relative wound confluence was calculated automatically by the IncuCyte™ software system at one-hour intervals for 72

hours (**Fig 2-9**). Scratch recovery rate was calculated as time to 50% wound closing ($T_{1/2}$). We found that dox-induced mutant group had the fastest scratch for closing 50% of the wound ($T_{1/2}$=18 hr), suggesting that the expression of R345W-Fibulin-3 increased the migration ability of RPE cells. Compared to the non-induced WT ($T_{1/2}$=31 hrs.) and dox-induced WT groups ($T_{1/2}$=29 hrs.), the non-induced mutant group had a faster scratch recovery rate ($T_{1/2}$=25 hrs.), and, relative to the dox-induced mutant group, it had a slower scratch recovery rate ($n=8$, $p<0.01$) (**Fig. 2-9 A**-**B**).

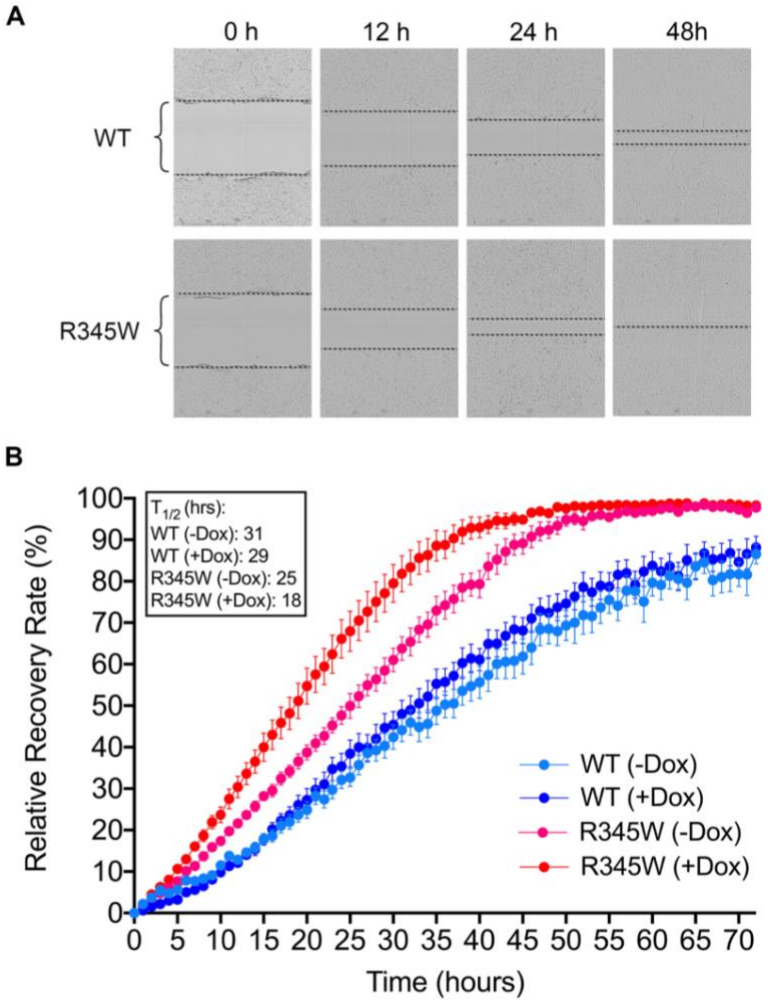

Figure 2-9. Expressing R345W-Fibulin-3 increases cell migration. Scratch assays were conducted in ARPE-19 cells overexpressing either WT-Fibulin-3 or R345W-Fibulin-3. (A,B) The experimental results showed that, relative to the WT group, ARPE-19 cells overexpressing R345W-Fibulin-3 had a significantly faster scratch recovery rate in would healing assays. Brackets represent wound distances (n = 8, $p < 0.01$).

Discussion

The current study sheds light on the potential impact of misfolded protein accumulation due to the R345W mutation in fibulin-3 in RPE cells. In this study, we cultured primary RPE cells on Transwells and observed their morphology under TEM. As in studies presented by others, our primary RPE cells showed robust tight junctions and

structural polarity under TEM (188, 195, 196). Unfolded protein response (UPR) activation involves several mechanisms aimed at reducing the load of aberrant protein accumulation, including attenuated protein translation to avoid worsening the accumulation, increased transcription of endoplasmic reticulum (ER) chaperones, including GRP-78 and GRP-94 to aid in the folding process, and an increase in ER-associated degradation (ERAD). Three ER transmembrane sensors, IRE1, PERK, and ATF6, regulate the UPR and determine the appropriate adaptive response, directing the cell to proliferate, change shape, or undergo apoptosis. Prior studies have also shown that mutant Fibulin-3 is misfolded and accumulated in the ER (89, 185). Our study showed that expression of mutant Fibulin-3 induces increased expression of ER chaperones and IRE1/XBP1 pathway. We found that, in primary RPE cells expressing R345W-Fibulin-3, barrier function was impaired, as evidenced by disrupted ZO-1 distribution and decreased TER. This is in line with a prior study which showed that RPE cells retained a differentiated phenotype if they maintained cell-cell contacts, whereas EMT was initiated when RPE cells lost tight junctions, suggesting that cell-cell contact plays an important role in the RPE transition from a well-differentiated phenotype to a fibroblast phenotype. This phenotypic switch may contribute to the development of fibrotic complications (71).

We next examined the effects of R345W-Fibulin-3 expression on the polarized secretion of proteins by RPE cells. In fully polarized RPE cells, VEGF is preferentially secreted to the basal side of the RPE monolayer for choroidal vasculogenesis, a function that may be impaired in AMD. For example, decreased thickness of the choroidal layer has been observed in AMD patients (197), while a previous study showed that RPE de-differentiation causes atrophy of the choriocapillaris (198). Our data are consistent with these findings, whereby the levels of basally secreted VEGF were significantly lower in the mutant group, indicating that the polarized secretion of VEGF was disrupted in RPE cells expressing R345W-Fibulin-3.

To our knowledge, this is the first study to delineate the directionality of impaired R345W-Fibulin-3 secretion. We found that WT-Fibulin-3 is preferentially secreted in the basal direction, substantiating the hypothesis that Fibulin-3 plays a role in maintaining the

RPE cell basement membrane (199, 200). We further found that R345W-Fibulin-3 secretion is severely impaired on the basal side and moderately impaired in the apical direction. These results suggest that expression of R345W-Fibulin-3 impairs polarized Fibulin-3 secretion in RPE cells. The reduction in total secretion of R345W Fibulin-3 may be due to accelerated degradation or to excessive intracellular accumulation.

We next showed that RPE cell signature genes were downregulated in primary RPE cells expressing R345W-Fibulin-3. Moreover, our data showed that four EMT markers, TGFB2, ZEB1, VIM, and CDH2, were upregulated and migration ability was enhanced in the mutant group, suggesting that the expression of R345W-Fibulin-3 not only attenuates RPE cell differentiation, but also facilitates EMT of RPE cells. This may explain the formation of sub-RPE deposits and increased thickness of Bruch's membrane in macular degeneration, as more extracellular matrix proteins are secreted by mesenchymal-like cells than epithelial cells. In addition, increased migration ability in mutant RPE cells may explain the presence of HRF in OCT images, which have been shown to display characteristics of RPE migration in published studies. **Figure 2-10** illustrates our working model for RPE cell dedifferentiation and EMT.

The current study shows that Fibulin-3 mutation leads to a phenotypic shift in RPE cells. However, the specific mechanisms by which mutant Fibulin-3 leads to EMT of RPE cells are unclear. Previous studies have shown that expression of mutant Fibulin-3 causes activation of the UPR in ARPE-19 cells (185). Emerging evidence suggests that the accumulation of misfolded proteins drives EMT via activation of the UPR (78, 97, 99). Thus, UPR activation may constitute one of the underlying mechanisms by which RPE cells undergo EMT.

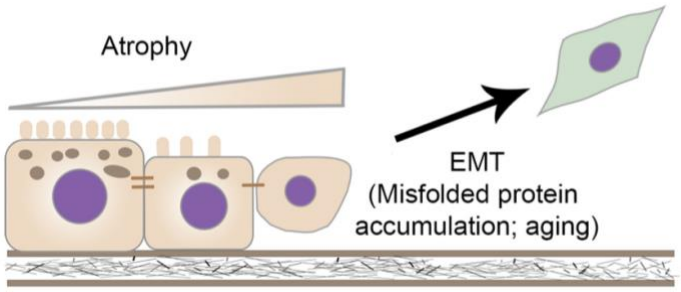

Figure 2-10. Working model for RPE cells dysfunction and undergoing EMT. RPE cells exhibit a well-differentiated epithelial phenotype, characterized by integrated tight junctions, a high degree of polarity, and proper RPE signature gene expression. Expression of R345W-Fibulin-3 in RPE cells leads to a mesenchymal-like phenotype with cytoskeletal changes, a transcriptional shift, and an increased capacity for migration. Potential mechanisms contributing to EMT in RPE cells include aging and misfolded protein accumulation.

In summary, our experimental results have shown that native and WT-fibulin-3 overexpressing RPE cells exhibit a terminally differentiated epithelial phenotype with continues, barrier-forming tight junctions, high polarization, and high expression of RPE signature genes. The expression of R345W-Fibulin-3 causes RPE cells to undergo EMT, as evidenced by upregulated EMT markers and an increased migration ability. The findings from this study will help us gain a better understanding of the role of misfolded proteins in RPE dysfunction.

CHAPTER 3.

EXTRACELLULAR VESICLES FROM RETINAL PIGMENT EPITHELIAL CELLS EXPRESSING R345W-FIBULIN-3 INDUCE EPITHELIAL-MESENCHYMAL TRANSITION IN RECIPIENT CELLS.

Abstract

Purpose: Previous studies in our lab found that expression of R345W-Fibulin-3 induces retinal pigment epithelial (RPE) cells to undergo epithelial-mesenchymal transition (EMT). The purpose of the current study was to investigate the size, cargo, and function of extracellular vesicles (EVs) derived from RPE cells expressing wild-type (WT)-Fibulin-3 compared to RPE cells expressing the R345W-Fibulin-3 mutation, and to determine the role of these EVs in RPE cell dysfunction.

Methods: ARPE-19 cells were infected with luciferase-tagged wild-type (WT)-Fibulin-3 or luciferase-tagged R345W-Fibulin-3 (R345W) using lentiviruses. EVs were isolated from the media of ARPE-19 cells by conventional ultracentrifugation or density gradient ultracentrifugation. Transmission electron microscopy (TEM) and cryogenic electron microscopy (Cryo-EM) were performed to study the morphology of the EVs. The amount and size distribution of EVs were determined by Nanoparticle Tracking Analysis (NTA). EV protein concentrations were quantified using the DCTM Protein Assay (Bio-Rad). EV markers were validated by conducting Western blot analysis. EV cargo were analyzed by unbiased proteomics using LC-MS/MS with subsequent pathway analysis (Advaita). The EV-associated transforming growth factor beta 1 (TGF-β1) protein was measured by enzyme-linked immunosorbent assay (ELISA). EV incubated with trypsin were conducted to determine the orientation of WT-Fibulin-3 and R345W-Fibulin-3 in EV. EV uptake was investigated by using PKH67-labeled vesicles and was analyzed by confocal imaging. The EV transplant study was conducted, and migration ability was evaluated in ARPE-19 cells with or without exposure to EVs by conducting scratch assays.

Pan-TGF-β-neutralizing antibody was used to determine whether EVs derived from RPE cells induce EMT via TGF-β signaling. mRNA expression levels of EMT markers were measured after EV treatment using RT-PCR.

Results: TEM imaging revealed concave-appearing vesicles, and Cryo-EM imaging showed spherical vesicles with two subpopulations of EVs: a group with diameters around 30 nm and a group with diameters over 100 nm. Imaging also indicated a greater number of small EVs (~30 nm) in the R345W group compared to the WT group. This result was further confirmed by NTA showing that, in the R345W group, the particle size distributions were smaller than those of the WT-ARPE-EV. There were no significant differences in EV protein concentrations per EV between WT and R345W groups. Pathway analysis revealed that primary cilia and sonic hedgehog (SHH) pathways were 3- to 5-fold more abundant in EVs derived from WT ARPE-19 cells. In contrast, EMT drivers, lysosome components, and ribosome components were found to be 3- to 7-fold more abundant in EVs secreted from R345W ARPE-19 cells. Subsequent studies revealed enhanced content of TGF-β1 associated with R345W-ARPE-EVs compared to WT-ARPE-EVs. Fibulin-3 can be digested with a low concentration of trypsin, but not EGFR, Flotillin-1, or ALIX, indicating that Fibulin-3 is outside of EV rather than within them. There were no significant differences in EV uptake between WT and R345W groups. Critically, EV transplant studies showed that treatment of recipient RPE cells with R345W-ARPE-EV was sufficient to induce an enhanced migration ability and elevated EMT marker expression in RPE cells. The effects were significantly inhibited after the addition of pan-TGF-β-neutralizing antibody.

Conclusions: The expression of R345W-Fibulin-3 alters the size, cargo, and function of EVs. Notably, EVs derived from RPE cells expressing R345W-Fibulin-3 are sufficient to enhance the rate of wound healing closure and elevate EMT marker expression in untransfected RPE cells.

Introduction

Extracellular vesicles (EVs) play a critical role in cell-cell communication and modulate cellular differentiation (115, 116, 201). In numerous tissues, EVs contribute to the regulation of epithelial-mesenchymal transition (EMT), including in the lungs, breasts, liver, and brain (117, 118, 120, 202). For example, myofibroblast-derived EVs are sufficient to induce normal fibroblasts to become myofibroblasts that possess mesenchymal features by upregulating transforming growth factor beta (TGF-β) pathways and EMT drivers (120). Recent studies have shown that alterations in EV size and cargo are dependent upon the secretory mechanisms and phenotypic status of their parental cells (203). This study examined the role of EVs secreted from retinal pigment epithelial (RPE) cells in the induction of EMT.

RPE cells form a monolayer of highly polarized cells that lie posterior to the neuroretina and are essential for maintaining the health and function of the adjacent photoreceptors. Loss of terminal differentiation and acquisition of a mesenchymal cell phenotype in RPE cells has been shown to occur in degenerative retinal diseases (26, 58, 91, 109, 204). As RPE cells become atrophic, the hallmark clinical lesions of sub-RPE lipoprotein deposits and pigmentary changes appear within the macula in diseases such as age-related macular degeneration (AMD) and Doyne honeycomb macular dystrophy (205-207). While RPE cells have been shown to secrete EVs (164, 208-210), their role in RPE function and dysfunction remains to be determined.

An inherited macular degeneration in which RPE dysfunction plays a significant role is Doyne honeycomb macular dystrophy, which results from a single arginine-to-tryptophan point mutation, R345W, in Fibulin-3 (86, 87). Fibulin-3 is an extracellular matrix protein that contains six epidermal growth factor (EGF)-like domains followed by a fibulin domain (184). The R345W mutation causes Fibulin-3 misfolding, poor Fibulin-3 secretion, and activation of the unfolded protein response (UPR) (89, 90). Previously, we found that overexpression of R345W-Fibulin-3 in RPE cells activates the UPR, attenuates RPE differentiation, and induces EMT in RPE cells (91). Previously, we found that overexpression of R345W-Fibulin-3 in RPE cells activates the UPR, attenuates RPE

differentiation, and induces EMT in RPE cells (91). Emerging evidence suggests that the accumulation of misfolded proteins drives EMT via activation of the UPR (78-81). Moreover, several studies have shown the interplay between ER stress and EV secretion (211-213). The mechanism by which the EV modulates cell fate has yet to be determined.

In this study, we investigated the mechanism by which EVs regulate EMT in RPE cells. EVs were isolated from media of cultured ARPE-19 cells expressing either WT or mutant Fibulin-3. Expression of the mutant protein altered the size of EVs and upregulated EMT markers including expression of transforming growth factor beta (TGF-β). EVs also enhanced the migration ability of RPE cells, indicating that EVs influence adjacent RPE cell differentiation. The data show that RPE-derived EVs strongly influence the phenotype of neighboring cells and likely play an important role in diseases of the posterior eye.

Results

Expression of R345W-Fibulin-3 alters EV size in RPE cells.

ARPE-19 cells were transfected with luciferase-tagged WT-Fibulin-3 or R345W-Fibulin-3 to overexpress these proteins. The cell lysate and cell culture media were collected to examine the extent of Fibulin3 secretion using the western blots and luciferase assay. Both western blots and luciferase assay results showed that Fibulin-3 secretion in the cell culture media of mutated ARPE-19 cells is significantly lower than that of WT cells (**Fig. 3-1 A-B**), suggesting that Fibulin-3 mutation led to reduced Fibulin-3 secretion in RPE cells.

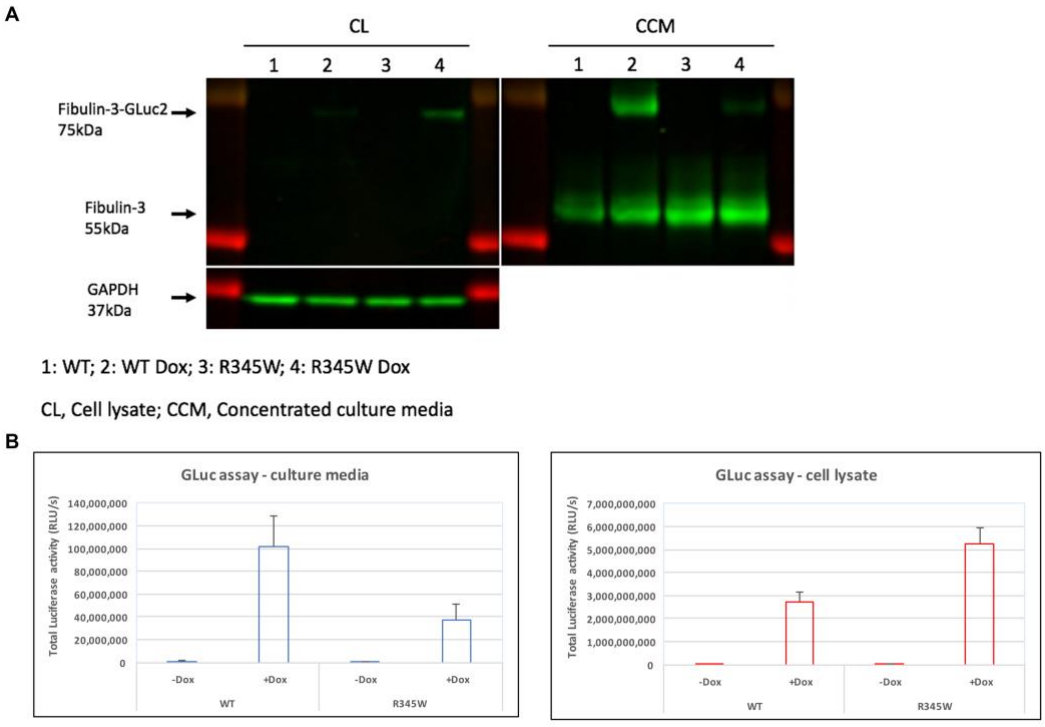

Figure 3-1. R345W-Fibulin-3 secretion is reduced in the mutated ARPE-19 cells. (A-B) ARPE-19 cells were transfected with luciferase-tagged WT-Fib3 or R345W-Fib3 to overexpress these proteins. The cell lysate and cell culture media were collected to examine the extent of Fibulin-3 secretion using the western blots and luciferase assay. The results show that in the cell lysate of R345W-ARPE is higher than that of WT-ARPE, whereas in the cell culture media of R345W-ARPE, the signal is lower than that of WT cells. All endogenous fibulin-3 (55 KD) was secreted to the cell culture media. GAPDH was used as an internal control. The results show that luciferase activity in the cell culture media of R345W-ARPE is also lower than that of WT cells. Taken together, these results suggest that R345W-Fibulin-3 leads to reduced Fibulin-3 secretion in RPE cells.

Conventional filtration and ultracentrifugation (P100K) and density gradient centrifugation (Pgrad) were used to isolate EVs. TEM and Cryo-EM were performed to study the morphology of the EVs (Pgrad). TEM imaging showed concave-appearing vesicles (**Fig. 3-2 A**) and cryo-EM showed spherical vesicles (**Fig. 3-2 B**), both with two subpopulations of EVs: a group with diameters around 30 nm and a group with diameters over 100 nm. NTA showed that, in the mutant group, the particle size distributions were smaller than those of the WT EVs **(Fig. 3-2 C**). There were no significant differences in the total amount of particles in these two groups or in the amount of protein per vesicle between WT and mutant groups (**Fig. 3-2 D-E**). Western immunoblots confirmed the presence of EV markers (P100K), including Alix, CD81, and CD63, in both WT and mutant EVs, as well as the absence of negative controls including mitochondrial import

inner membrane translocase subunit Tim23 (TIM23), Golgi matrix protein 130 (GM130), calnexin, and histone H3 (**Fig. 3-2 F).** GAPDH was not detected in EVs derived from ARPE-19 cells. A loading gel was used as a reference for protein amounts in different samples (**Fig. 3-3**).

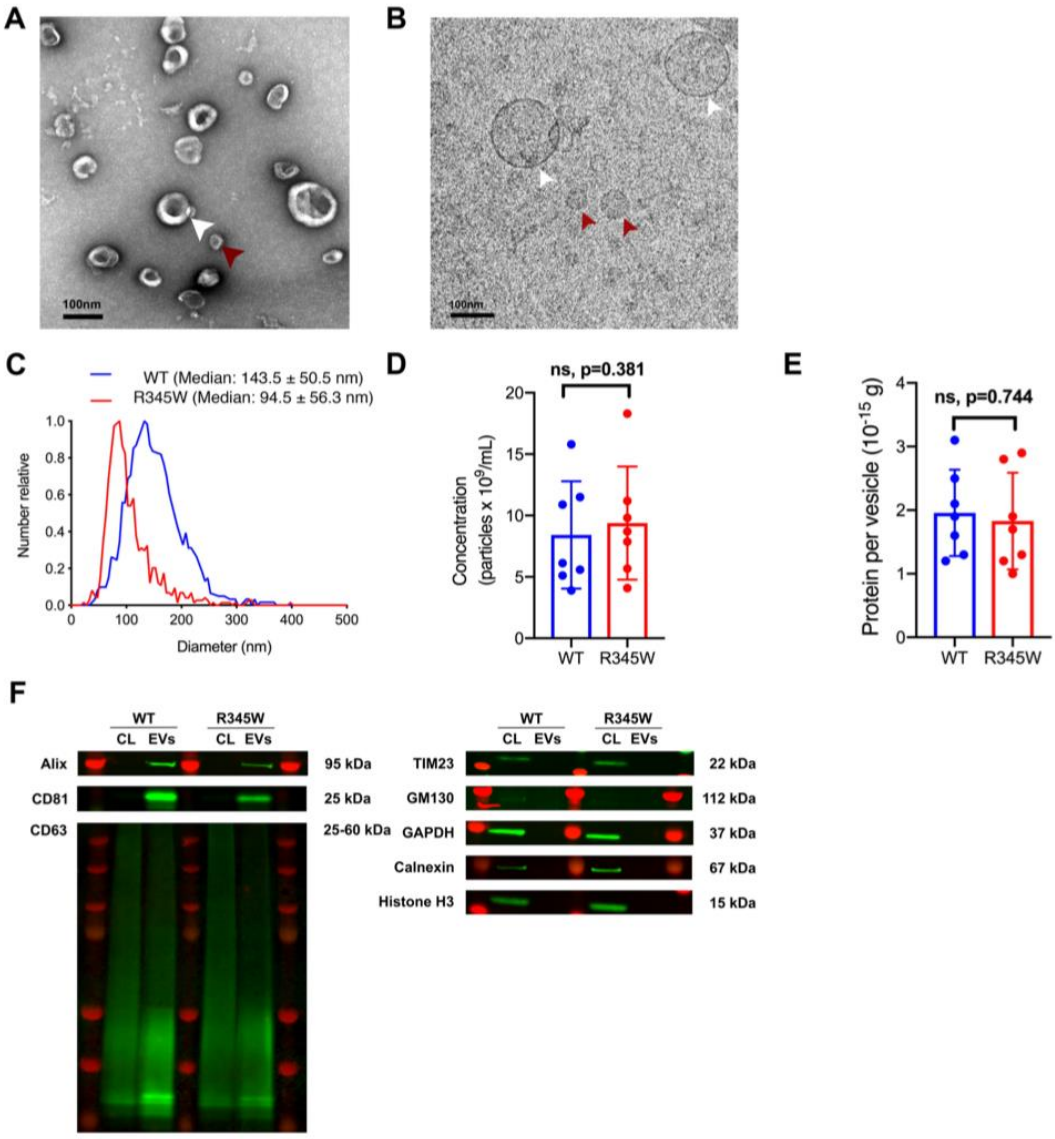

Figure 3-2. Expression of R345W-Fibulin-3 in RPE cells alters EV size. (A-B) TEM and cryoEM of EVs reveals two subpopulations: vesicles ~30 nm in diameter (red arrowhead) and vesicles over 100 nm in diameter (white arrowhead). Scale bar: 100 nm. (C) Nanoparticle tracking analysis confirms a median diameter of 143.5 nm and 94.5 nm for WT and mutant EVs, respectively. (DE) No significant differences in the total amount of vesicles or in the amount of protein per vesicle between WT and mutant groups are observed. (F) Western immunoblots confirmed the presence of EV markers (P100K), including Alix, CD81, and CD63, in both WT and mutant EVs and the absence of negative controls including TIM23, GM130, GAPDH, calnexin, and histone H3.

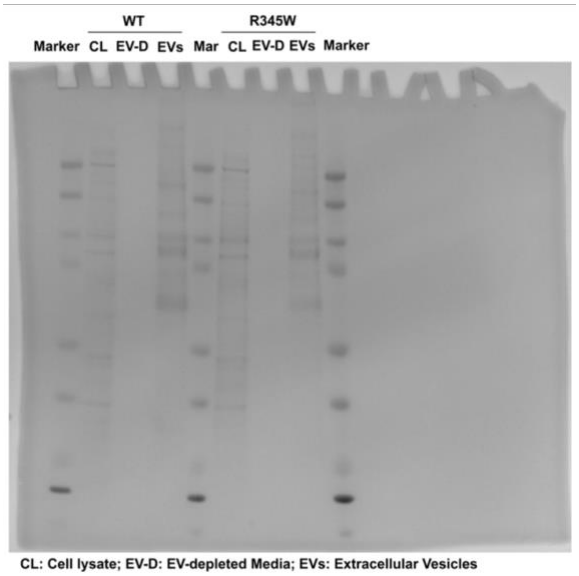

Figure 3-3. Loading gel. SDS-PAGE gel image showed the protein patterns of EVs isolated by differential centrifugation from WT and R345W cells, cell lysates (CL), and EV-depleted media (EV-D) after ultracentrifugation.

Expression of R345W-Fibulin-3 in RPE cells partially alters their EV cargo content.

EVs derived from WT and mutant ARPE-19 cells were purified using sucrose cushion and iodixanol buoyant density gradient ultracentrifugation (Pgrad). Final ultracentrifugation yields 10 remaining fractions, with EVs in the third fraction from the top (density = 1.096) (214). Ten fractions were collected, and each 1 mL fraction was diluted to 10 mL with HBS and spun at 150,000 g for 3 hours at 4°C. The supernatant was removed and the pellet was re-suspended in 50 µL HBS. SDS-PAGE gels showed distinct differences in protein distribution pattern between these groups in both fraction and pellet samples (**Fig. 3-4 A-B**). Western immunoblots confirmed the presence of EV markers (Pgrad), including Alix, HSP70, Flotillin-1, CD81, and CD63 in the WT EV pellets (**Fig. 3-4 C**).

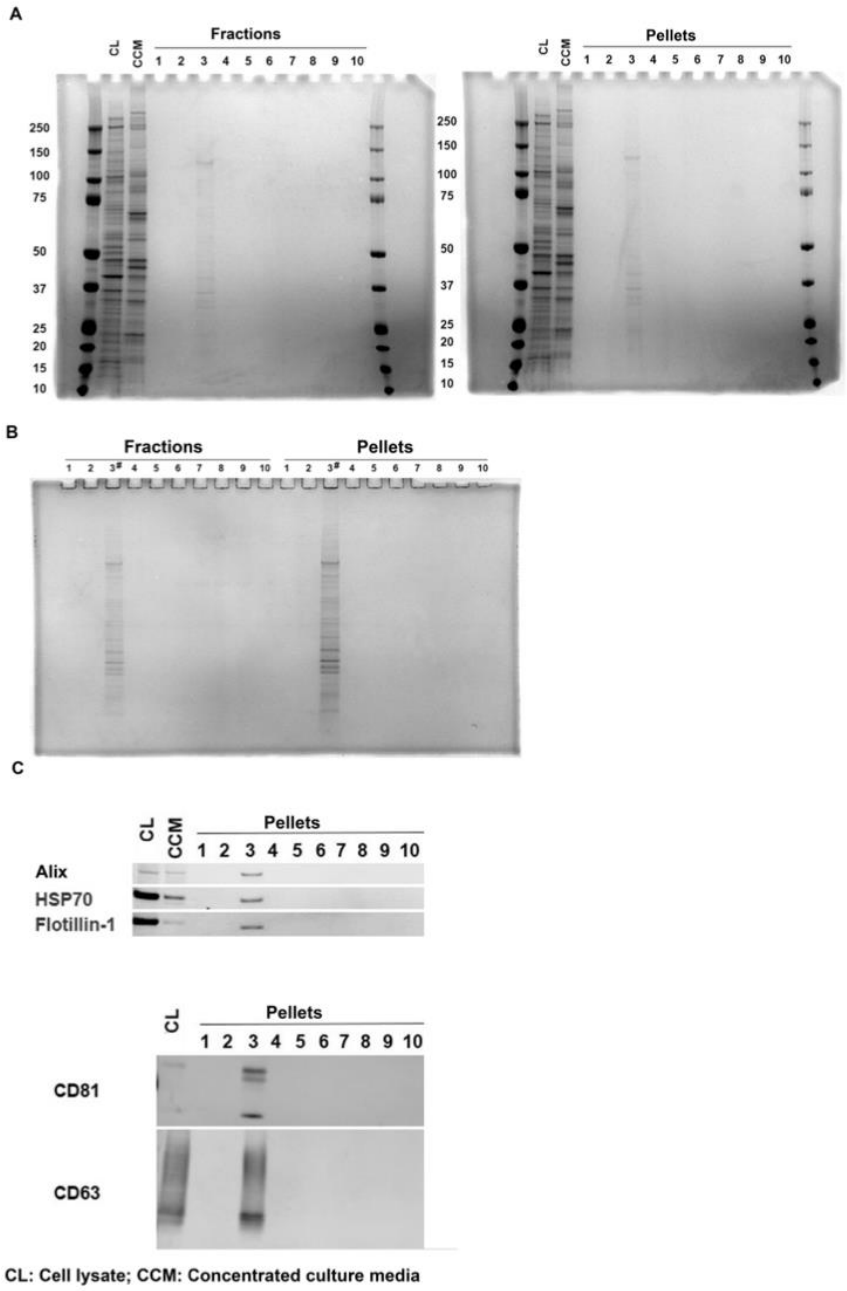

Figure 3-4: Expression of R345W-Fibulin-3 in RPE cells alters EV content. (A) EVs derived from ARPE-19 cells expressing WT-Fibulin-3 or (B) EVs derived from ARPE-19 cells expressing R345W-Fibulin-3 were purified using sucrose cushion and iodixanol buoyant density gradient ultracentrifugation. SDS-PAGE gels showed distinct differences in protein distribution patterns between these groups in both fraction and pellet samples. Cell lysates (CL) and concentrated culture media (CCM) were used as controls. (C) Western immunoblots showed EV markers in the third fraction, including Alix, HSP70, Flotillin-1, CD81 and CD63.

EVs (Pgrad) derived from WT and mutant ARPE-19 cells were subjected to proteomic analysis. A total of 2,852 proteins were identified in WT-Fibulin-3 EVs, and 2,868 proteins were identified in mutant Fibulin-3 EVs (**Fig. 3-5 A**). The log differential expression (Log_2DE) was calculated by determining the differential expression of R345W and WT, then taking the log base 2 of that value. Downregulated proteins in the sonic hedgehog signaling (SHH) and primary cilia pathways and upregulated EMT markers are listed in the table (**Fig. 3-5 B**). Pathway analysis revealed that SHH pathway was found to be, 3- to 5-fold, significantly more abundant in EVs derived from WT ARPE-19 cells, suggesting a role for RPE EVs in the maintenance of RPE cell and photoreceptor differentiation (8, 215). In contrast, lysosome components, and ribosome components were found to be, 3- to 7-fold, significantly more abundant in EVs secreted from mutant ARPE-19 cells (**Fig. 3-5 B-C, Fig. 3-6**). Moreover, Pathway analysis revealed that primary cilia, EV assembly, and ESCRT I complex pathways were found to be more abundant in EVs derived from WT ARPE-19 cells. In contrast, large ribosomal subunit was found to be more abundant in EVs secreted from mutant ARPE-19 cells (**Fig. 3-7**). Western blocts were used to validate the proteomic data. Proteomic analyses and protein expression quantification of western blots (band density using Fiji) show that WT-ARPE-EV exhibit greater ALIX, ZO-1, CD63 and CD81, and lesser Flotilin-1, Annexin A5 and Fibulin-3 content compared to R345W-ARPE-EV (**Fig. 3-8**).

A

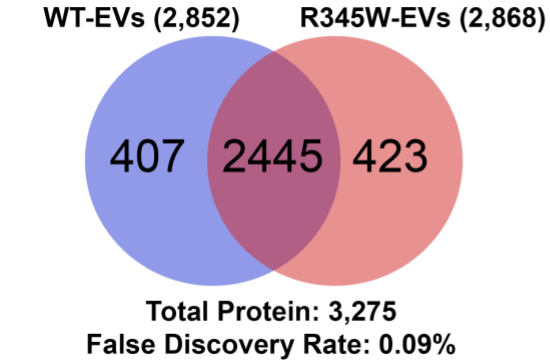

B

Proteins	Differential Expression (R345W-WT)
SHH and primary cilia	
ULK3	0.36
KIF7	0.31
SMO	0.29
CSNK1G1	0.18
CSNK1G2	0.26
EMT markers	
VIM	7.5
HTRA1	3.2
MMP14	3.9
MMP15	3.6
SMAD4	2.0

C

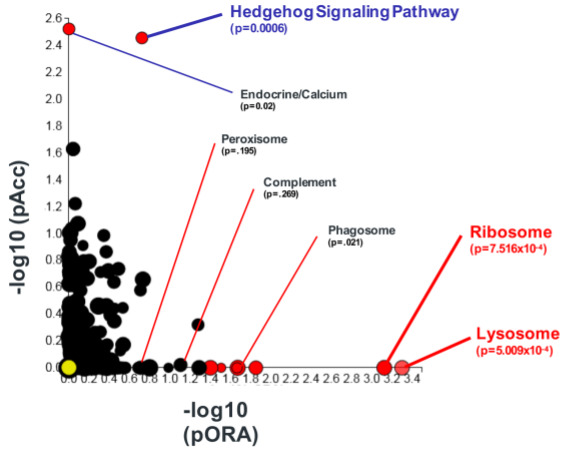

Figure 3-5. Proteomic analysis of RPE EVs reveal markers of EMT. (A) A total of 2,852 proteins were identified in WT-Fibulin-3 EVs, and 2,868 proteins were identified in R345W-Fibulin-3 EVs. (B) Table of selected proteins and fold-change in spectral counts from proteomic profiling between WT RPE EVs and mutant RPE EVs. (C) Pathway analysis revealed that sonic hedgehog (SHH) pathways was found to be 3- to 5-fold more abundant in EVs derived from WT ARPE-19 cells. In contrast, EMT drivers, lysosome components, and ribosome components were found to be 3- to 7-fold more abundant in EVs secreted from mutant ARPE-19 cells.

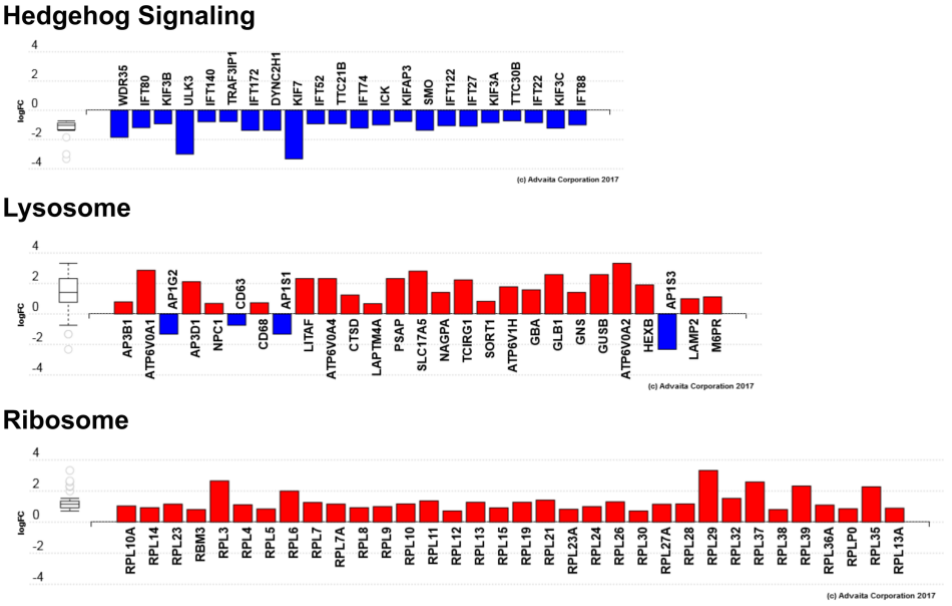

Figure 3-6. Pathway analysis 1. (A) Pathway analysis revealed that SHH pathways was found to be significantly more abundant in EVs derived from WT ARPE-19 cells. (B) In contrast, lysosome components, and ribosome components were found to be significantly more abundant in EVs secreted from mutant ARPE-19 cells.

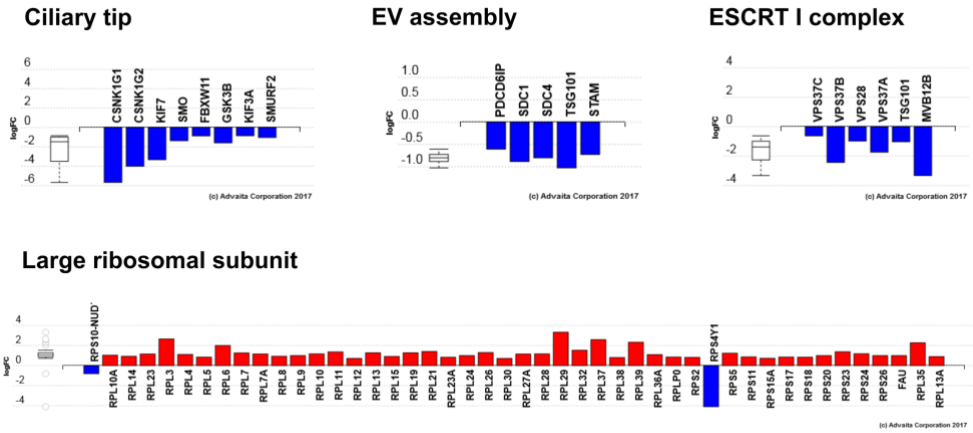

Figure 3-7. Pathway analysis 2. (A) Pathway analysis revealed that primary cilia, EV assembly, and ESCRT I complex pathways were found to be more abundant in EVs derived from WT ARPE-19 cells. (B) In contrast, large ribosomal subunit was found to be more abundant in EVs secreted from mutant ARPE-19 cells.

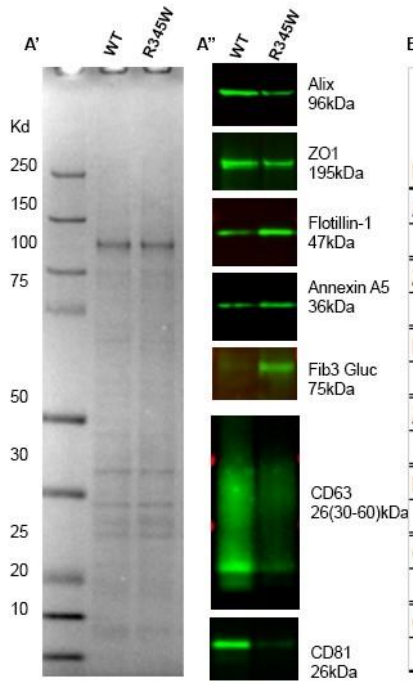

B

Protein	Quantification	WT	R345W	Fold change from WT
ALIX	Spectral Count	837	550	-1.52
	Protein expression	0.69	0.24	-2.81
ZO1	Spectral Count	269	81	-3.32
	Protein expression	0.68	0.33	-2.06
Flotilin	Spectral Count	119	166	1.39
	Protein expression	0.39	0.50	1.26
Annexin A5	Spectral Count	358	487	1.36
	Protein expression	0.28	0.36	1.28
Fibulin 3	Spectral Count	0	13	N/A
	Protein expression	0.06	0.14	2.46
CD63	Spectral Count	367	219	-1.68
	Protein expression	0.59	0.19	-3.08
CD81	Spectral Count	222	86	-2.58
	Protein expression	0.83	0.11	-7.29

Figure 3-8. Validation of proteomics. Our proteomic analyses and protein expression quantification of western blots (band density using Fiji) show that WT-ARPE-EV exhibit greater ALIX, ZO-1, CD63 and CD81, and lesser Flotilin-1, Annexin A5 and Fibulin-3 content compared to R345W-ARPE-EV.

R345W-RPE-derived EVs have increased TGF-β1 protein.

TGF-β is a well-known regulator of EMT (100). Recent studies have shown that EV-bound TGF-β1 can induce EMT in recipient cells (120). Studies in post-mortem AMD eyes found upregulation of well-known drivers of EMT, namely, TGF-β and vimentin (VIM) (26, 41, 43). Recent studies have shown that EV-bound TGF-β1 can induce EMT in recipient cells (120).

To test whether induction of mutant Fibulin-3 alters TGF-β protein content, we quantified TGF-β1 protein in cell culture media, EV-depleted media, and EVs in both WT and mutant groups using a commercial ELISA. Cell culture media were collected from ARPE-19 cells expressing either WT-Fibulin-3 or R345W-Fibulin-3 after culturing for 48 hours. EVs (P100K) were isolated from WT and mutant ARPE-19 cells and EV-depleted media was collected as well. Media left over after EVs are centrifuged out were collected as EV-depleted media. Our experimental results revealed that, compared to the WT media

and EV-depleted media, the amount of TGF-β1 protein was significantly greater in the mutant media and EV-depleted media (each experiment was performed in duplicate, n=3, $p<0.01$) (**Fig. 3-9 A**). In addition, compared to the WT EVs, TGF-β1 protein was significantly more abundant in the mutant EVs (each experiment was performed in duplicate, n=3, $p<0.01$) (**Fig. 3-9 B**). These results suggest that expression of mutant Fibulin-3 induces a higher abundance of TGF-β1 protein in RPE cells and EVs derived from RPE cells. We have quantified the ratio of EV-bound TGF-β1 to free TGF-β1. The results show that EV-bound:free TGF-β1 is approximately 3:1 and 2:1 for WT and R345W, respectively, suggesting that EV-derived TGF-β1 might play an important role in mediating EMT in RPE cells (**Fig. 3-9 C**).

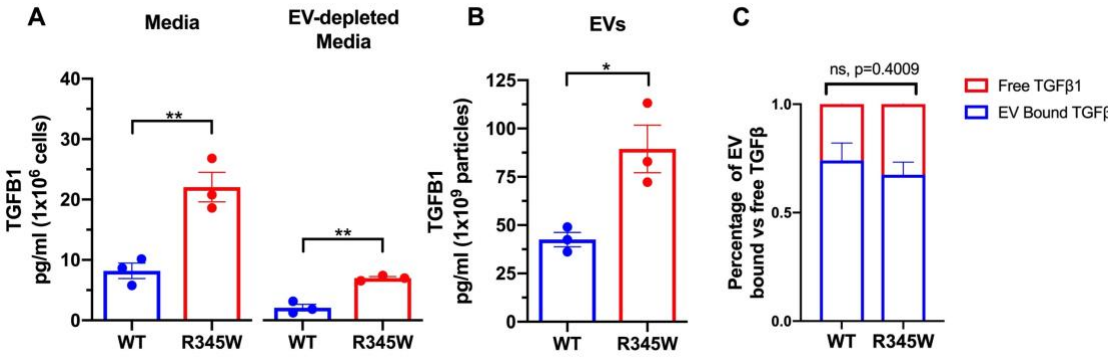

*Figure 3-9. R345W EVs demonstrate increased TGF-β1 content. TGF-β1 content in media, EV-depleted media, and EVs from WT and R345W groups were quantified by ELISA. (A) R345W media and EV-depleted media contain significantly more TGF-β1protein (n=3, each experiment was performed in duplicate). (B) R345W EVs show significantly greater TGF-β1 protein compared to WT EVs (n=3, each experiment was performed in duplicate). (C) We have quantified the ratio of EV-bound TGFB1 to free TGFB1. The results show that EV-bound:free TGFB1 is approximately 3:1 and 2:1 for WT and R345W, respectively, suggesting that EV-derived TGFB1 play an important role in mediating EMT in RPE cells. A student's unpaired t-test was used to compare differences between groups. Data are presented as mean ± SEM, *p< 0.05, **p< 0.01.*

<u>RPE-derived EVs are taken up by recipient RPE cells.</u>

Confocal images show green puncta located within the cell body of ARPE-19 cells (labeled for phalloidin staining for actin [greyscale]) that were incubated with PKH67-labeled WT- or R345W-EVs at $1x10^{10}$ vesicles/mL for 8 hours. No green puncta were present in cells that were not incubated with EVs (**Fig. 3-10**). Number of EVs was quantified using ImageJ. There are no significant differences regarding EV uptake per area ($1mm^2$) between WT and R345W groups (n=3, ns, p=0.3391) (**Fig. 3-11**).

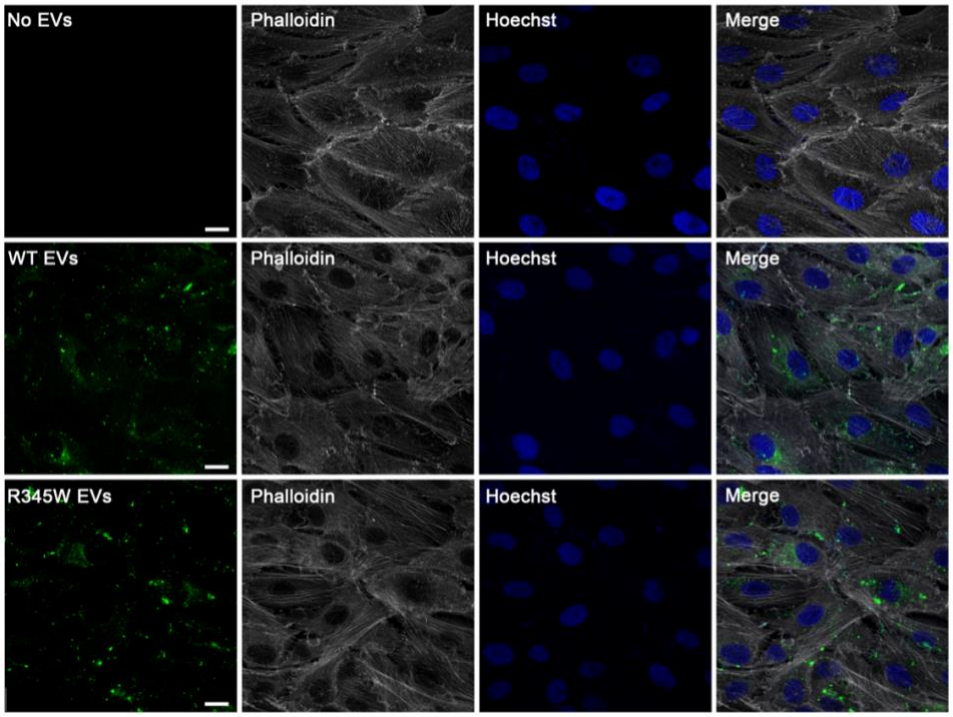

Figure 3-10. EVs were taken up by ARPE-19 cells. Confocal images (1024 x 1024; z-stack: 2.8µm; z-step: 0.186µm) showing PKH67-labeled WT- or R345W-EVs (green) were taken up by ARPE19 cells after an 8 hours incubation period. Phalloidin staining for actin was used to label the cell body (greyscale); Hoechst was used to label the nuclei (blue). Scale bar = 15 µm.

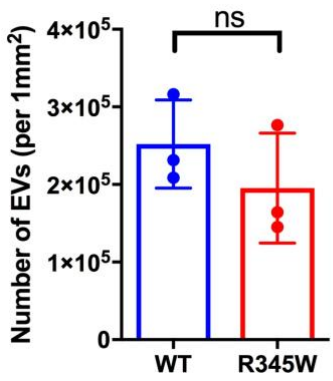

Figure 3-11: No differences regarding EV e between WT and mutant groups. Number of was quantified using the Analyze Particle on in Fiji. There are no significant differences ding EV uptake per area (1mm²) between WT R345W groups (n=3, 3 regions per n, p=0.3391).

Fibulin-3 is outside of EV rather than within them.

To determine the orientation of WT-Fibulin-3 and R345W-Fibulin-3 in EV, EV were incubated with trypsin. A low concentration of trypsin can only digest proteins outside of EV. However, a high concentration of trypsin can destabilize the EV membrane, enabling access to the inside of the vesicles and digestion of proteins on both the inside and outside of the vesicles (216). EGFR and Flotillin-1, which are known to be transmembrane members of EVs, and ALIX, a protein known to be present within the EV lumen, were used as controls. Western blots were conducted to quantify the remaining proteins. We found that both WT-fibulin-3 and R345W-fibulin-3 can be digested with a concentration of trypsin (0.1 g/g), but not EGFR, Flotillin-1, or ALIX. These results indicate that Fibulin-3 is outside of EV rather than within them. (**Fig. 3-12**).

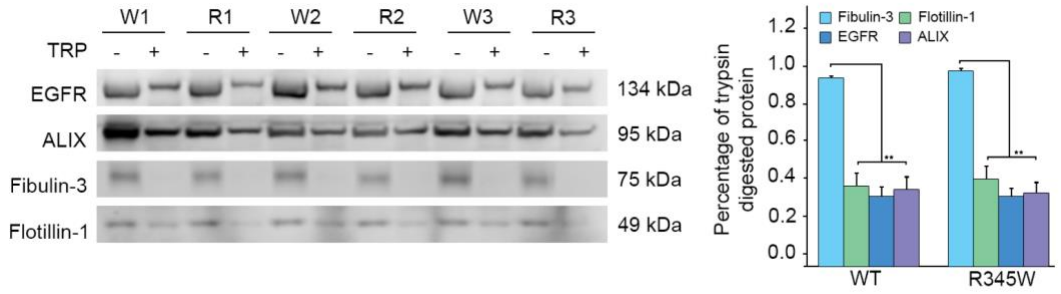

*Figure 3-12. Fibulin-3 is located on the outside of EVs. Trypsin (0.1 g/g) was incubated with EVs derived from ARPE-19 cells for 30 minutes. (n=3). Western blots were then conducted. A) Only Fibulin-3 was fully digested, bands for EGFR, Flotilin-1 or ALIX were still prominent following trypsin digestion, B) Western blots were analyzed using Image J software. Both WT-fibulin-3 and R345W-fibulin-3 can be digested for approximate 90% with a concentration of trypsin (0.1 g/g), but EGFR, Flotillin-1, or ALIX can only be digested for approximate 30%. Data are presented as mean ± SEM, **p< 0.01. Abbreviations: W, WT-ARPE-EV; R, R345W-ARPE-EV; TRP, Trypsin; EGFR, epidermal growth factor receptor; Alix, apoptosis-linked gene-2 interacting protein X.*

R345W-RPE-derived EVs are sufficient to enhance migration abilities and upregulate EMT markers in recipient RPE cells.

EV transfer experiments were conducted to determine if EVs from mutant cells are sufficient to promote EMT in naive cells. EVs (P100K) were isolated from ARPE-19 cells expressing WT-Fibulin-3 or R345W-Fibulin-3. Naive ARPE-19 cells were seeded onto a

96-well plate ($5x10^4$/well). On Day 1, the wound was created, each well was rinsed with PBS, and media containing WT or mutant EVs were added to the appropriate wells. ARPE-19 cells grown on FBS depleted media without adding EVs were used as controls. A total of n=8 was used for each group, and the experiment was repeated three times with new EV preparations. EV concentrations were chosen according to a previously published study (120). For these studies, 1 $x10^{10}$/mL EVs were used. A schematic for the scratch assay timeline is shown (**Fig. 3-13 A**). To compare across groups, the maximum recovery at 72 hours was used to determine the time required to close half of the wound area. The mean half-max wound recovery time across three experiments revealed that EVs from mutant cells had the fastest wound recovery time (**Fig. 3-13 B-C**). No significant differences were found between no EV and WT EV groups (p=0.116).

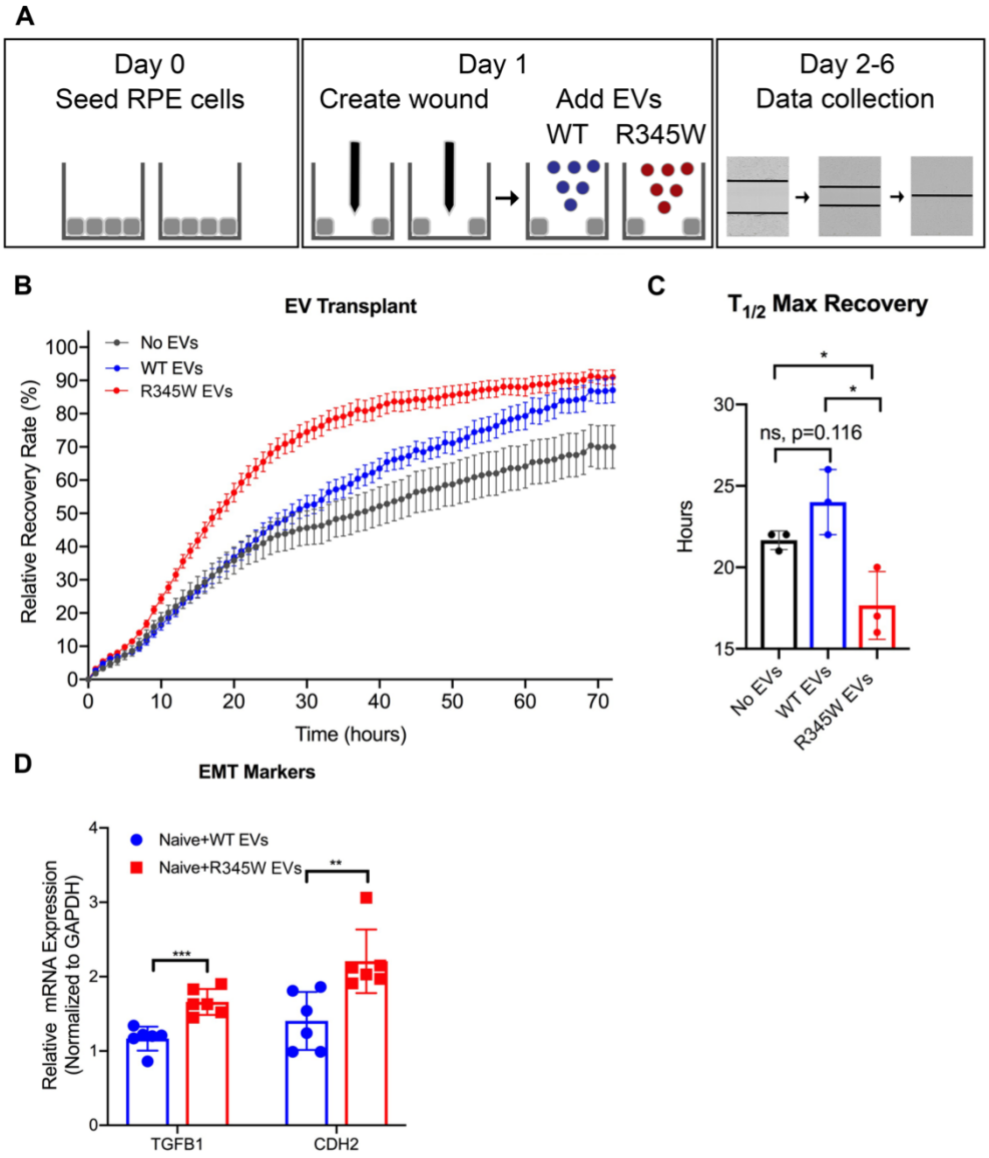

*Figure 3-13. RPE-derived EVs are sufficient to enhance migration abilities in RPE cells. (A) On Day 0, naive ARPE-19 cells were seeded onto a 96-well plate. On Day 1, the wound was created, each well was rinsed with PBS, and media containing WT or mutant EVs were added to the appropriate wells. On Days 2-6, recovery rate was automatically analyzed by the software. (B-C) Scratch assays show that, compared to the cell-only (T 1/2 = 21± 0.5 hours) and cells exposed to WT EVs groups (T 1/2 = 24± 1.6 hours), exposing ARPE-19 cells to mutant RPE cell-derived EVs resulted in a faster rate of 50% wound closure (T 1/2 = 17± 1.7 hours). One-way analysis of variance (ANOVA) was used with a Tukey post-test. Data are presented as mean ± SEM, *p<0.05. (D) The relative quantity of mRNA in naive ARPE-19 cells was normalized to GAPDH and then normalized to the control group (No EVs). RT-PCR analysis show that, compared to the control (No EVs) and WT EVs, the mRNA expression levels of EMT markers TGF-β1 and CDH2 were significantly greater in cells treated with mutant EVs (n=6). Student's unpaired t-test was used to compare differences between groups. Data are presented as mean ± SEM, **p<0.01, **p< 0.001.*

Using RT-PCR, we compared the expression levels of EMT-promoting factors (TGF-β1, cadherin 2 (CDH2)) in each group 24 hours after EV treatment. ARPE-19 cells grown on FBS depleted media without adding EVs were used as controls. The relative quantity of mRNA was normalized to GAPDH and then normalized to the control group (no EVs). GAPDH was validated as an internal control. Compared to the control group (No EVs) and WT EVs, increased mRNA expression levels of EMT markers were found in cells treated with mutant EVs (n=6, **p<0.01, ***p<0.001) (**Fig. 3-13 D**).

EV surface TGF-β1 inducing EMT has been shown in several studies (117, 217, 218). We found that the groups pre-incubated with pan-TGF-β-neutralizing antibody had a significant slower recovery rate compared to the control group and isotype IgG group, suggesting that TGF-β signaling is important for the EMT effects of EVs on recipient RPE cells (n=6, *p<0.05, **p<0.01, ***p<0.001) (**Fig. 3-14 A-C**).

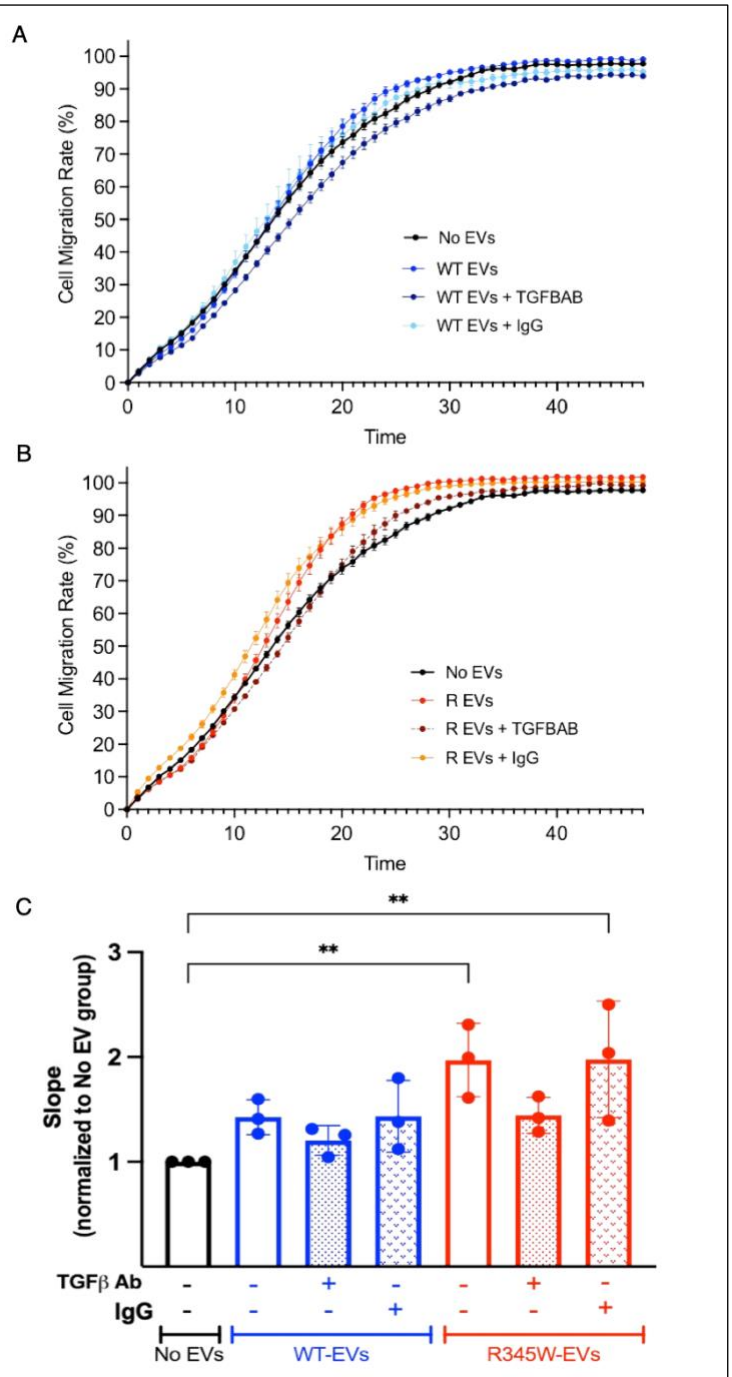

*Figure 3-14. Pre-incubated with pan-TGF-β-neutralizing antibody had a significant slower recovery rate compared to the control group and isotype IgG group. (A) WT EVs; (B) R345W-EVs; (C) Statistic analysis showed that in mutant groups, pan-TGF-β-neutralizing antibody had a significant slower recovery rate compared to the control group and isotype IgG group (n=6, *p<0.05, **p<0.01, ***p<0.001).*

Discussion

Under normal conditions, RPE cells are terminally differentiated cells that rarely divide or proliferate (219). Recent studies in post-mortem age-related macular degeneration (AMD) eyes have found upregulation of critical EMT drivers such as TGF-β, VIM, and Snail (26, 41, 43). These findings suggest that dysfunctional RPE cells are capable of migration and proliferation. In other tissues, EMT is regulated, in part, by EVs, suggesting that this mechanism may also be possible in RPE cells (117, 118, 202).

In this study, we investigate the role of EVs in the induction of EMT in RPE cells. We first showed that expression of the misfolded protein R345W-Fibulin-3 alters the size of EVs. TEM showed concave-appearing vesicles while cryo-EM imaging showed spherical vesicles. In both forms of imaging there were a variety of different sizes which segregated as about 30 nm diameter and over 100 nm diameter using NTA, confirming that EVs derived from mutant cells were smaller on average than those derived from WT cells. Despite this difference in vesicle size, the amount of protein was not significantly different between the two vesicle types, suggesting that the size difference alone between these two populations does not have a broad impact on the amount of vesicle cargo. A recent study demonstrated, however, that the complexities of heterogeneous EV subpopulations may imply distinct biological functions (203), further emphasizing the importance of separating and studying subpopulations of EVs.

We next examined whether expression of R345W-Fibulin-3 alters EV cargo. Interestingly, we found that EVs derived from RPE cells overexpressing WT-Fibulin-3 contain critical members of SHH and primary cilium pathways. SHH coordinates photoreceptor differentiation during development (220), and the primary cilium pathway regulates cellular differentiation and division by mediating hedgehog and Wnt signaling (221). Prior studies have shown that abnormal activation or absence of primary ciliary signaling is associated with less differentiation and uncontrolled cell division (222). A reduction of 3- to 5- fold in SHH and ciliary tip signaling in EVs derived from RPE cells overexpressing R345W-Fibulin-3 suggests that the RPE cells may lose their capacity to provide effective support mechanisms that maintain photoreceptor outer segments.

ALIX, an ESCRT-related protein, is required for EV secretion(128). Tetraspanins, such as CD63 and CD81, are highly enriched in EVs relative to their content in the respective producing cells(128). Both our proteomic analyses and western blot analysis have shown that WT-ARPE-EV exhibit greater ALIX, CD63 and CD81 content compared to R345W-ARPE-EV. This EV compositional heterogeneity results from EV biogenesis operating across a spectrum of endosomal and plasma membranes (223, 224). These results suggest that expression of R345W-Fibulin-3 may alter the mechanism of EV secretion from an ESCRT-dependent to an ESCRT-independent mechanism.

TGF-β ELISAs revealed greater TGF-β1 protein content in mutant EVs, consistent with the proteomic data showing that EMT drivers were found to be 3- to 7-fold more abundant in R345W EVs compared to WT EVs. This finding is consistent with our prior work showing that expression of R345W-Fibulin-3 activates the UPR in RPE cells. Specifically, the IRE1/XBP1 pathway is preferentially upregulated after expression of R345W-Fibulin-3 in primary RPE cells (91). The UPR and TGF-β-induced EMT signaling pathways interact in an IRE1-dependent manner (94-96). Taken together, these data suggest a role for TGF-β1 in EV-induced EMT of ARPE-19 cells.

EV transplant experiments were conducted to determine if EVs from mutant cells are sufficient to enhance migration abilities. Previous studies in our lab showed that expression of mutant Fibulin-3 accelerates wound healing (91). In this study, our experiments reveal that mutant EVs accelerate RPE proliferation and migration to a similar extent as does the expression of mutant Fibulin-3, suggesting that EVs play a major role in driving EMT of RPE cells. Moreover, the data show that expression levels of EMT-promoting factors were greater after mutant EV treatment.

Conclusion

In summary, our experimental results indicate that misfolded proteins in RPE cells alter specific EV cargo, resulting in EVs that are able to enhance migration abilities in the recipient cells. **Fig. 3-15** illustrates our working model for EV-induced RPE cell EMT. The

findings from this study will help elucidate the mechanisms underlying RPE dysfunction in macular degenerations.

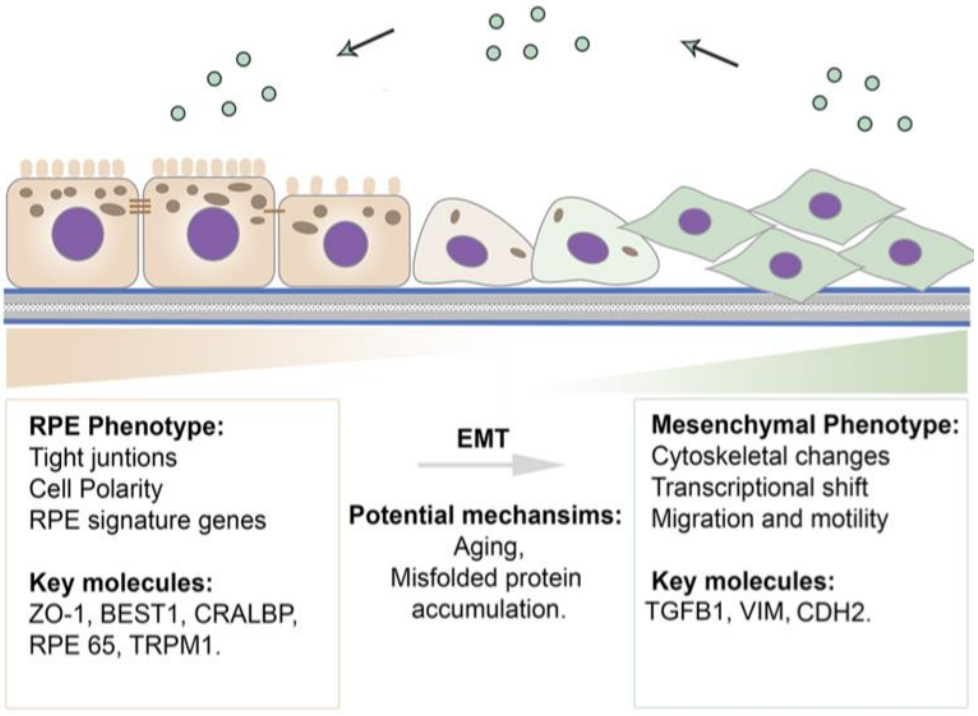

Figure 3-15. RPE EVs impact adjacent RPE cell differentiation. Schematic illustration showing the proposed theory that EVs impact adjacent RPE cell differentiation. The green circles represent EVs derived from RPE cells expressing R345W-Fibulin-3.

CHAPTER 4. SUMMARY OF RESEARCH, IMPLICATIONS, AND FUTURE RESEARCH DIRECTIONS

Preface

In early chapters, I described the central role that retinal pigment epithelial (RPE) cells play in maintaining the health and functional integrity of both photoreceptors and the choroid. This functional unit is required for maintaining proper visual function. Numerous retinal degenerative diseases are initiated by RPE dysfunction, including several inherited retinal degenerations and age-related macular degeneration (AMD). However, the molecular mechanisms underlying RPE dysfunction in retinal degeneration remain unknown. This gap in knowledge hinders the design of therapeutics aimed at preventing or reversing retinal degeneration prior to the development of severe vision loss. Therefore, the goal of the current study was to identify the molecular mechanisms that initiate and exacerbate RPE dysfunction so that future work can target early-stage disease and prevent vision loss.

Accumulation of misfolded protein induce RPE cells undergo EMT.

Recent studies have found that epithelial-mesenchymal transition (EMT) plays an essential role in many ocular degenerative diseases, including proliferative vitreoretinopathy (PVR) (27, 50, 182), neovascular ("wet") age-related macular degeneration (AMD) (41, 225), atrophic ("dry") AMD (26, 226), and diabetic retinopathy (DR)(227). The Age-Related Eye Disease Study (AREDS) identified two clinical risk factors for disease progression, namely, 1) drusen burden and 2) presence of pigment abnormalities (4). Intraretinal hyperreflective foci (HRF) detectable on optical coherence tomography (OCT) imaging were found to correlate with pigment on fundus imaging (39, 40). Studies using polarimetry with autofluorescence imaging suggest that these HRF are actually RPE cells that have migrated into the neuroretina (41, 42). Consistent with these

studies, our data suggest that RPE cells retain a reprogramming capacity to move along a continuum between polarized epithelial cells and mesenchymal cells and RPE dysfunction is the movement along this continuum toward a mesenchymal phenotype. As such, we propose that those pigment abnormalities RPE cells that have migrated into the neuroretina.

The data presented in this dissertation elucidate the underlying mechanisms that contribute to the retina pathophysiology. The first major finding focused on the role of misfolded protein accumulation in RPE dedifferentiation and EMT. The data shown in Chapter 2 demonstrated that expression of misfolded fibulin-3 in RPE cells activates ER stress via the IRE1α/XBP1 pathway, which in turn activates the EMT pathway and attenuates differentiation in RPE cells, as indicated by disrupted tight junctions, impairment of polarized proteins, and downregulated RPE signature gene expression. Furthermore, we reported that the expression of misfolded Fibulin-3 upregulates EMT markers and enhances the migration ability of RPE cells.

Numerous studies have implicated disrupted RPE cell proteostasis as a contributing factor to the pathogenesis of AMD (228-230). Age, a major risk factor for AMD, is associated with chronic low-grade oxidative stress and accumulation of misfolded proteins (229). The serine protease HTRA1 is associated with several protein misfolding disorders (231, 232), and a large genome-wide association study revealed that HTRA-1 is a major genetic risk factor for AMD (233). However, the underlying mechanisms by which misfolded protein accumulation leads to RPE cell dysfunction in AMD remains to be determined. ts045-VSVG is misfolded and retained in the ER at 39 °C, and it is able to refold and exit the ER at 32 °C (234). In RPE cells, ts045-VSVG has been used as a positive control for studying the underlying mechanisms by which the accumulation of misfolded proteins activate ER stress (235). Further study should focus on whether the expression of ts045-VSVG in RPE cells at 39 °C attenuates RPE differentiation and promotes EMT of RPE cells.

Several inherited macular degenerations are phenotypically similar to AMD and are frequently used to gain insight into AMD pathogenesis (89, 236, 237). Three autosomal dominant macular degenerations are of particular interest, as they result from a single point

mutation in proteins uniquely expressed and secreted by RPE cells (89, 237, 238). 1) Doyne honeycomb macular dystrophy (DHC) results from an R345W mutation in Fibulin-3 (86, 87), an extracellular matrix protein and downstream target of HTRA1 (88). The R345W mutation causes Fibulin-3 misfolding, poor Fibulin-3 secretion, and activation of the unfolded protein response (UPR) (89, 90). 2) Several mutations in the tissue inhibitor of metalloproteinases 3 (TIMP3) gene also cause protein misfolding and the development of the clinical condition Sorsby's fundus dystrophy (SFD) (238). TIMP3 is present within an AMD risk locus (233), and prior studies have shown that Fibulin-3 and TIMP3 are bound together within the extracellular matrix (239). 3) Mutations in Complement C1q Tumor Necrosis Factor-Related Protein 5 (C1QTNF5) also lead to protein misfolding and the development of the clinical condition known as Late-Onset Retinal Degeneration (LORD) (240). We have shown that mutant Fibulin-3 induces EMT in RPE cells. Future studies should focus on TIMP3 and C1QTNF5 mutations to investigate the causative role of protein misfolding in the development of RPE dysfunction.

Emerging evidence suggests that the accumulation of misfolded proteins drives EMT via activation of the UPR (78-81). UPR activation involves several mechanisms aimed at reducing the load of aberrant protein accumulation. Three ER transmembrane sensors, IRE1, PERK, and ATF6, determine the proper adaptive response by promoting cells to proliferate, change shape, or undergo apoptosis (92, 93) (**Fig. 4-1**). New evidence is emerging that accumulation of misfolded protein activates IRE-XBP1, which in turn modulates cell fate and can induce EMT (92, 97, 98) by altering specific EV cargo (241). In RPE cells, loss of IRE-XBP1 expression results in apoptosis (242, 243).

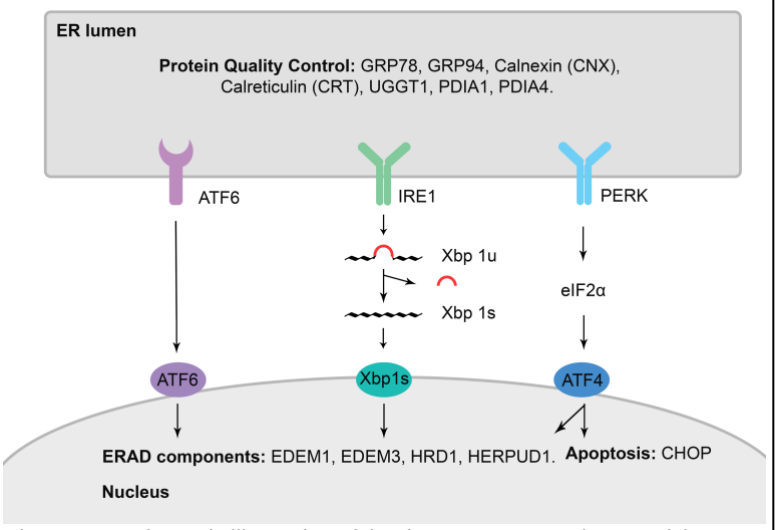

Figure 4-1. Schematic illustration of the three common pathways of the UPR.

In Chapter 2, we showed that, although the expression of each of the three ER transmembrane sensors were elevated, the IRE1/XBP1 pathway was primarily elevated compared to controls. These results suggest that expression of mutant Fibulin-3 activates ER stress in RPE cells primarily through the IRE/XBP1 pathway. Accumulation of misfolded proteins activates the NK/p38-MAPK pathway, which crosstalks with TGF-β-induced non-Smad pathways in an IRE-dependent manner. The molecular mechanisms by which the UPR modulates cell fate are yet to be determined.

Interaction between Fibulin-3 and TGFβ1

Fibulins are a family of eight extracellular glycoproteins that play a critical role in maintaining the normal function of extracellular matrix. Fibulins consists predominantly of repeated calcium-binding epidermal growth factor (cbEGF)-like modules followed by fibulin domain. Fibulin-3 belongs to the Fibulin family and has six EGF-like domains followed by a fibulin domain (**Fig. 4-2**) (184). TGF β1 is a dimeric polypeptide. Pro-TGFβ1 consists of a dimer TGFβ1and a latency-associated peptide (LAP). Activation of TGFβ1 requires the cleavage of TGFβ1 from the LAP. The latent TGFβ binding proteins (LTBP) are a family of carrier proteins. Previous studies have shown that fibulins modulate TGFβ

activation and signaling in extracellular matrix (244). Particularly, cbEGF-like domains regulate TGFβ by interacting LTBP (245, 246). In addition, Fibulin-2 is present on the

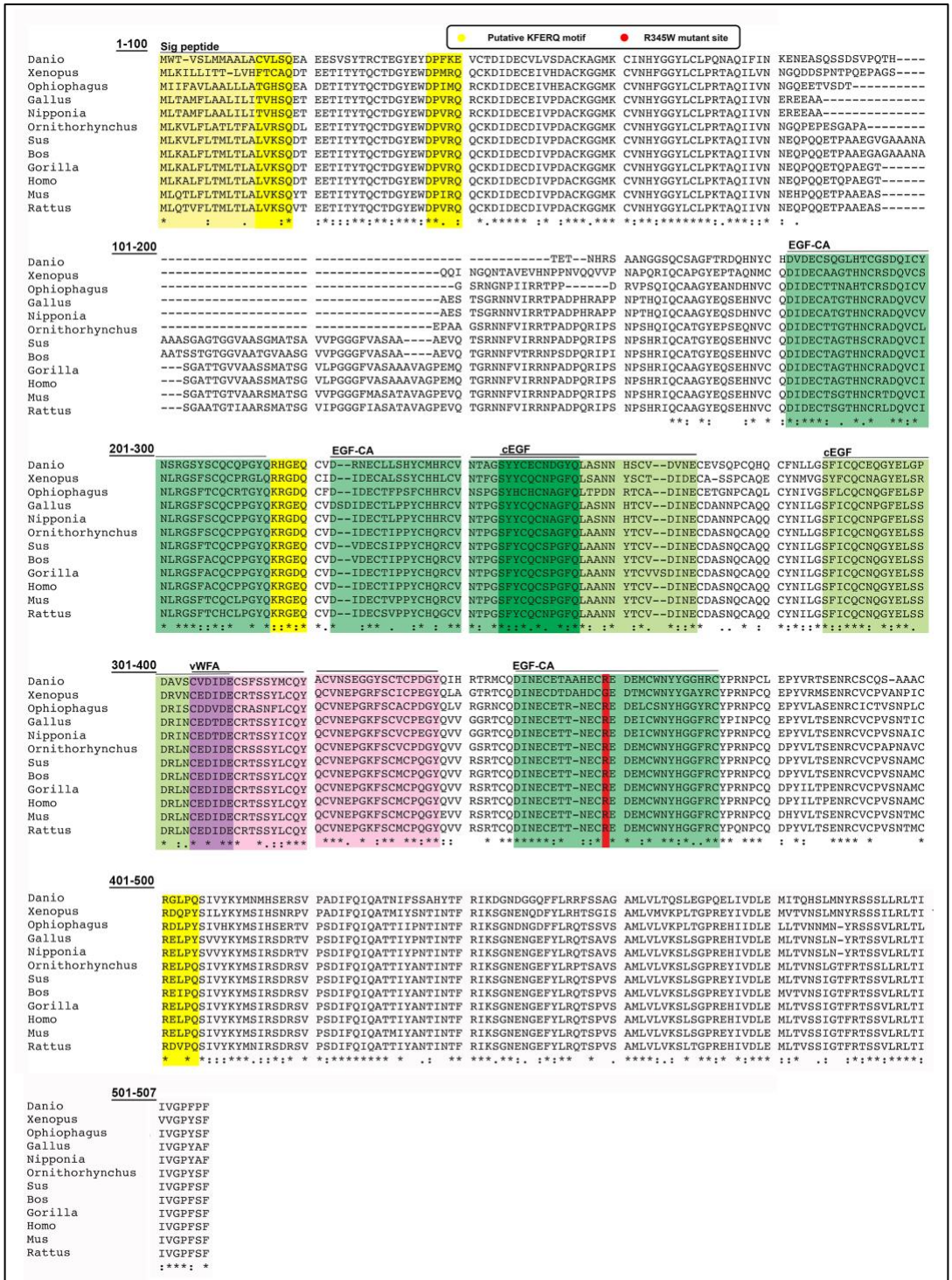

Figure 4-2. Fibulin-3 sequence. cEGF: complement C1r-likeEGF domain; cbEGF: calcium binding EGF domain.

outside of EVs derived from astrocyte and active TGFβ1 signaling (247). The mechanisms by which Fibulin-3 and Fibulin-3 on EV regulate TGFβ1 are yet to be determined.

Induced pluripotent stem cell-derived RPE (iPSC-RPE)

Induced pluripotent stem cells (iPSCs) are a cell type derived from adult somatic cells that have been genetically reprogrammed to generate patient-specific cell lines. iPSC-derived RPE (iPSC-RPE), after differentiation from iPSC, can be generated reproducibly and monitored closely. These cells behave in a manner close to primary human RPE cells both morphologically and functionally.

In our lab, we have successfully cultured iPSC-RPE cells to terminal differentiation. iPSC-RPE cells were cultured according to the triphasic RPE differentiation protocol provided (248). Briefly, iPSCs (Week 0) were differentiated into committed RPE (Week 4), immature RPE (Week 6), and mature RPE (Week 11). Each phase of differentiation required specific media and additives (248) (**Fig. 4-3**). Several endpoints were developed to evaluate the differentiation state of these cells at various time points. Further studies should focus on whether the expression of mutant Fibulin-3, TIMP3, and C1QTNF5 attenuate RPE differentiation and promote EMT in iPSC-derived RPE cells and whether the expression of mutant Fibulin-3, TIMP3, and C1QTNF5 alters EV size and cargo derived from iPSC-RPE cells.

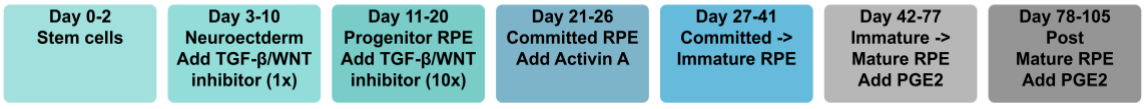

Figure 4-3. Triphasic RPE differentiation protocol.

EV secretion and uptake

Extracellular vesicles (EVs) play a critical role in cell-cell communication and modulate cellular differentiation (115, 116). Recent studies have shown that alterations in

EV size and cargo are dependent upon the secretion mechanisms and phenotypic status of their parental cells (203). Two different mechanisms have been identified for EV formation, including the transport endosomal sorting complexes required for transport machinery (ESCRT)-dependent pathway (128) and a non-ESCRT, ceramide-dependent pathway (129). EV compositional heterogeneity results from EV biogenesis operating across a spectrum of endosome and plasma membranes (223, 224). Our second major finding explored the role of misfolded protein R345W-Fibulin-3 in altering EV size and cargo. Both TEM and NTA showed mutant EVs were smaller on average than those derived from WT cells. Proteomic analysis revealed substantial changes in EV cargo. ALIX, an ESCRT-related protein, is required for EV secretion (128), and Tetraspanins, such as CD63 and CD81, are highly enriched in EVs relative to their content in the respective producing cells (128). Both our proteomic analyses and western blot analysis have shown that WT-ARPE-EVs exhibit greater ALIX, CD63 and CD81 content compared to R345W-ARPE-EVs. These results suggest that expression of R345W-Fibulin-3 may alter the mechanism of EV secretion from an ESCRT-dependent to an ESCRT-independent mechanism. It is important to determine how mutant EVs are secreted from RPE cells by blocking the ESCRT pathway or by adding ceramide inhibitors (Manumycin A and GW4869).

EVs are taken up by a variety of endocytic pathways, including clathrin-dependent endocytosis and clathrin-independent pathways, including caveolin-mediated uptake, macropinocytosis, phagocytosis, and lipid raft-mediated internalization (249). Some studies suggest that vesicular uptake is a highly specific process which can only occur if cell and EV share the right combination of ligand and receptor (250, 251). Our data presented in Chapter 3 have shown that EVs are taken up by recipient RPE cells after incubation for 12 hours. It will be important for future studies to determine the uptake mechanism for RPE-EVs in recipient RPE cells.

EV cargo

TGFβ1

EVs regulating EMT have been found to promote cancer metastasis in many tissues, including the lungs, breasts, liver, and brain (117-120). Proteins on the surface of EVs, including TGFβ, have been shown to promote EMT (117, 217). Our proteomic analysis revealed that expression of misfolded fibulin-3 substantially alters EV cargo; proteins that play a central role in EMT were found to be 3- to 7-fold more abundant R345W EVs compared to WT EVs. Our next major finding explored the roles of EVs in regulating RPE dysfunction. In chapter 3, we quantified TGFβ1 protein in cell culture media, EV-depleted media, and EVs in both WT-Fib3 and R345W-Fib3 groups. Compared to the WT media and EV-depleted media, the amount of TGFβ1 protein was significantly greater in the R345W media and EV-depleted media. Compared to the WT EVs, TGFβ1 protein was significantly more abundant in the R345W EVs. In addition, EV transplant studies demonstrate that EVs from cells expressing R345W-Fibulin-3 are sufficient to induce EMT in recipient RPE cells. Taken together, these results suggest that TGFβ1 proteins on EVs play a role in regulating EMT in RPE cells.

microRNA-204/211

miRNA-204/211 plays a critical role in RPE cell differentiation. Prior studies demonstrated that the TGF-β receptor is a direct target of miRNA-204/211 in RPE cells. Transient receptor potential cation channel (TRPM)1 and TRPM3 are two signature genes of RPE cells. miRNA-204 resides in the sixth intron of TRPM3, and miR-211 resides in the sixth intron of TRPM1. miRNA-204/211 and TRPM3/1 co-translate in RPE cells (12). miRNA-204 and miRNA-211 are highly expressed in fully differentiated RPE cells, allowing maintenance of RPE terminal differentiation (13). Further, anti-miRNA-204/211 leads to elevations in the levels of several EMT transcriptional factors, including TGFBR2, JNK, SNAIL1, SNAIL2, Smad3, and Smad4. Together, these data demonstrate the importance of miRNA-204/211 in preventing EMT in RPE cells (**Fig. 4-4**).

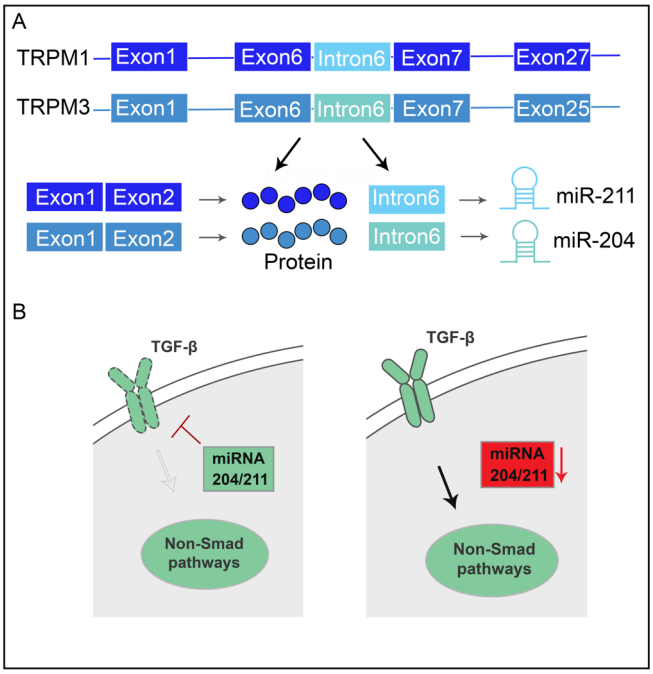

Figure 4-4. microRNA 204/211 regulates RPE differentiation. (A) Schematic illustration of the coding sequences of miRNA-204/211 lies within intron 6 of TRPM3 and intron 6 of TRPM1 respectively. (B) miRNA 204/211 directly targets TGFβ receptor and inhibits the phosphorylation of downstream targets. Downregulated miRNA 204/211 allows TGFβ pathway activation.

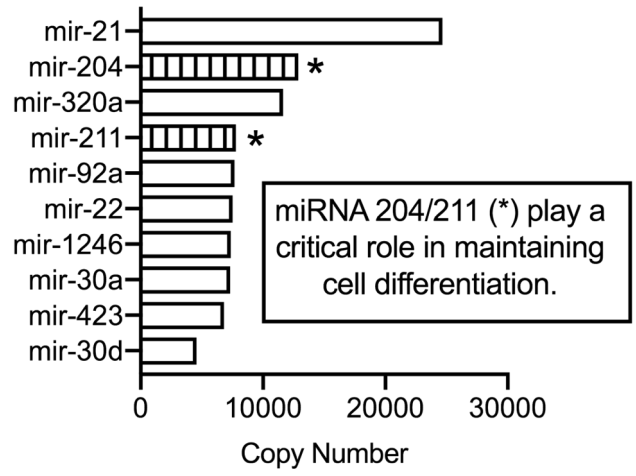

Figure 4-5. Top 10 miRNAs in EVs derived from primary RPE.

Preliminary data in our lab show that miRNA-204/211 are two of the top ten miRNAs in EVs derived from terminally differentiated human fetal RPE (hfRPE) cells (**Fig. 4-5**). Additionally, we found that terminally differentiated RPE-derived EVs contain abundant miRNA-204/211. Our most recent study showed that expression of R345W-Fibuin-3 downregulates miRNA204/211 in EVs derived from iPSC-RPE cells (**Fig. 4-6**). Taken together, these results suggest that mutant EVs induce EMT via a TGFβ and/or miRNA pathway.

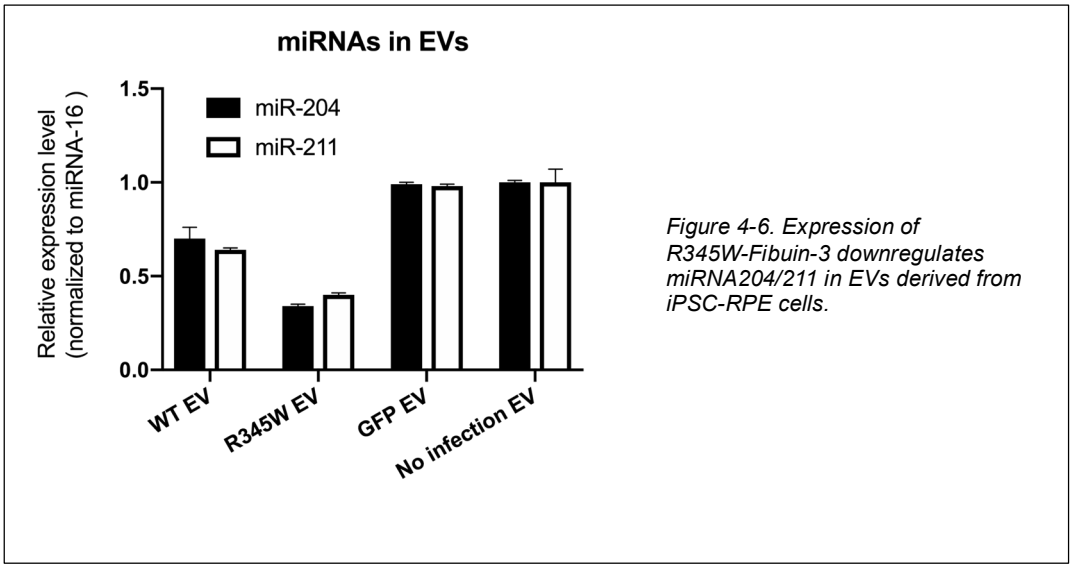

Figure 4-6. Expression of R345W-Fibuin-3 downregulates miRNA204/211 in EVs derived from iPSC-RPE cells.

Nicotinamide

Nicotinamide (NAM), a vitamin B3 derivative, has both antioxidant and anti-inflammatory properties. NAM has been shown to enhance RPE phenotype and prevent EMT in multiple RPE cell model systems (107, 252-254). The ARPE-19 cell line is typically thought not to be well differentiated but does offer relative convenience and consistency. NAM has been shown to rapidly promote ARPE-19 cell differentiation (252). In human adult stem cell-derived RPE, NAM prevents and reverses RPE EMT that is induced by TGF-β and TNF-α treatment (107). In a human iPSC model of AMD, NAM ameliorates disease phenotype by inhibiting drusen proteins and inflammatory and complement factors (254). Potential mechanisms by which NAM promoted RPE cell

survival and differentiation include inhibition of Rho-associated protein kinase (ROCK) and casein kinase 1 (CK1) (253).

Concluding remarks

In summary, our study identified a novel mechanism by which accumulation of misfolded proteins in the retinal pigment epithelium (RPE) impairs extracellular vesicle (EV) cargo, and this results in the epithelial to mesenchymal transition (EMT). Mutant EVs have increased TGFβ protein and decreased miRNA-204/211 and are sufficient to induce EMT (**Fig. 4-7**). Future work will examine the role of EVs in in model systems of additional inherited retinal degenerations caused by misfolded proteins expressed in RPE cells as well as in models of AMD. If successful, it will provide a novel therapeutic mechanism to reverse EMT in RPE cells. Conceptually, approaches aimed at modulating aberrant ECM, sub-RPE deposits, or restoring proteostasis are inherently complicated and lack specificity. In contrast, the use of EVs with specific cargo to modulate specific cells is a rapidly expanding field for the treatment of numerous diseases (250, 255-257).

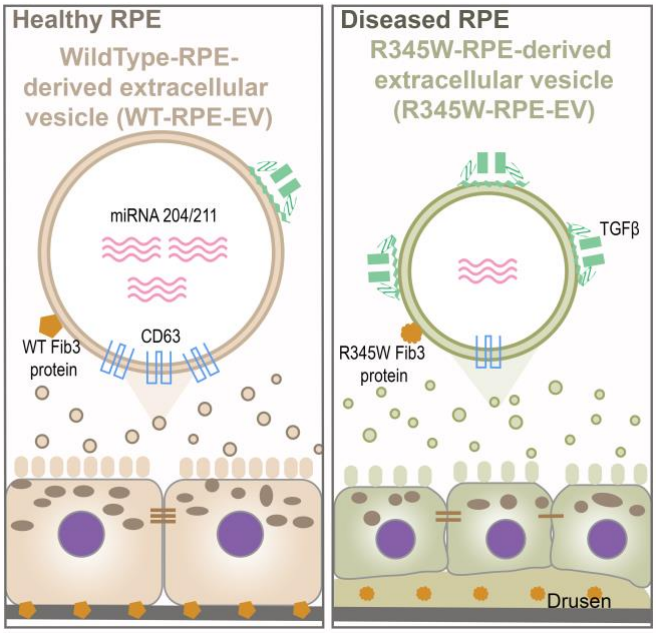

Figure 4-7: WT-EV vs R345W-EV. 1) have increased TGFβ protein and decreased miRNA-204/211 (known to promote RPE differentiation); 2) have reduced ALIX and CD63 content, suggesting an alternate secretion mechanism; and 3) are sufficient to induce EMT.

APPENDIX

Common Materials and Methods

Plasmids

Lentiviral constructs containing naturally secreted *Gaussia* Luciferase (GLuc) and GLuc tagged wild type or R345W Fibulin-3 were described previously (194). ViraPower™ Lentiviral Expression systems (Thermo Fisher Scientific, Waltham, MA, USA) were used to produce lentiviruses in 293T cells by calcium phosphate transfection.

Cell Culture

Human fetal RPE (hfRPE) cells were generously provided by Dr. Sheldon S. Miller, Dr. Kapil Bharti, and Dr. Arvydas Maminishkis (National Eye Institute, Bethesda, MD, USA) and cultured following the protocol published previously (188). In brief, hfRPE cells were maintained in MEM medium (α modification) with N1 supplement, glutamine, non-essential amino acid, penicillin-streptomycin, taurine, hydrocortisone, triiodothyronine, and 5% fetal bovine serum (heat inactivated) at 37°C with 5% CO_2. hfRPE cells were seeded on human extracellular matrix (ECM, #354237, Corning Life Sciences, Tewksbury, MA, USA) coated 12mm polyester (PET) Transwell® inserts with 0.4um pores in 12-well plate (#3460, Corning Life Sciences, Tewksbury, MA, USA) with 150K cells per well. Medium was changed twice a week. At the beginning of seven weeks after seeding, hfRPE cells were infected with Lentiviral GLuc-tagged wild-type (WT)-Fibulin-3, GLuc-tagged R345W-Fibulin-3, or GLuc tag only at MOI 10 with 6ug/ml hexadimethrine bromide (#H9268, MilliporeSigma, Burlington, MA, USA) for 4 hours a day for 5 days, resulting in a copy number of 55 ± 9 (mean ± SEM) in WT group versus 57 ± 3 (mean ± SEM) in mutant group.

ARPE-19 cells (CRL-2302, p19) were purchased from American Type Culture Collection (ATCC), which originated from a 19-year-old male human. ARPE-19 cell lines were maintained in DMEM (Dulbecco's Modified Eagle's Medium)/Hams F-12 (10-092-CV, Corning) supplemented with 10% fetal bovine serum (100106, Gemini) and penicillin/streptomycin (30-002-CI, Corning) at 37°C and 5% CO_2. Viability and phenotype were assessed by a microplate fluorometer and microscopy routinely. Trypan blue (25-900-CI, 0.4%, Corning) was used to stain cells with 1:1 dilution. Over 95% of cells were considered viable for analysis. ARPE-19 Tet-On cells with Lentiviral GLuc-tagged WT- or R345W-Fibulin-3 were described previously (91, 194). Inserted genes have inducible expression in the presence of doxycycline (1ug/ml, Dox, D9891, MilliporeSigma, Burlington, MA, USA).

Immunocytochemistry (ICC)

Cells in Transwell® inserts were washed twice with PBS and fixed with 4% paraformaldehyde for 15 minutes at room temperature. Cells were washed twice with PBS, then treated with 0.1 M glycine for 15 minutes and permeabilized with 0.1% Triton X-100 for 3 times, 2 minutes each. Cells were blocked with 10% normal donkey serum for 2 hours at room temperature then incubated with rabbit polyclonal anti-ZO-1 (1:100, #61-7300, Thermo Fisher Scientific, Waltham, MA, USA) overnight at 4°C. Cells were washed 3 times in PBS and incubated with Alexa Fluor® 488 donkey anti-rabbit IgG (H+L) for 1 hour (1:500, #711-546-152, Jackson ImmunoResearch Laboratories, Inc., West Grove, PA, USA). Nuclei were counterstained with Hoechst 33342 (1ug/ml, #B2261, MilliporeSigma, Burlington, MA, USA). The Transwell® membranes with cells were mounted on microscope slides with Aqua-Poly/Mount medium (#18606-20, Polysciences, Warrington, PA, USA). Images were acquired using a Leica SP8 confocal microscope (Leica Microsystems, Wetzlar, Germany).

VEGF Enzyme-linked immunosorbent assays (ELISAs)

Cell culture media were collected from the upper and lower chambers of Transwells after incubation for 48 hours. Vascular endothelial growth factor (VEGF) ELISAs

(Quantikine; R&D Systems, Minneapolis, MN, USA) were performed according to kit instructions. Optical densities were determined within 30 min with a SpectraMax 190 microplate reader (Molecular Devices, San Jose, CA, USA) at 450 nm with wavelength correction at 570 nm. All VEGF ELISA experiments were run in biological and technical triplicate.

TGF-β1 Enzyme-Linked Immunosorbent Assays (ELISAs)

Cell culture media (serum-free) was collected from ARPE-19 cells expressing either WT-Fibulin-3 or R345W-Fibulin-3. EVs from media were isolated by using conventional ultracentrifugation, and media left over after EVs were centrifuged out were collected as EV-depleted media. TGF-β1 ELISAs (Quantikine; R&D Systems, Minneapolis, MN, USA) were performed on media, EV-depleted media, and EVs from both groups according to kit instructions. Fifty microliters of media, EV, or EV-depleted media was used for loading on each test. Before the analysis, dilution factor was first determined to ensure all the values fell within the detection range of the assay. To activate latent TGF-β1 to immunoreactive TGF-β1 detectable by the Quantikine® TGF-β1 immunoassay, all samples were incubated with 1 N HCL for 10 minutes and neutralized by 1.2 N NaOH/0.5 M HEPES. Activated samples were assayed immediately after activation. Optical densities were determined within 30 minutes. with a SpectraMax 190 microplate reader (Molecular Devices, San Jose, CA, USA) at 450 nm with wavelength correction at 570 nm. All TGF-β1 ELISA experiments were run in technical duplicates and biological triplicates.

Luciferase assay

Cell culture media was collected weekly from apical and basal compartments of Transwell® inserts after Lentiviral infection, spun at 12,000g, 15 min at 4°C, and stored at -20°C. Cells were lysed in 1x Passive Lysis Buffer (#E1941, Promega, Madison, WI, USA). *Gaussia* Luciferase activities were measured by BioLux® *Gaussia* Luciferase Assay Kit (#E3300, New England BioLabs, Ipswich, MA, USA) in triplicate according to the

manufacturer's standard protocol using a Sirius Tube Luminometer (Berthold Detection Systems GmbH, Pforzheim, Germany).

Real-time PCR

Total RNA was extracted from samples using the AllPrep DNA/RNA/Protein Mini Kit (#80004, Qiagen Sciences, Inc., Germantown, MD, USA) according to the manufacturer's protocol. RNA was eluted with RNase-free water. Total RNA was quantified using a NanoDrop 2000 Spectrophotometer (Thermo Fisher Scientific, Waltham, MA, USA). For reverse transcription, 0.25 µg of total RNA was used in the SuperScript™ IV First-Strand cDNA Synthesis System (#18091050, Thermo Fisher Scientific, Waltham, MA, USA) with a mixture of 50uM oligo-dT and 50ng/ul random hexamers as primers. Real-time primers were designed with Primer3web, version 4.4.0 (http://bioinfo.ut.ee/primer3/) and validated using melt curve analysis and agarose gel electrophoresis. PCR primers used in this study are shown in Appendix Table 1. Significant gene expression was evaluated using the FastStart Universal SYBR Green Master (ROX) (#4913850001, Roche Molecular Systems, Inc., Branchburg, NJ, USA) in triplicate in QuantStudio™ 3 Real-Time PCR Systems (Thermo Fisher Scientific, Waltham, MA, USA). The relative quantity of mRNA was normalized to glyceraldehyde 3-phosphate dehydrogenase (GAPDH) using the comparative $2^{-\Delta\Delta Ct}$ method.

Genes		Forward / Reverse primer (5' --> 3')	Amplicon size (bp)
BEST1	bestrophin 1	TCCGTCGAGCCTCCTTTATG	
		CCTGATTGGGCTGGAACTCC	78bp
CRALBP	cellular retinaldehyde binding protein	TCCGGACTTCAGATCTCAGG	
		CATGGCTGGTGGATGAAGTG	91bp
RPE65	retinal pigment epithelium-specific 65 kDa protein	AGAGCCTGATTCATACCCATCA	
		ACCACACTCAGAACTACACCA	87bp
TRPM1	transient receptor potential cation channel subfamily M member 1	GCATCCGGGTCACTTCTGA	
		GTCGAAGGTCAACAGTCTGC	108bp
TGFB2	transforming growth factor beta 2	CAGTTCCCTTCTGCGACATA	
		GCTCGATAAGGTGGTGCTTG	101bp
ZEB1	zinc finger E-box binding homeobox 1	CCCTTGAAAGTGATCCAGCC	
		GGGCGGTGTAGAATCAGAGT	108bp
VIM	vimentin	GATTCACTCCCTCTGGTTGAT	
		CGTGATGCTGAGAAGTTTCGT	103bp
CDH2	cadherin 2	CCAGTATCCGGTCCGATCTG	
		GGGAGTCATATGGTGGAGCT	110bp
GAPDH	glyceraldehyde 3-phosphate dehydrogenase	CGTGGAAGGACTCATGACCA	
		CATCACGCCACAGTTTCCC	86bp

Appendix Table 1. PCR Primers.

Cell Migration assay

ARPE-19 cells were cultured in 96-well ImageLock Microplates (Essen Bioscience Inc., Ann Arbor, MI, USA) to confluence (n=8), and scratches were made using a 96-pin WoundMaker™ (Essen Bioscience Inc., Ann Arbor, MI, USA). The wells were then washed with PBS to remove cell debris. Wound images were acquired automatically by the IncuCyte™ software system (Essen Bioscience Inc., Ann Arbor, MI, USA). Images were collected at one-hour intervals for the duration of the experiment (72 hours). The data were then analyzed via IncuCyte S3 Software (Essen Bioscience Inc., Ann Arbor, MI, USA) using the Relative Wound Confluence integrated metric.

Trans-epithelial electrical resistance (TER)

TER of hfRPE cells was measured weekly after seeding in Transwell® inserts using the EVOM^2 Epithelial Voltohmmeter (World Precision Instruments, Sarasota FL, USA). In each plate, one coated insert without cells was measured as blank and final resistance was calculated by multiplication of net resistance (R_{Total}-R_{blank}, Ω) with effective membrane area (cm^2). The electrodes were rinsed with 70% ethanol and sterile pre-warmed culture medium.

Transmission electron microscopy (TEM)

Cells were washed twice with PBS and fixed in ½ strength Karnovsky fixative (2% paraformaldehyde, 2.5% glyceraldehyde, pH7.3) for 1 hour at room temperature and further fixed in 1% osmium tetroxide in 0.1 M cacodylate buffer (pH 7.4) for 1 hour. Samples were dehydrated in a graduated ethanol series terminating in pure acetone and embedded in LX-112 (Ladd Research, Williston, VT). Ultrathin sections (60nm) were stained with uranyl acetate and lead citrate and viewed with a JEOL JEM1400 Transmission Electron Microscope (JEOL USA Inc., Peabody, MA, USA), Penn State College of Medicine Imaging Core Facility.

Extracellular Vesicle Isolation

ARPE-19 Tet-On WT or R345W Fibulin-3 eGLuc2 cells were seeded in 100 mm dishes (Corning) initially in DMEM/F12 media supplemented with 10% FBS and penicillin/streptomycin. When cells reached 60-70% confluency, they were rinsed 3 times with PBS containing Ca^{2+} and Mg^{2+}, and serum-free DMEM/F12 with doxycycline (1 µg/ml) was added. Two days later, EVs were collected from conditioned media after cells were grown in FBS-depleted media (serum-free).

EVs used for characterization and Western blot studies were isolated by differential centrifugation. Briefly, cell culture media was filtered using a 0.22-µm filter and then concentrated to 1/10th of its original volume (Amicon Centrifugal Filter Ultra-15mL 3K, UFC900324, Millipore Sigma). Concentrated cell culture media was ultracentrifuged at 100,000 g for 17 hours and washed using HBS at 100,000 g for 5 hours. EV pellets were re-suspended in HEPES based saline (HBS, 150 mM NaCl, 20 mM HEPES, pH 7.4, 0.22 µm filtered) buffer. Fresh EVs were stored at 4°C for use within 1 week. Unused EVs were frozen at -20 °C and kept for less than 6 months with ≤ 3 freeze/thaw cycles.

EVs used in proteomics studies were isolated using iodixanol buoyant density gradient ultracentrifugation in order to isolate a more homogeneous fraction (258, 259). Concentrated culture media was loaded over 1 mL of 0.8 M sucrose buffer (0.8 M sucrose, 150 mM NaCl, 20 mM HEPES, pH 7.4) and 0.5 mL of 2.0 M sucrose buffer (2.0 M sucrose,

150 mM NaCl, 20 mM HEPES, pH7.4) and spun at 100,000 g for 2 hours at 4°C. Two mL of interface between 0.8 M and 2.0 M sucrose cushion was diluted 1:5 in HBS, loaded over 0.35 ml of 0.8 M sucrose buffer and 0.15 mL of 2.0 M sucrose and spun at 100,000 g for 2 hours at 4°C. The interface (0.5 mL) between 0.8 M and 2.0 M sucrose cushion buffers was collected and stored at 4°C. The sample was mixed with 1.42 mL HBS and 2.88 mL 50% iodixanol prepared from 5 volumes of OptiPrep™ Density Gradient Medium (D1556, Millipore Sigma) and 1 volume of the buffer containing 0.25 M Sucrose, 900 mM NaCl and 120 mM HEPES (pH 7.4), resulting in 30% iodixanol solution and overlaid with 3 mL of 20% and 2.5 mL 5% iodixanol, and then spun at 200,000 g for 2 hours at 4°C.

Ten fractions were collected, and each 1 mL fraction was diluted to 10 mL with HBS and spun at 150,000 g for 3 hours at 4°C. The supernatant was removed and the pellet was re-suspended in 50 µL HBS. EV sample was collected from the 3rd fraction (Pgrad). Fifteen µL of each sample were stored at 4°C for protein assay, electrophoresis, and TEM. EV samples for proteomics were stored at -80°C for 2 weeks until shipment to MS Bioworks for mass spectrometry analysis.

Sample Preparation and Proteomic Analysis

EVs for proteomics analysis were isolated using iodixanol buoyant density gradient ultracentrifugation as described above. A total of 20 µg of protein was processed using sodium dodecyl sulfate-polyacrylamide gel electrophoresis (SDS-PAGE) with a 4-12% Bis-Tris Mini-gel (Thermo Fisher) and the 3-(N-morpholino) propanesulfonic acid (MOPS) buffer system. Following electrophoresis, the gel lanes were excised into 40 equal-sized segments and processed by in-gel digestion with trypsin (DigiLab). Briefly, fragments were washed with 25 mM ammonium bicarbonate followed by acetonitrile. Samples were reduced with 10 mM dithiothreitol at 60°C followed by alkylation with 50 mM iodoacetamide at room temperature. Digestion was performed with Sequencing Grade Trypsin (Promega, Madison, WI, USA) at 37°C for 4 hours. Samples were quenched with formic acid, and the supernatant was analyzed directly without further processing.

Half of each gel digest was analyzed by nano LC-MS/MS with a Waters NanoAcquity high performance liquid chromatography system interfaced to a ThermoFisher Q Exactive mass spectrometer. Peptides were loaded on a trapping column and eluted over a 75 μm analytical column at 350 nL/min. Both columns were packed with Luna C18 resin (Phenomenex). The mass spectrometer was operated in data-dependent mode, with the Orbitrap operating at 60,000 and 17,500 full widths at half maximum (FWHM) for MS and MS/MS, respectively. The 15 most abundant ions were selected for MS/MS. The mass spectra were processed using Mascot set to search the SwissProt Human database (forward and reverse appended with common contaminant proteins) set with Trypsin/P as the enzyme. The resultant Mascot DAT files were parsed into Scaffold (Proteome software) for validation, filtering, and creation of non-redundant protein lists for samples. Data were filtered using a 1% protein and peptide false discovery rate (FDR) and requiring at least two unique peptides per protein.

Bioinformatics

Proteomic analyses were performed using Advaita iPathway Guide. The log differential expression (Log_2DE) was calculated by determining the differential expression of R345W and WT proteins, then taking the log base 2 of that value. Bos Taurus proteins (from bovine serum) and uncharacterized proteins were removed from the analysis.

Nanoparticle Tracking Analysis

EV suspensions (n=6 per group) were diluted to 1 mL (1:50 to 1:1000) with particle-free water. Each sample was loaded by syringe pump into the NanoSight NS300 (Malvern Instruments Ltd, Malvern, Worcestershire, UK) set in scatter mode, and five 60-second videos were generated. The size distribution and concentration of particles were analyzed and images were acquired using NanoSight software version 3.2 (Malvern Instruments Ltd).

EV uptake and confocal imaging

The EV concentration (1 $x10^{10}$ vesicles/mL) for EV uptake studies was chosen according to a previously published study (120). To confirm that EVs at this concentration are taken up by the cells, isolated WT- or R345W-EVs were labelled with the green fluorescent membrane dye PKH67 (Mini 67-1KT Millipore Sigma, 2 x 10^{-6} M final concentration), for 5 minutes at room temperature. The reaction was stopped by adding 1% BSA, then the EVs were ultracentrifuged for 2 hours at 110,000 g at 4°C. The pellet was resuspended in PBS and ultracentrifuged for 2 hours at 110,000 g at 4°C, at which point the final pellet was resuspended in PBS. These PKH67-labelled WT- or R345W-EVs were incubated with ARPE-19 cells at the chosen EV concentration (1 $x10^{10}$ vesicles/mL) for 8 hours. The media was removed and cells were washed with PBS, then fixed with 4% paraformaldehyde in PBS for 15 minutes at room temperature. The cells were washed twice with PBS and incubated with 0.1 M glycine for 15 minutes at room temperature to quench unreacted aldehyde. The cells were then permeabilized with two washes with 0.1% Triton-X-100 in PBS (PBS-T), and washed twice with PBS. The cells were blocked with blocking buffer (10% donkey serum in PBS-T) for 1.5 hours at room temperature, then were labeled with phalloidin (1:66, A22287, Thermo Fisher Scientific) diluted in blocking buffer for 30 minutes. They were then thrice rinsed with PBS and coverslipped using Aqua Poly/Mount (18606-20Polysciences, PA), then allowed to dry at room temperature. Confocal images (1024 x 1024; z-stack: 2.8 µm; z-step: 0.186 µm) were collected using a Leica TCS SP8 confocal microscope.

EV Transplant and Cell Migration Assay

Cell migration assays were performed as described previously (91). Briefly, ARPE-19 cells were cultured in 96-well ImageLock Microplates (Essen Bioscience Inc., Ann Arbor, MI, USA) to confluence (n=8). A 96-pin WoundMaker™ (Essen Bioscience Inc., Ann Arbor, MI, USA) was used to make scratches. The wells were then washed with PBS to remove cell debris. EVs were added to the cell culture media. The EV concentration (1 $x10^{10}$ vesicles/mL) was chosen according to a previously published study (120), and EV uptake in ARPE-19 cells was confirmed as described in the previous section. To determine

whether EVs derived from RPE cells induce EMT via TGF-β signaling, after the wounds were created, ARPE-19 cells were treated with EVs purified from WT or R345W ARPE-19 cells, or TGF-β1 (10 ng/mL, Cat# DCPU0821041, Quantikine; R&D Systems, Minneapolis, MN, USA) as a positive control. The EVs or protein were pre-incubated with pan-TGF-β-neutralizing antibody (10 μg/mL; Cat# MAB1835-100, Quantikine; R&D Systems, Minneapolis, MN, USA) or the isotype IgG (10 μg/mL; Cat # IX2721082, Quantikine; R&D Systems, Minneapolis, MN, USA) as a negative control prior to scratch assays. EVs without pre-incubation with antibody or IgG served as an additional control. Relative wound recovery time were monitored. Wound images were acquired automatically and data were analyzed by the IncuCyte™ software system (Essen Bioscience Inc., Ann Arbor, MI, USA).

Western Blot Analysis

Cells were lysed in RIPA buffer (R0278, Millipore Sigma) and sonicated for 8 pulses. Protein concentrations in cell lysate and EVs were quantified using the DC™ Protein Assay (5000116, Bio-Rad). Total protein (2.5 μg) for each sample was mixed with LDS sample buffer (NP0007, Thermo Fisher Scientific) and 0.1 M dithiothreitol (except when probing with CD63 or CD81 antibodies) and heated at 70°C for 15 minutes, then loaded on NuPAGE 4-12% gradient (NP0323BOX, Thermo Fisher Scientific) or 12% (NP0343BOX, Thermo Fisher Scientific) Tris-Bis Gel and ran for 1.5 hour at 150 V in MOPS SDS Running buffer (NP0001, Thermo Fisher Scientific). For protein staining, gels were incubated in staining buffer (0.25% Coomassie brilliant blue R250 (97063-820, VWR), 45% methanol, 10% acetic acid) overnight at room temperature, and then de-staining buffer (45% methanol, 10% acetic acid) and scanned using FluorChem M imaging System (ProteinSimple, San Jose, CA). For Western blot, samples were transferred from gel to 0.22 μm nitrocellulose membrane (EP2HY00010, Fisher) at 100 V for 1.5 hours in Transfer buffer (NP0006-1) with 20% methanol and 0.05% SDS. The membrane was blocked at room temperature for 1 hour in blocking buffer (5% non-fat milk in TBST (10 mM Tris, 150 mM NaCl, 0.05% Tween-20, pH 7.2)). The membrane was then incubated with primary antibodies (**Appendix Table 2**) diluted in blocking buffer at 4°C overnight,

washed in TBST 4 times for 10 minutes each time, incubated with secondary antibody diluted (1: 5,000) in blocking buffer for 1.5 hour at room temperature, and washed another 4 times in TBST for 10 minutes. each time. In this study, we used either alkaline phosphatase conjugated goat anti-rabbit IgG (H+L) (111-055-144, Jackson ImmunoResearch Laboratories, Inc.) or anti-mouse IgG+IgM (H+L) (115-055-068, Jackson ImmunoResearch Laboratories, Inc.) secondary antibodies and Vistra ECF Substrate (RPN5785, GE Healthcare) to detect signals and then Typhoon 9400 (GE Healthcare) to scan the image; or IRDye 800CW goat anti-rabbit IgG (H+L) (925-32211, LI-COR) or anti-mouse IgG (H+L) (925-32210, LI-COR) secondary antibodies to detect signals and Odyssey CLx Imaging system (LI-COR) to scan the image using software Image Studio Ver 5.2 (LI-COR).

Trypsin digestion and Western Blot analysis

EVs were first incubated with Sequencing Grade Trypsin (Promega) 0.1g/g at 37°C for 30 min with gentle mixing every 5 min. EVs preps were then incubated with 0.1 M proteinase inhibitors (Sigma) for an additional 10 min at room temperature to neutralize the effects of trypsin. Total protein (10 µg) was loaded for each sample. Western blots were performed as described previously. The primary antibodies were shown in the **Appendix Table 2**. Western blots were analyzed using Image J software.

Antigen	Full name	Host species	Manufacture	Catalog number	Western blotting dilution
Alix	apoptosis-linked gene-2 interacting protein X	Rabbit polyclonal	Millipore Sigma	ABC40	1:1,000
HSP70	heat shock protein 70 kD	Rabbit polyclonal	Santa Cruz	sc-1060-R	1:1,000
Flotillin-1	--	Mouse monoclonal	BD	610821	1:500
CD63	--	Mouse monoclonal	Santa Cruz	sc-5275	1:500
CD81	--	Mouse monoclonal	BD	555675	1:500
GM130	golgi matrix protein 130 kD	Rabbit monoclonal	Abcam	ab52649	1:500
TIM23	translocase of inner mitochondrial membrane 23	Mouse monoclonal	BD	611222	1:500
Histone H3	--	Rabbit polyclonal	Cell Signaling	9715	1:1,000
Calnexin	--	Rabbit polyclonal	Santa Cruz	sc-11397	1:1,000
GAPDH	glyceraldehyde 3-phosphate dehydrogenase	Mouse monoclonal	Santa Cruz	sc-32233	1:500

Appendix Table 2. Antibodies used for Western Blot analysis.

EV Transmission Electron Microscopy (TEM)

Negative staining was conducted as follows. Briefly, the resuspended pellet was fixed in 2% paraformaldehyde. The fixed vesicles (10 uL) were deposited on Formvar carbon-coated TEM grids and incubated for 20 minutes. The grids were then washed with PBS, incubated with glutaraldehyde, and washed with water. The vesicles were then stained with uranyl acetate solution and air dried. Vesicles were observed using the JEM1400 TEM (JEOL Ltd., Tokyo, Japan). TEM images were from gradient ultracentrifugation isolation. WT EVs had 11 images and R345W had 10. Magnification was 10,000x.

EV Cryogenic Electron Microscopy (Cryo-EM)

Four microliters of EV extract was pipetted onto a freshly glow-discharged Quantifoil R2/2 holey carbon grid. Grids were hand blotted from behind using Whatman paper #1 and plunged into liquid ethane using a Mark IV Vitrobot (Thermo Fisher

Scientific) for vitrification. Samples were then transferred under liquid nitrogen into a cryo side-entry holder (Gatan) and loaded into a JEM 2100 cryo TEM (JEOL) operating at 200 k. Holes containing vesicles were targeted for data collection. A nominal magnification of 40,000x was used, which corresponded to a pixel size of 0.29 nm/pixel on our 4k ultrascan CCD (Gatan).

Statistics

Power analyses were conducted using Graphpad StatMate software 2.0 (Graphpad, San Diego, CA, USA), Type I error (alpha) was set to 0.05 and type II error (beta) was set to 80%. Based on the power analysis, a group size of n=6 will provide more than 99% power to confirm the results. Data are presented as mean ± standard error of the mean (SEM). Statistical analysis was performed by using Prism 8 (GraphPad, Inc., La Jolla, CA, USA). One-way analysis of variance (ANOVA) was used to determine differences among multiple groups, where individual differences were tested using the Tukey post-test. Where appropriate, an unpaired Student's t-test was used to compare differences between groups. A p-value of < 0.05 was considered statistically significant.

BIBLIOGRAPHY

1. Kalluri R & Weinberg RA (2009) The basics of epithelial-mesenchymal transition. *J Clin Invest* 119(6):1420-1428.
2. Acloque H, Adams MS, Fishwick K, Bronner-Fraser M, & Nieto MA (2009) Epithelial-mesenchymal transitions: the importance of changing cell state in development and disease. *J Clin Invest* 119(6):1438-1449.
3. Kalluri R (2009) EMT: when epithelial cells decide to become mesenchymal-like cells. *J Clin Invest* 119(6):1417-1419.
4. Huang RY, Guilford P, & Thiery JP (2012) Early events in cell adhesion and polarity during epithelial-mesenchymal transition. *J Cell Sci* 125(Pt 19):4417-4422.
5. Huang RY, *et al.* (2013) An EMT spectrum defines an anoikis-resistant and spheroidogenic intermediate mesenchymal state that is sensitive to e-cadherin restoration by a src-kinase inhibitor, saracatinib (AZD0530). *Cell Death Dis* 4:e915.
6. Nieto MA, Huang RY, Jackson RA, & Thiery JP (2016) Emt: 2016. *Cell* 166(1):21-45.
7. Panda-Jonas S, Jonas JB, & Jakobczyk-Zmija M (1996) Retinal pigment epithelial cell count, distribution, and correlations in normal human eyes. *Am J Ophthalmol* 121(2):181-189.
8. Amirpour N, *et al.* (2012) Differentiation of human embryonic stem cell-derived retinal progenitors into retinal cells by Sonic hedgehog and/or retinal pigmented epithelium and transplantation into the subretinal space of sodium iodate-injected rabbits. *Stem Cells Dev* 21(1):42-53.
9. Perron M, *et al.* (2003) A novel function for Hedgehog signalling in retinal pigment epithelium differentiation. *Development* 130(8):1565-1577.
10. Schouwey K, Aydin IT, Radtke F, & Beermann F (2011) RBP-Jkappa-dependent Notch signaling enhances retinal pigment epithelial cell proliferation in transgenic mice. *Oncogene* 30(3):313-322.
11. Burke JM (2008) Epithelial phenotype and the RPE: is the answer blowing in the Wnt? *Prog Retin Eye Res* 27(6):579-595.
12. Adijanto J, *et al.* (2012) Microphthalmia-associated transcription factor (MITF) promotes differentiation of human retinal pigment epithelium (RPE) by regulating microRNAs-204/211 expression. *J Biol Chem* 287(24):20491-20503.
13. Wang FE, *et al.* (2010) MicroRNA-204/211 alters epithelial physiology. *FASEB J* 24(5):1552-1571.
14. Sundelin SP, Nilsson SE, & Brunk UT (2001) Lipofuscin-formation in cultured retinal pigment epithelial cells is related to their melanin content. *Free radical biology & medicine* 30(1):74-81.
15. Libby RT, Brunken WJ, & Hunter DD (2000) Roles of the extracellular matrix in retinal development and maintenance. *Results Probl Cell Differ* 31:115-140.
16. Wimmers S, Karl MO, & Strauss O (2007) Ion channels in the RPE. *Prog Retin Eye Res* 26(3):263-301.
17. Tarnowski BI, Shepherd VL, & McLaughlin BJ (1988) Mannose 6-phosphate receptors on the plasma membrane on rat retinal pigment epithelial cells. *Invest Ophthalmol Vis Sci* 29(2):291-297.
18. Deora AA, Philp N, Hu J, Bok D, & Rodriguez-Boulan E (2005) Mechanisms regulating tissue-specific polarity of monocarboxylate transporters and their chaperone CD147 in kidney and retinal epithelia. *Proc Natl Acad Sci U S A* 102(45):16245-16250.

19. Ryeom SW, Sparrow JR, & Silverstein RL (1996) CD36 participates in the phagocytosis of rod outer segments by retinal pigment epithelium. *J Cell Sci* 109 (Pt 2):387-395.
20. Yoon H, Fanelli A, Grollman EF, & Philp NJ (1997) Identification of a unique monocarboxylate transporter (MCT3) in retinal pigment epithelium. *Biochem Biophys Res Commun* 234(1):90-94.
21. Milenkovic VM, Krejcova S, Reichhart N, Wagner A, & Strauss O (2011) Interaction of bestrophin-1 and Ca2+ channel beta-subunits: identification of new binding domains on the bestrophin-1 C-terminus. *PLoS One* 6(4):e19364.
22. Bhutto IA, *et al.* (2006) Pigment epithelium-derived factor (PEDF) and vascular endothelial growth factor (VEGF) in aged human choroid and eyes with age-related macular degeneration. *Experimental Eye Research* 82(1):99-110.
23. Bonilha VL, Finnemann SC, & Rodriguez-Boulan E (1999) Ezrin promotes morphogenesis of apical microvilli and basal infoldings in retinal pigment epithelium. *J Cell Biol* 147(7):1533-1548.
24. Senanayake P, *et al.* (2006) Glucose utilization by the retinal pigment epithelium: evidence for rapid uptake and storage in glycogen, followed by glycogen utilization. *Exp Eye Res* 83(2):235-246.
25. Wu J, *et al.* (2018) Autophagy regulates TGF-beta2-induced epithelial-mesenchymal transition in human retinal pigment epithelium cells. *Mol Med Rep* 17(3):3607-3614.
26. Ghosh S, *et al.* (2018) A Role for betaA3/A1-Crystallin in Type 2 EMT of RPE Cells Occurring in Dry Age-Related Macular Degeneration. *Invest Ophthalmol Vis Sci* 59(4):AMD104-AMD113.
27. Tamiya S & Kaplan HJ (2016) Role of epithelial-mesenchymal transition in proliferative vitreoretinopathy. *Exp Eye Res* 142:26-31.
28. Roy R, Saurabh K, Shah D, Chowdhury M, & Goel S (2019) Choroidal Hyperreflective Foci: A Novel Spectral Domain Optical Coherence Tomography Biomarker in Eyes With Diabetic Macular Edema. *Asia Pac J Ophthalmol (Phila)* 8(4):314-318.
29. Liu S, Wang D, Chen F, & Zhang X (2019) Hyperreflective foci in OCT image as a biomarker of poor prognosis in diabetic macular edema patients treating with Conbercept in China. *BMC Ophthalmology* 19(1).
30. Miura M, *et al.* (2017) Evaluation of intraretinal migration of retinal pigment epithelial cells in age-related macular degeneration using polarimetric imaging. *Sci Rep* 7(1):3150.
31. Kuroda M, *et al.* (2014) Intraretinal hyperreflective foci on spectral-domain optical coherence tomographic images of patients with retinitis pigmentosa. *Clin Ophthalmol* 8:435-440.
32. Piri N, Nesmith BL, & Schaal S (2015) Choroidal hyperreflective foci in Stargardt disease shown by spectral-domain optical coherence tomography imaging: correlation with disease severity. *JAMA Ophthalmol* 133(4):398-405.
33. Chen KC, *et al.* (2016) Intraretinal Hyperreflective Foci in Acquired Vitelliform Lesions of the Macula: Clinical and Histologic Study. *Am J Ophthalmol* 164:89-98.
34. Christenbury JG, *et al.* (2013) Progression of intermediate age-related macular degeneration with proliferation and inner retinal migration of hyperreflective foci. *Ophthalmology* 120(5):1038-1045.
35. Abri Aghdam K, Pielen A, Framme C, & Junker B (2015) Correlation Between Hyperreflective Foci and Clinical Outcomes in Neovascular Age-Related Macular Degeneration After Switching to Aflibercept. *Invest Ophthalmol Vis Sci* 56(11):6448-6455.

36. Friedman DS, *et al.* (2004) Prevalence of age-related macular degeneration in the United States. *Arch Ophthalmol* 122(4):564-572.
37. Balaratnasingam C, *et al.* (2016) Associations Between Retinal Pigment Epithelium and Drusen Volume Changes During the Lifecycle of Large Drusenoid Pigment Epithelial Detachments. *Invest Ophthalmol Vis Sci* 57(13):5479-5489.
38. Miura M, *et al.* (2019) Evaluation of focal damage in the retinal pigment epithelium layer in serous retinal pigment epithelium detachment. *Sci Rep* 9(1):3278.
39. Ferris FL, *et al.* (2005) A simplified severity scale for age-related macular degeneration: AREDS Report No. 18. *Arch Ophthalmol* 123(11):1570-1574.
40. Folgar FA, *et al.* (2012) Spatial Correlation between Hyperpigmentary Changes on Color Fundus Photography and Hyperreflective Foci on SDOCT in Intermediate AMD. *Investigative Opthalmology & Visual Science* 53(8).
41. Hirasawa M, *et al.* (2011) Transcriptional factors associated with epithelial-mesenchymal transition in choroidal neovascularization. *Mol Vis* 17:1222-1230.
42. Roberts P, *et al.* (2016) Automated Identification and Quantification of Subretinal Fibrosis in Neovascular Age-Related Macular Degeneration Using Polarization-Sensitive OCT. *Invest Ophthalmol Vis Sci* 57(4):1699-1705.
43. Ishikawa K, Kannan R, & Hinton DR (2016) Molecular mechanisms of subretinal fibrosis in age-related macular degeneration. *Exp Eye Res* 142:19-25.
44. Rosales MAB, Shu DY, Iacovelli J, & Saint-Geniez M (2019) Loss of PGC-1alpha in RPE induces mesenchymal transition and promotes retinal degeneration. *Life Sci Alliance* 2(3).
45. Kobayashi M, *et al.* (2019) Suppression of Epithelial-Mesenchymal Transition in Retinal Pigment Epithelial Cells by an MRTF-A Inhibitor. *Investigative ophthalmology & visual science* 60(2):528-537.
46. Kim JW, Kang KH, Burrola P, Mak TW, & Lemke G (2008) Retinal degeneration triggered by inactivation of PTEN in the retinal pigment epithelium. *Genes Dev* 22(22):3147-3157.
47. Ishikawa K, *et al.* (2016) alphaB-Crystallin Regulates Subretinal Fibrosis by Modulation of Epithelial-Mesenchymal Transition. *Am J Pathol* 186(4):859-873.
48. Bonnet M, *et al.* (1996) [Has the incidence of postoperative PVR in rhegmatogenous retinal detachment decreased?]. *J Fr Ophtalmol* 19(11):696-704.
49. Rodriguez de la Rua E, *et al.* (2003) [Clinical risk factors for postoperative proliferative vitreoretinopathy (PVR). A prospective study]. *Arch Soc Esp Oftalmol* 78(2):91-97.
50. Casaroli-Marano RP, Pagan R, & Vilaro S (1999) Epithelial-mesenchymal transition in proliferative vitreoretinopathy: intermediate filament protein expression in retinal pigment epithelial cells. *Invest Ophthalmol Vis Sci* 40(9):2062-2072.
51. Morino I, Hiscott P, McKechnie N, & Grierson I (1990) Variation in epiretinal membrane components with clinical duration of the proliferative tissue. *Br J Ophthalmol* 74(7):393-399.
52. Yamashita H, Hori S, & Masuda K (1986) Population and proportion of component cells in preretinal membranes. *Jpn J Ophthalmol* 30(3):269-281.
53. Feist RM, Jr., King JL, Morris R, Witherspoon CD, & Guidry C (2014) Myofibroblast and extracellular matrix origins in proliferative vitreoretinopathy. *Graefes Arch Clin Exp Ophthalmol* 252(2):347-357.
54. Saika S, *et al.* (2004) Smad3 is required for dedifferentiation of retinal pigment epithelium following retinal detachment in mice. *Laboratory investigation; a journal of technical methods and pathology* 84(10):1245-1258.
55. Yoo K, *et al.* (2017) Substance P prevents development of proliferative vitreoretinopathy in mice by modulating TNF-alpha. *Molecular vision* 23:933-943.

56. Zhang J, *et al.* (2017) Notch signaling modulates proliferative vitreoretinopathy via regulating retinal pigment epithelial-to-mesenchymal transition. *Histochemistry and cell biology* 147(3):367-375.
57. Nagasaki YK, H.; Ye, F.; Kachi, S.; Asami, T.; Kato, S.; Takayami, K.; Hwang, S.; Kataoka, K.; Shimizu, H.; Iwase, T.; Funahashi, Y.; Higuchi, A.; Senga, T.; Terasaki, H. (2016) Role of Caveolin-1 for Blocking the Epithelial-Mesenchymal TRansition in Proliferative Vitreoretinopathy. *Invest Ophthalmol Vis Sci* 58.
58. Goldberg MF, *et al.* (2018) Ocular Histopathology and Immunohistochemical Analysis in the Oldest Known Individual with Autosomal Dominant Vitreoretinochoroidopathy. *Ophthalmol Retina* 2(4):360-378.
59. Li ZY, Possin DE, & Milam AH (1995) Histopathology of bone spicule pigmentation in retinitis pigmentosa. *Ophthalmology* 102(5):805-816.
60. Szamier RB & Berson EL (1977) Retinal ultrastructure in advanced retinitis pigmentosa. *Invest Ophthalmol Vis Sci* 16(10):947-962.
61. Fox KR (1981) Dominantly inherited retinitis pigmentosa. *Ann Ophthalmol* 13(7):817-821.
62. Flannery JG, Farber DB, Bird AC, & Bok D (1989) Degenerative changes in a retina affected with autosomal dominant retinitis pigmentosa. *Invest Ophthalmol Vis Sci* 30(2):191-211.
63. Tso MO (1973) Photic maculopathy in rhesus monkey. A light and electron microscopic study. *Invest Ophthalmol* 12(1):17-34.
64. Anderson DH, Stern WH, Fisher SK, Erickson PA, & Borgula GA (1981) The onset of pigment epithelial proliferation after retinal detachment. *Invest Ophthalmol Vis Sci* 21(1 Pt 1):10-16.
65. MacDonald IM, Russell L, & Chan CC (2009) Choroideremia: new findings from ocular pathology and review of recent literature. *Surv Ophthalmol* 54(3):401-407.
66. Curcio CA, Saunders PL, Younger PW, & Malek G (2000) Peripapillary chorioretinal atrophy: Bruch's membrane changes and photoreceptor loss. *Ophthalmology* 107(2):334-343.
67. Jonasson F, Hardarson S, Olafsson BM, & Klintworth GK (2007) Sveinsson chorioretinal atrophy/helicoid peripapillary chorioretinal degeneration: first histopathology report. *Ophthalmology* 114(8):1541-1546.
68. Foulds WS, Moseley H, Eadie A, & McNaught E (1980) Vitreal, retinal, and pigment epithelial contribution to the posterior blood-ocular barrier. *Trans Ophthalmol Soc U K* 100(3):341-342.
69. Tash BR, *et al.* (2012) The occludin and ZO-1 complex, defined by small angle X-ray scattering and NMR, has implications for modulating tight junction permeability. *Proc Natl Acad Sci U S A* 109(27):10855-10860.
70. Erickson KK, Sundstrom JM, & Antonetti DA (2007) Vascular permeability in ocular disease and the role of tight junctions. *Angiogenesis* 10(2):103-117.
71. Tamiya S, Liu L, & Kaplan HJ (2010) Epithelial-mesenchymal transition and proliferation of retinal pigment epithelial cells initiated upon loss of cell-cell contact. *Invest Ophthalmol Vis Sci* 51(5):2755-2763.
72. Georgiadis A, *et al.* (2010) The tight junction associated signalling proteins ZO-1 and ZONAB regulate retinal pigment epithelium homeostasis in mice. *PloS one* 5(12):e15730.
73. Ikenouchi J, Matsuda M, Furuse M, & Tsukita S (2003) Regulation of tight junctions during the epithelium-mesenchyme transition: direct repression of the gene expression of claudins/occludin by Snail. *J Cell Sci* 116(Pt 10):1959-1967.

74. Gonzalez-Mariscal L, *et al.* (2014) Tight junctions and the regulation of gene expression. *Semin Cell Dev Biol* 36:213-223.
75. Gonzalez DM & Medici D (2014) Signaling mechanisms of the epithelial-mesenchymal transition. *Sci Signal* 7(344):re8.
76. Lei QY, *et al.* (2008) TAZ promotes cell proliferation and epithelial-mesenchymal transition and is inhibited by the hippo pathway. *Mol Cell Biol* 28(7):2426-2436.
77. Liu Y, *et al.* (2010) Taz-tead1 links cell-cell contact to zeb1 expression, proliferation, and dedifferentiation in retinal pigment epithelial cells. *Investigative ophthalmology & visual science* 51(7):3372-3378.
78. Santamaria PG, Mazon MJ, Eraso P, & Portillo F (2019) UPR: An Upstream Signal to EMT Induction in Cancer. *J Clin Med* 8(5).
79. Lenna S & Trojanowska M (2012) The role of endoplasmic reticulum stress and the unfolded protein response in fibrosis. *Curr Opin Rheumatol* 24(6):663-668.
80. Zhong Q, *et al.* (2011) Role of endoplasmic reticulum stress in epithelial-mesenchymal transition of alveolar epithelial cells: effects of misfolded surfactant protein. *Am J Respir Cell Mol Biol* 45(3):498-509.
81. Pang XX, *et al.* (2016) Urotensin II Induces ER Stress and EMT and Increase Extracellular Matrix Production in Renal Tubular Epithelial Cell in Early Diabetic Mice. *Kidney Blood Press Res* 41(4):434-449.
82. Johnson AA, *et al.* (2017) Bestrophin 1 and retinal disease. *Progress in retinal and eye research* 58:45-69.
83. Johnson AA, *et al.* (2014) Disease-causing mutations associated with four bestrophinopathies exhibit disparate effects on the localization, but not the oligomerization, of Bestrophin-1. *Exp Eye Res* 121:74-85.
84. Park SW, *et al.* (2014) Intracellular amyloid beta alters the tight junction of retinal pigment epithelium in 5XFAD mice. *Neurobiol Aging* 35(9):2013-2020.
85. Zigler JS, Jr. & Sinha D (2015) betaA3/A1-crystallin: more than a lens protein. *Prog Retin Eye Res* 44:62-85.
86. Narendran N, Guymer RH, Cain M, & Baird PN (2005) Analysis of the EFEMP1 gene in individuals and families with early onset drusen. *Eye (Lond)* 19(1):11-15.
87. Marmorstein L (2004) Association of EFEMP1 with malattia leventinese and age-related macular degeneration: a mini-review. *Ophthalmic Genet* 25(3):219-226.
88. Lin MK, *et al.* (2018) HTRA1, an age-related macular degeneration protease, processes extracellular matrix proteins EFEMP1 and TSP1. *Aging cell*:e12710.
89. Marmorstein LY, *et al.* (2002) Aberrant accumulation of EFEMP1 underlies drusen formation in Malattia Leventinese and age-related macular degeneration. *Proc Natl Acad Sci U S A* 99(20):13067-13072.
90. Hulleman JD & Kelly JW (2015) Genetic ablation of N-linked glycosylation reveals two key folding pathways for R345W fibulin-3, a secreted protein associated with retinal degeneration. *FASEB J* 29(2):565-575.
91. Zhou M, *et al.* (2020) Expression of R345W-Fibulin-3 Induces Epithelial-Mesenchymal Transition in Retinal Pigment Epithelial Cells. *Frontiers in Cell and Developmental Biology* 8.
92. Lin JH, *et al.* (2007) IRE1 signaling affects cell fate during the unfolded protein response. *Science* 318(5852):944-949.
93. Walter P & Ron D (2011) The unfolded protein response: from stress pathway to homeostatic regulation. *Science* 334(6059):1081-1086.

94. Santibanez JF (2006) JNK mediates TGF-beta1-induced epithelial mesenchymal transdifferentiation of mouse transformed keratinocytes. *FEBS Lett* 580(22):5385-5391.
95. Urano F, *et al.* (2000) Coupling of stress in the ER to activation of JNK protein kinases by transmembrane protein kinase IRE1. *Science* 287(5453):664-666.
96. Liu Z, *et al.* (2019) Transforming growth factor beta (TGFbeta) cross-talk with the unfolded protein response is critical for hepatic stellate cell activation. *J Biol Chem* 294(9):3137-3151.
97. Mo XT, *et al.* (2015) Inositol-requiring protein 1 - X-box-binding protein 1 pathway promotes epithelial-mesenchymal transition via mediating snail expression in pulmonary fibrosis. *Int J Biochem Cell Biol* 65:230-238.
98. Li H, *et al.* (2015) XBP1 induces snail expression to promote epithelial- to-mesenchymal transition and invasion of breast cancer cells. *Cell Signal* 27(1):82-89.
99. Cuevas EP, *et al.* (2017) LOXL2 drives epithelial-mesenchymal transition via activation of IRE1-XBP1 signalling pathway. *Sci Rep* 7:44988.
100. Xu J, Lamouille S, & Derynck R (2009) TGF-beta-induced epithelial to mesenchymal transition. *Cell Res* 19(2):156-172.
101. Valcourt U, Kowanetz M, Niimi H, Heldin CH, & Moustakas A (2005) TGF-beta and the Smad signaling pathway support transcriptomic reprogramming during epithelial-mesenchymal cell transition. *Mol Biol Cell* 16(4):1987-2002.
102. Zhou BP, *et al.* (2004) Dual regulation of Snail by GSK-3beta-mediated phosphorylation in control of epithelial-mesenchymal transition. *Nat Cell Biol* 6(10):931-940.
103. Engel ME, McDonnell MA, Law BK, & Moses HL (1999) Interdependent SMAD and JNK signaling in transforming growth factor-beta-mediated transcription. *J Biol Chem* 274(52):37413-37420.
104. Connor TB, Jr., *et al.* (1989) Correlation of fibrosis and transforming growth factor-beta type 2 levels in the eye. *J Clin Invest* 83(5):1661-1666.
105. Kita T, *et al.* (2008) Role of TGF-beta in proliferative vitreoretinal diseases and ROCK as a therapeutic target. *Proc Natl Acad Sci U S A* 105(45):17504-17509.
106. Radeke MJ, *et al.* (2015) Restoration of mesenchymal retinal pigmented epithelial cells by TGFbeta pathway inhibitors: implications for age-related macular degeneration. *Genome Med* 7(1):58.
107. Boles NC, *et al.* (2020) Epigenomic and Transcriptomic Changes During Human RPE EMT in a Stem Cell Model of Epiretinal Membrane Pathogenesis and Prevention by Nicotinamide. *Stem Cell Reports* 14(4):631-647.
108. Kuroda T, Ando S, Takeno Y, Kishino A, & Kimura T (2019) Robust induction of retinal pigment epithelium cells from human induced pluripotent stem cells by inhibiting FGF/MAPK signaling. *Stem Cell Res* 39:101514.
109. Wu D, *et al.* (2019) Galectin-1 promotes choroidal neovascularization and subretinal fibrosis mediated via epithelial-mesenchymal transition. *FASEB J* 33(2):2498-2513.
110. Ishikawa K, *et al.* (2015) Resveratrol inhibits epithelial-mesenchymal transition of retinal pigment epithelium and development of proliferative vitreoretinopathy. *Sci Rep* 5:16386.
111. Cui L, *et al.* (2019) miR-194 suppresses epithelial-mesenchymal transition of retinal pigment epithelial cells by directly targeting ZEB1. *Annals of translational medicine* 7(23):751.
112. Han JW, Lyu J, Park YJ, Jang SY, & Park TK (2015) Wnt/beta-Catenin Signaling Mediates Regeneration of Retinal Pigment Epithelium After Laser Photocoagulation in Mouse Eye. *Invest Ophthalmol Vis Sci* 56(13):8314-8324.

113. Chen HC, Zhu YT, Chen SY, & Tseng SC (2012) Wnt signaling induces epithelial-mesenchymal transition with proliferation in ARPE-19 cells upon loss of contact inhibition. *Lab Invest* 92(5):676-687.
114. Iriyama A, Iriyama T, Tamaki Y, & Yanagi Y (2008) Effects of white light on beta-catenin signaling pathway in retinal pigment epithelium. *Biochem Biophys Res Commun* 375(1):173-177.
115. Yuyama K, Yamamoto N, & Yanagisawa K (2008) Accelerated release of exosome-associated GM1 ganglioside (GM1) by endocytic pathway abnormality: another putative pathway for GM1-induced amyloid fibril formation. *J Neurochem* 105(1):217-224.
116. Alvarez-Erviti L, *et al.* (2011) Lysosomal dysfunction increases exosome-mediated alpha-synuclein release and transmission. *Neurobiol Dis* 42(3):360-367.
117. Kim J, *et al.* (2016) Exosome cargo reflects TGF-beta1-mediated epithelial-to-mesenchymal transition (EMT) status in A549 human lung adenocarcinoma cells. *Biochem. Biophys. Res. Commun.* 478(2):643-648.
118. Vella LJ (2014) The emerging role of exosomes in epithelial-mesenchymal-transition in cancer. *Frontiers in oncology* 4:361.
119. Chen Y, *et al.* (2017) Aberrant low expression of p85alpha in stromal fibroblasts promotes breast cancer cell metastasis through exosome-mediated paracrine Wnt10b. *Oncogene*.
120. van de Vlekkert D, *et al.* (2019) Excessive exosome release is the pathogenic pathway linking a lysosomal deficiency to generalized fibrosis. *Sci Adv* 5(7):eaav3270.
121. Thery C, Zitvogel L, & Amigorena S (2002) Exosomes: composition, biogenesis and function. *Nat Rev Immunol* 2(8):569-579.
122. Kalra H, *et al.* (2013) Comparative proteomics evaluation of plasma exosome isolation techniques and assessment of the stability of exosomes in normal human blood plasma. *Proteomics* 13(22):3354-3364.
123. Gonzales PA, *et al.* (2009) Large-scale proteomics and phosphoproteomics of urinary exosomes. *J Am Soc Nephrol* 20(2):363-379.
124. Stuendl A, *et al.* (2016) Induction of alpha-synuclein aggregate formation by CSF exosomes from patients with Parkinson's disease and dementia with Lewy bodies. *Brain* 139(Pt 2):481-494.
125. Zhao Y, *et al.* (2018) Liquid Biopsy of Vitreous Reveals an Abundant Vesicle Population Consistent With the Size and Morphology of Exosomes. *Transl Vis Sci Technol* 7(3):6.
126. Runz S, *et al.* (2007) Malignant ascites-derived exosomes of ovarian carcinoma patients contain CD24 and EpCAM. *Gynecol Oncol* 107(3):563-571.
127. Torregrosa Paredes P, *et al.* (2014) Differences in exosome populations in human breast milk in relation to allergic sensitization and lifestyle. *Allergy* 69(4):463-471.
128. Colombo M, *et al.* (2013) Analysis of ESCRT functions in exosome biogenesis, composition and secretion highlights the heterogeneity of extracellular vesicles. *J Cell Sci* 126(Pt 24):5553-5565.
129. Katarina Trajkovic CH, Salvatore Chiantia, Lawrence Rajendran, Dirk Wenzel, & Felix Wieland PS, Britta Brügger, Mikael Simons (2008) Ceramide Triggers Budding of Exosome Vesicles into Multivesicular Endosomes. *Science* 319.
130. Ostrowski M, *et al.* (2010) Rab27a and Rab27b control different steps of the exosome secretion pathway. *Nat Cell Biol* 12(1):19-30; sup pp 11-13.
131. Bobrie A, Colombo M, Krumeich S, Raposo G, & Thery C (2012) Diverse subpopulations of vesicles secreted by different intracellular mechanisms are present in exosome preparations obtained by differential ultracentrifugation. *J Extracell Vesicles* 1.

132. Johnstone RM, Adam M, Hammond JR, Orr L, & Turbide C (1987) Vesicle formation during reticulocyte maturation. Association of plasma membrane activities with released vesicles (exosomes). *J Biol Chem* 262(19):9412-9420.
133. Kowal J, *et al.* (2016) Proteomic comparison defines novel markers to characterize heterogeneous populations of extracellular vesicle subtypes. *Proc Natl Acad Sci U S A* 113(8):E968-977.
134. Van Veldhoven PP, Baumgart E, & Mannaerts GP (1996) Iodixanol (Optiprep), an improved density gradient medium for the iso-osmotic isolation of rat liver peroxisomes. *Anal Biochem* 237(1):17-23.
135. Greening DW, Xu R, Ji H, Tauro BJ, & Simpson RJ (2015) A protocol for exosome isolation and characterization: evaluation of ultracentrifugation, density-gradient separation, and immunoaffinity capture methods. *Methods Mol Biol* 1295:179-209.
136. Choi D, Gho, Y.S. (2016) Isolation of Extracellular Vesicles for Proteomic Profiling. *Proteomic Profiling: Methods and Protocols, Methods in Molecular Biology* 1295.
137. Clayton A, *et al.* (2001) Analysis of antigen presenting cell derived exosomes, based on immuno-magnetic isolation and flow cytometry. *J Immunol Methods* 247(1-2):163-174.
138. Sharma P, *et al.* (2018) Immunoaffinity-based isolation of melanoma cell-derived exosomes from plasma of patients with melanoma. *J Extracell Vesicles* 7(1):1435138.
139. Lugini L, *et al.* (2012) Immune surveillance properties of human NK cell-derived exosomes. *J Immunol* 189(6):2833-2842.
140. Mustapic M, *et al.* (2017) Plasma Extracellular Vesicles Enriched for Neuronal Origin: A Potential Window into Brain Pathologic Processes. *Front Neurosci* 11:278.
141. Van Deun J, *et al.* (2014) The impact of disparate isolation methods for extracellular vesicles on downstream RNA profiling. *J Extracell Vesicles* 3.
142. Tang YT, *et al.* (2017) Comparison of isolation methods of exosomes and exosomal RNA from cell culture medium and serum. *Int J Mol Med* 40(3):834-844.
143. Kim J, Shin H, Kim J, Kim J, & Park J (2015) Isolation of High-Purity Extracellular Vesicles by Extracting Proteins Using Aqueous Two-Phase System. *PLoS One* 10(6):e0129760.
144. Lobb RJ, *et al.* (2015) Optimized exosome isolation protocol for cell culture supernatant and human plasma. *J Extracell Vesicles* 4:27031.
145. Yuana Y, *et al.* (2015) Handling and storage of human body fluids for analysis of extracellular vesicles. *J Extracell Vesicles* 4:29260.
146. Jung MK & Mun JY (2018) Sample Preparation and Imaging of Exosomes by Transmission Electron Microscopy. *J Vis Exp* (131).
147. Sokolova V, *et al.* (2011) Characterisation of exosomes derived from human cells by nanoparticle tracking analysis and scanning electron microscopy. *Colloids Surf B Biointerfaces* 87(1):146-150.
148. Sharma S, *et al.* (2010) Structural-mechanical characterization of nanoparticle exosomes in human saliva, using correlative AFM, FESEM, and force spectroscopy. *ACS Nano* 4(4):1921-1926.
149. Tatischeff I, Larquet E, Falcon-Perez JM, Turpin PY, & Kruglik SG (2012) Fast characterisation of cell-derived extracellular vesicles by nanoparticles tracking analysis, cryo-electron microscopy, and Raman tweezers microspectroscopy. *J Extracell Vesicles* 1.
150. Yuana Y, *et al.* (2013) Cryo-electron microscopy of extracellular vesicles in fresh plasma. *J Extracell Vesicles* 2.
151. Shivani Sharma HIR, Viswanathan Palanisamy, Cliff Mathisen, Michael Schmidt, & David T. Wong aJKG (2010) Structural-Mechanical Characterization of Nanoparticle

Exosomes in Human Saliva, Using Correlative AFM, FESEM, and Force Spectroscopy. *ACSNANO* 4(4):1921-1926.

152. Zhang H, Freitas, D., Kim, H.S. (2018) Identification of distinct nanoparticles and subsets of extracellular vesicles by asymmetric flow field-flow fractionation. *Nat Cell Biol* 20:332-343.
153. Petersen KE, *et al.* (2014) A review of exosome separation techniques and characterization of B16-F10 mouse melanoma exosomes with AF4-UV-MALS-DLS-TEM. *Anal Bioanal Chem* 406(30):7855-7866.
154. Sitar S, *et al.* (2015) Size characterization and quantification of exosomes by asymmetrical-flow field-flow fractionation. *Anal Chem* 87(18):9225-9233.
155. Grabarek AD, Weinbuch D, Jiskoot W, & Hawe A (2018) Critical Evaluation of Microfluidic Resistive Pulse Sensing for Quantification and Sizing of Nanometer- and Micrometer-Sized Particles in Biopharmaceutical Products. *J Pharm Sci*.
156. Suarez H, *et al.* (2017) A bead-assisted flow cytometry method for the semi-quantitative analysis of Extracellular Vesicles. *Sci Rep* 7(1):11271.
157. Melo SA, *et al.* (2015) Glypican-1 identifies cancer exosomes and detects early pancreatic cancer. *Nature* 523(7559):177-182.
158. Daaboul GG, *et al.* (2016) Digital Detection of Exosomes by Interferometric Imaging. *Sci Rep* 6:37246.
159. Takahashi Y, *et al.* (2013) Visualization and in vivo tracking of the exosomes of murine melanoma B16-BL6 cells in mice after intravenous injection. *J Biotechnol* 165(2):77-84.
160. Suetsugu A, *et al.* (2013) Imaging exosome transfer from breast cancer cells to stroma at metastatic sites in orthotopic nude-mouse models. *Adv Drug Deliv Rev* 65(3):383-390.
161. Yoshimura A, *et al.* (2016) Generation of a novel transgenic rat model for tracing extracellular vesicles in body fluids. *Sci Rep* 6:31172.
162. Epple LM, *et al.* (2012) Medulloblastoma exosome proteomics yield functional roles for extracellular vesicles. *PLoS One* 7(7):e42064.
163. Schey KL, Luther JM, & Rose KL (2015) Proteomics characterization of exosome cargo. *Methods* 87:75-82.
164. Klingeborn M, *et al.* (2017) Directional Exosome Proteomes Reflect Polarity-Specific Functions in Retinal Pigmented Epithelium Monolayers. *Sci Rep* 7(1):4901.
165. van Niel G & Heyman M (2002) The epithelial cell cytoskeleton and intracellular trafficking. II. Intestinal epithelial cell exosomes: perspectives on their structure and function. *Am J Physiol Gastrointest Liver Physiol* 283(2):G251-255.
166. Mittelbrunn M, *et al.* (2011) Unidirectional transfer of microRNA-loaded exosomes from T cells to antigen-presenting cells. *Nat Commun* 2:282.
167. Azmi AS, Bao B, & Sarkar FH (2013) Exosomes in cancer development, metastasis, and drug resistance: a comprehensive review. *Cancer Metastasis Rev* 32(3-4):623-642.
168. Rajendran L, *et al.* (2006) Alzheimer's disease beta-amyloid peptides are released in association with exosomes. *Proc Natl Acad Sci U S A* 103(30):11172-11177.
169. Lin J, *et al.* (2015) Exosomes: novel biomarkers for clinical diagnosis. *ScientificWorldJournal* 2015:657086.
170. Phinney DG & Pittenger MF (2017) Concise Review: MSC-Derived Exosomes for Cell-Free Therapy. *Stem Cells* 35(4):851-858.
171. Kamerkar S, *et al.* (2017) Exosomes facilitate therapeutic targeting of oncogenic KRAS in pancreatic cancer. *Nature* 546(7659):498-503.
172. Skog J, *et al.* (2008) Glioblastoma microvesicles transport RNA and proteins that promote tumour growth and provide diagnostic biomarkers. *Nat Cell Biol* 10(12):1470-1476.

173. Momen-Heravi GSF (2017) Extracellular vesicles in liver disease and potential as biomarkers and therapeutic targets. *Nature Reviews Gastroenterology & Hepatology* 14:455-466.
174. Fitzgerald W, *et al.* (2018) A System of Cytokines Encapsulated in ExtraCellular Vesicles. *Sci Rep* 8(1):8973.
175. Skliar M, *et al.* (2018) Membrane proteins significantly restrict exosome mobility. *Biochem Biophys Res Commun* 501(4):1055-1059.
176. Taylor DD & Gercel-Taylor C (2008) MicroRNA signatures of tumor-derived exosomes as diagnostic biomarkers of ovarian cancer. *Gynecol Oncol* 110(1):13-21.
177. Bala S, *et al.* (2012) Circulating microRNAs in exosomes indicate hepatocyte injury and inflammation in alcoholic, drug-induced, and inflammatory liver diseases. *Hepatology* 56(5):1946-1957.
178. Van Giau V & An SS (2016) Emergence of exosomal miRNAs as a diagnostic biomarker for Alzheimer's disease. *J Neurol Sci* 360:141-152.
179. Zarbin MA, Casaroli-Marano RP, & Rosenfeld PJ (2014) Age-related macular degeneration: clinical findings, histopathology and imaging techniques. *Developments in ophthalmology* 53:1-32.
180. Wang JJ, Foran S, Smith W, & Mitchell P (2003) Risk of age-related macular degeneration in eyes with macular drusen or hyperpigmentation: the Blue Mountains Eye Study cohort. *Arch Ophthalmol* 121(5):658-663.
181. Klein R, *et al.* (2007) Fifteen-year cumulative incidence of age-related macular degeneration: the Beaver Dam Eye Study. *Ophthalmology* 114(2):253-262.
182. Lamouille S, Xu J, & Derynck R (2014) Molecular mechanisms of epithelial-mesenchymal transition. *Nat Rev Mol Cell Biol* 15(3):178-196.
183. Pallet N (2012) New insights on stress-induced epithelial phenotypic changes. *Nephrol Dial Transplant* 27(2):483-485.
184. Zhang Y & Marmorstein LY (2010) Focus on molecules: fibulin-3 (EFEMP1). *Exp Eye Res* 90(3):374-375.
185. Roybal CN, Marmorstein LY, Vander Jagt DL, & Abcouwer SF (2005) Aberrant accumulation of fibulin-3 in the endoplasmic reticulum leads to activation of the unfolded protein response and VEGF expression. *Invest Ophthalmol Vis Sci* 46(11):3973-3979.
186. Garland DL, *et al.* (2014) Mouse genetics and proteomic analyses demonstrate a critical role for complement in a model of DHRD/ML, an inherited macular degeneration. *Hum Mol Genet* 23(1):52-68.
187. Fernandez-Godino R, Bujakowska KM, & Pierce EA (2018) Changes in extracellular matrix cause RPE cells to make basal deposits and activate the alternative complement pathway. *Human Molecular Genetics* 27(1):147-159.
188. Maminishkis A, *et al.* (2006) Confluent monolayers of cultured human fetal retinal pigment epithelium exhibit morphology and physiology of native tissue. *Invest Ophthalmol Vis Sci* 47(8):3612-3624.
189. Marneros AG, *et al.* (2005) Vascular endothelial growth factor expression in the retinal pigment epithelium is essential for choriocapillaris development and visual function. *The American journal of pathology* 167(5):1451-1459.
190. Hulleman JD, Kaushal S, Balch WE, & Kelly JW (2011) Compromised mutant EFEMP1 secretion associated with macular dystrophy remedied by proteostasis network alteration. *Mol Biol Cell* 22(24):4765-4775.
191. Liao JL, *et al.* (2010) Molecular signature of primary retinal pigment epithelium and stem-cell-derived RPE cells. *Hum Mol Genet* 19(21):4229-4238.

192. Strunnikova NV, *et al.* (2010) Transcriptome analysis and molecular signature of human retinal pigment epithelium. *Hum Mol Genet* 19(12):2468-2486.
193. Johno H & Kitamura M (2013) Pathological in Situ Reprogramming of Somatic Cells by the Unfolded Protein Response. *The American Journal of Pathology* 183(3):644-654.
194. Hulleman JD, Brown SJ, Rosen H, & Kelly JW (2013) A high-throughput cell-based Gaussia luciferase reporter assay for identifying modulators of fibulin-3 secretion. *J Biomol Screen* 18(6):647-658.
195. Maminishkis A & Miller SS (2010) Experimental models for study of retinal pigment epithelial physiology and pathophysiology. *Journal of visualized experiments : JoVE* (45).
196. Sonoda S, *et al.* (2009) A protocol for the culture and differentiation of highly polarized human retinal pigment epithelial cells. *Nature protocols* 4(5):662-673.
197. Lee JY, Lee DH, Lee JY, & Yoon YH (2013) Correlation between subfoveal choroidal thickness and the severity or progression of nonexudative age-related macular degeneration. *Invest Ophthalmol Vis Sci* 54(12):7812-7818.
198. Ohlmann A, Scholz M, Koch M, & Tamm ER (2016) Epithelial-mesenchymal transition of the retinal pigment epithelium causes choriocapillaris atrophy. *Histochem Cell Biol* 146(6):769-780.
199. Segade F (2010) Molecular evolution of the fibulins: implications on the functionality of the elastic fibulins. *Gene* 464(1-2):17-31.
200. Giltay R, Timpl R, & Kostka G (1999) Sequence, recombinant expression and tissue localization of two novel extracellular matrix proteins, fibulin-3 and fibulin-4. *Matrix biology : journal of the International Society for Matrix Biology* 18(5):469-480.
201. Weber SR, Zhou M, Zhao Y, & Sundstrom JM (2020) Exosomes in retinal diseases. *Exosomes*), pp 415-431.
202. Chen Y, *et al.* (2017) Aberrant low expression of p85alpha in stromal fibroblasts promotes breast cancer cell metastasis through exosome-mediated paracrine Wnt10b. *Oncogene* 36(33):4692-4705.
203. Zhang H, *et al.* (2018) Identification of distinct nanoparticles and subsets of extracellular vesicles by asymmetric flow field-flow fractionation. *Nat Cell Biol* 20(3):332-343.
204. Zhou M, *et al.* (2020) Role of Epithelial-Mesenchymal Transition in Retinal Pigment Epithelium Dysfunction. *Frontiers in Cell and Developmental Biology* 8.
205. Stone EM, *et al.* (1999) A single EFEMP1 mutation associated with both Malattia Leventinese and Doyne honeycomb retinal dystrophy. *Nat. Genet.* 22(2):199-202.
206. Weber BH, Vogt G, Pruett RC, Stohr H, & Felbor U (1994) Mutations in the tissue inhibitor of metalloproteinases-3 (TIMP3) in patients with Sorsby's fundus dystrophy. *Nat. Genet.* 8(4):352-356.
207. Vincent A, *et al.* (2012) The characterization of retinal phenotype in a family with C1QTNF5-related late-onset retinal degeneration. *Retina* 32(8):1643-1651.
208. Atienzar-Aroca S, *et al.* (2018) Role of retinal pigment epithelium-derived exosomes and autophagy in new blood vessel formation. *J Cell Mol Med* 22(11):5244-5256.
209. Biasutto L, Chiechi A, Couch R, Liotta LA, & Espina V (2013) Retinal pigment epithelium (RPE) exosomes contain signaling phosphoproteins affected by oxidative stress. *Exp Cell Res* 319(13):2113-2123.
210. Shah N, *et al.* (2018) Extracellular vesicle-mediated long-range communication in stressed retinal pigment epithelial cell monolayers. *Biochim Biophys Acta Mol Basis Dis* 1864(8):2610-2622.
211. Hosoi T, Nakashima M, & Ozawa K (2018) Incorporation of the Endoplasmic Reticulum Stress-Induced Spliced Form of XBP1 mRNA in the Exosomes. *Front Physiol* 9:1357.

212. Osman A, *et al.* (2020) Endoplasmic Reticulum (ER) Stress-Generated Extracellular Vesicles (Microparticles) Self-Perpetuate ER Stress and Mediate Endothelial Cell Dysfunction Independently of Cell Survival. *Front Cardiovasc Med* 7:584791.
213. Furmanik M, *et al.* (2021) Endoplasmic Reticulum Stress Mediates Vascular Smooth Muscle Cell Calcification via Increased Release of Grp78 (Glucose-Regulated Protein, 78 kDa)-Loaded Extracellular Vesicles. *Arterioscler Thromb Vasc Biol* 41(2):898-914.
214. Choi DS & Gho YS (2015) Isolation of extracellular vesicles for proteomic profiling. *Methods Mol Biol* 1295:167-177.
215. Wan J, Zheng H, Xiao HL, She ZJ, & Zhou GM (2007) Sonic hedgehog promotes stem-cell potential of Muller glia in the mammalian retina. *Biochem. Biophys. Res. Commun.* 363(2):347-354.
216. Besingi RN & Clark PL (2015) Extracellular protease digestion to evaluate membrane protein cell surface localization. *Nat Protoc* 10(12):2074-2080.
217. Shelke GV, *et al.* (2019) Endosomal signalling via exosome surface TGFbeta-1. *J Extracell Vesicles* 8(1):1650458.
218. Webber J, Steadman R, Mason MD, Tabi Z, & Clayton A (2010) Cancer exosomes trigger fibroblast to myofibroblast differentiation. *Cancer Res* 70(23):9621-9630.
219. Kozlowski MR (2012) RPE cell senescence: a key contributor to age-related macular degeneration. *Med Hypotheses* 78(4):505-510.
220. Stenkamp DL, Frey RA, Prabhudesai SN, & Raymond PA (2000) Function for Hedgehog genes in zebrafish retinal development. *Dev. Biol.* 220(2):238-252.
221. Oh EC & Katsanis N (2012) Cilia in vertebrate development and disease. *Development* 139(3):443-448.
222. Spalluto C, Wilson DI, & Hearn T (2013) Evidence for reciliation of RPE1 cells in late G1 phase, and ciliary localisation of cyclin B1. *FEBS Open Bio* 3:334-340.
223. Kowal J, Tkach M, & Thery C (2014) Biogenesis and secretion of exosomes. *Curr Opin Cell Biol* 29:116-125.
224. Thery C, *et al.* (2018) Minimal information for studies of extracellular vesicles 2018 (MISEV2018): a position statement of the International Society for Extracellular Vesicles and update of the MISEV2014 guidelines. *J Extracell Vesicles* 7(1):1535750.
225. Lopez PF, Sippy BD, Lambert HM, Thach AB, & Hinton DR (1996) Transdifferentiated retinal pigment epithelial cells are immunoreactive for vascular endothelial growth factor in surgically excised age-related macular degeneration-related choroidal neovascular membranes. *Invest Ophthalmol Vis Sci* 37(5):855-868.
226. Shih YH, Radeke MJ, Radeke CM, & Coffey PJ (2017) Restoration of Mesenchymal RPE by Transcription Factor-Mediated Reprogramming. *Invest Ophthalmol Vis Sci* 58(1):430-441.
227. Saika S, *et al.* (2009) TGF beta in fibroproliferative diseases in the eye. *Front Biosci (Schol Ed)* 1:376-390.
228. Lin JH & Lavail MM (2010) Misfolded proteins and retinal dystrophies. *Advances in experimental medicine and biology* 664:115-121.
229. Basaiawmoit RV & Rattan SI (2010) Cellular stress and protein misfolding during aging. *Methods Mol Biol* 648:107-117.
230. Tzekov R, Stein L, & Kaushal S (2011) Protein Misfolding and Retinal Degeneration. *Cold Spring Harbor Perspectives in Biology* 3(11):a007492-a007492.
231. Launay S, *et al.* (2008) HtrA1-dependent proteolysis of TGF-beta controls both neuronal maturation and developmental survival. *Cell Death Differ* 15(9):1408-1416.

232. Poulsen ET, *et al.* (2019) The serine protease HtrA1 cleaves misfolded transforming growth factor beta-induced protein (TGFBIp) and induces amyloid formation. *J Biol Chem* 294(31):11817-11828.
233. Fritsche LG, *et al.* (2016) A large genome-wide association study of age-related macular degeneration highlights contributions of rare and common variants. *Nat Genet* 48(2):134-143.
234. Ellgaard L & Helenius A (2003) Quality control in the endoplasmic reticulum. *Nature Reviews Molecular Cell Biology* 4(3):181-191.
235. Farr GA, Hull M, Mellman I, & Caplan MJ (2009) Membrane proteins follow multiple pathways to the basolateral cell surface in polarized epithelial cells. *J Cell Biol* 186(2):269-282.
236. Gourier HC & Chong NV (2015) Can Novel Treatment of Age-Related Macular Degeneration Be Developed by Better Understanding of Sorsby's Fundus Dystrophy. *Journal of clinical medicine* 4(5):874-883.
237. Jacobson SG, Cideciyan AV, Sumaroka A, Roman AJ, & Wright AF (2014) Late-onset retinal degeneration caused by C1QTNF5 mutation: sub-retinal pigment epithelium deposits and visual consequences. *JAMA ophthalmology* 132(10):1252-1255.
238. Fariss RN, Apte SS, Luthert PJ, Bird AC, & Milam AH (1998) Accumulation of tissue inhibitor of metalloproteinases-3 in human eyes with Sorsby's fundus dystrophy or retinitis pigmentosa. *The British journal of ophthalmology* 82(11):1329-1334.
239. Klenotic PA, Munier FL, Marmorstein LY, & Anand-Apte B (2004) Tissue inhibitor of metalloproteinases-3 (TIMP-3) is a binding partner of epithelial growth factor-containing fibulin-like extracellular matrix protein 1 (EFEMP1). Implications for macular degenerations. *J Biol Chem* 279(29):30469-30473.
240. Soumplis V, *et al.* (2013) Phenotypic findings in C1QTNF5 retinopathy (late-onset retinal degeneration). *Acta Ophthalmol* 91(3):e191-195.
241. Zhao Y, *et al.* (2016) XBP1 splicing triggers miR-150 transfer from smooth muscle cells to endothelial cells via extracellular vesicles. *Sci Rep* 6:28627.
242. McLaughlin T, *et al.* (2018) Loss of XBP1 accelerates age-related decline in retinal function and neurodegeneration. *Mol Neurodegener* 13(1):16.
243. Ma JH, *et al.* (2016) The Role of IRE-XBP1 Pathway in Regulation of Retinal Pigment Epithelium Tight Junctions. *Invest Ophthalmol Vis Sci* 57(13):5244-5252.
244. Tsuda T (2018) Extracellular Interactions between Fibulins and Transforming Growth Factor (TGF)-beta in Physiological and Pathological Conditions. *Int J Mol Sci* 19(9).
245. Chaudhry SS, *et al.* (2007) Fibrillin-1 regulates the bioavailability of TGFbeta1. *J Cell Biol* 176(3):355-367.
246. Robertson I, Jensen S, & Handford P (2011) TB domain proteins: evolutionary insights into the multifaceted roles of fibrillins and LTBPs. *Biochem J* 433(2):263-276.
247. Patel MR & Weaver AM (2021) Astrocyte-derived small extracellular vesicles promote synapse formation via fibulin-2-mediated TGF-beta signaling. *Cell Rep* 34(10):108829.
248. Sharma R, *et al.* (2019) Clinical-grade stem cell-derived retinal pigment epithelium patch rescues retinal degeneration in rodents and pigs. *Sci Transl Med* 11(475).
249. Mulcahy LA, Pink RC, & Carter DR (2014) Routes and mechanisms of extracellular vesicle uptake. *J Extracell Vesicles* 3.
250. Xie Y, *et al.* (2010) Dendritic cells recruit T cell exosomes via exosomal LFA-1 leading to inhibition of CD8+ CTL responses through downregulation of peptide/MHC class I and Fas ligand-mediated cytotoxicity. *J Immunol* 185(9):5268-5278.

251. Hawari FI, *et al.* (2004) Release of full-length 55-kDa TNF receptor 1 in exosome-like vesicles: a mechanism for generation of soluble cytokine receptors. *Proc Natl Acad Sci U S A* 101(5):1297-1302.
252. Hazim RA, Volland S, Yen A, Burgess BL, & Williams DS (2019) Rapid differentiation of the human RPE cell line, ARPE-19, induced by nicotinamide. *Exp Eye Res* 179:18-24.
253. Meng Y, *et al.* (2018) Nicotinamide Promotes Cell Survival and Differentiation as Kinase Inhibitor in Human Pluripotent Stem Cells. *Stem Cell Reports* 11(6):1347-1356.
254. Saini JS, *et al.* (2017) Nicotinamide Ameliorates Disease Phenotypes in a Human iPSC Model of Age-Related Macular Degeneration. *Cell Stem Cell* 20(5):635-647 e637.
255. Johnsen KB, *et al.* (2014) A comprehensive overview of exosomes as drug delivery vehicles - endogenous nanocarriers for targeted cancer therapy. *Biochim Biophys Acta* 1846(1):75-87.
256. Wiklander OPB, Brennan MA, Lotvall J, Breakefield XO, & El Andaloussi S (2019) Advances in therapeutic applications of extracellular vesicles. *Sci Transl Med* 11(492).
257. S ELA, Mager I, Breakefield XO, & Wood MJ (2013) Extracellular vesicles: biology and emerging therapeutic opportunities. *Nat Rev Drug Discov* 12(5):347-357.
258. Choi DS GY (2016) Isolation of Extracellular Vesicles for Proteomic Profiling. *Methods Mol Biol* 1295:167-177.
259. Zhou M, Weber SR, Zhao Y, Chen H, & Sundstrom JM (2020) Methods for exosome isolation and characterization. *Exosomes*), pp 23-38.

VITA

Mi Zhou

Education

Ph.D. **Biomedical Sciences**, Pennsylvania State University College of Medicine, 2022

M.D. **Clinical Medicine**, China Medical University, 2012

Publications and Manuscripts

Zhou M, Zhao Y, Weber SR, Chen H, Ford M, Swulius MT, Liu X, Wang HG, Barber AJ, Grillo SL, Sundstrom JM. Extracellular Vesicles from Retinal Pigment Epithelial Cells Expressing R345W-Fibulin-3 Induce Epithelial-Mesenchymal Transition in Recipient Cells. Journal of Extracellular Vesicles. Pub Status: Under revision.

Liu X, Wills CA, Chen L, Zhang J, Zhao Y, **Zhou M**, Sundstrom JM, Schell T, Spiegelman V, Young MM, and Wang HG. Tipifarnib inhibits the secretion of tumor-derived small extracellular vesicles and enhances the immunotherapeutic efficacy of Dinutuximab in neuroblastoma. Journal for ImmunoTherapy of Cancer. Pub Status: Accepted.

Sundstrom JM, Weber S, **Zhou M**, Hogan RN. (2021). The Eye in Aging. In Albert D, Miller J, Azar D, Young LH (Ed.), Albert and Jakobiec's Principles and Practices of Ophthalmology, 4th edition (pp. 1-100). Cham: Springer Nature Switzerland AG.

Zhou M, Geathers JS, Grillo SL, Weber SR, Wang W, Zhao Y, Sundstrom JM. (2020, Jun). Role of Epithelial Mesenchymal Transition in Retinal Pigment Epithelium Dysfunction. Frontiers in Cell and Developmental Biology, 8(-), -. Cited in PubMed; PMID: 32671066. Pub Status: Published.

Zhou M, Weber SR, Zhao Y, Chen H, Barber AJ, Grillo SL, Wills CA, Wang H, Hulleman JD, Sundstrom JM. (2020, Jun). Expression of R345W-Fibulin-3 Induces Epithelial-Mesenchymal Transition in Retinal Pigment Epithelial Cells. Frontiers Cell and Developmental Biology, 8(-), -. Cited in PubMed; PMID: 32637411. Pub Status: Published.

Weber S**, Zhou M**, Zhao Y, Sundstrom JM. (2020). Exosomes in Retinal Diseases. In Edelstein LR, Smythies JR, Quesenberry PJ, Noble D (Ed.), Exosomes: A Clinical Compendium (pp. 415-426). Cambridge: Academic Press; 1st edition.

Zhou M, Weber S, Zhao Y, Sundstrom JM. (2020). Methods for Exosome Isolation and Characterization. In Edelstein LR, Smythies JR, Quesenberry PJ, Noble D (Ed.), Exosomes: A Clinical Compendium (pp. 23-35). Cambridge: Academic Press; 1st edition.